

CHARACTERIZATION OF NEGATIVE  
ELECTROLYTE– ALIZARIN RED S AND  
POSITIVE ELECTRODE FELT FOR ORGANIC  
REDOX FLOW BATTERY APPLICATION



KHOR AI CHIA

اونيورسيتي مليسيا قهغ

UNIVERSITI MALAYSIA PAHANG

DOCTOR OF PHILOSOPHY

UNIVERSITI MALAYSIA PAHANG

UNIVERSITI MALAYSIA PAHANG

**DECLARATION OF THESIS AND COPYRIGHT**

Author's Full Name : KHOR AI CHIA

Date of Birth : 31 JANUARY 1989

Title : CHARACTERIZATION OF NEGATIVE ELECTROLYTE-  
ALIZARIN RED S AND POSITIVE ELECTRODE FELT FOR  
ORGANIC REDOX FLOW BATTERY APPLICATION

Academic Session : 2018 / 2019

I declare that this thesis is classified as:

- CONFIDENTIAL (Contains confidential information under the Official Secret Act 1997)\*
- RESTRICTED (Contains restricted information as specified by the organization where research was done)\*
- OPEN ACCESS I agree that my thesis to be published as online open access (Full Text)

I acknowledge that Universiti Malaysia Pahang reserves the following rights:

1. The Thesis is the Property of Universiti Malaysia Pahang
2. The Library of Universiti Malaysia Pahang has the right to make copies of the thesis for the purpose of research only.
3. The Library has the right to make copies of the thesis for academic exchange.

Certified by:

KhorAichia

(Student's Signature)

890131-02-5468

New IC/Passport Number

Date: 5/4/2021

Mohd Ruslim

(Supervisor's Signature)

Asso. Prof. Ts. Dr. Mohd Ruslim Mohamed

Name of Supervisor

Date: 5/4/2021

اونيورسيتي ملايسيا قهق  
UNIVERSITI MALAYSIA PAHANG

### SUPERVISOR'S DECLARATION

We hereby declare that we have checked this thesis and in our opinion, this thesis is adequate in terms of scope and quality for the award of the degree of Doctor of Philosophy.



---

(Supervisor's Signature)

Full Name : Ts. Dr. MOHD RUSLLIM MOHAMED

Position : ASSOCIATE PROFESSOR

Date : 5/4/2021



---

(Co-supervisor's Signature)

Full Name : Dr. CHONG KWOK FENG

Position : ASSOCIATE PROFESSOR

Date : 5/4/2021

## STUDENT'S DECLARATION

I hereby declare that the work in this thesis is based on my original work except for quotations and citations which have been duly acknowledged. I also declare that it has not been previously or concurrently submitted for any other degree at Universiti Malaysia Pahang or any other institutions.

---

(Student's Signature)

Full Name : KHOR AI CHIA

ID Number : PEE15010

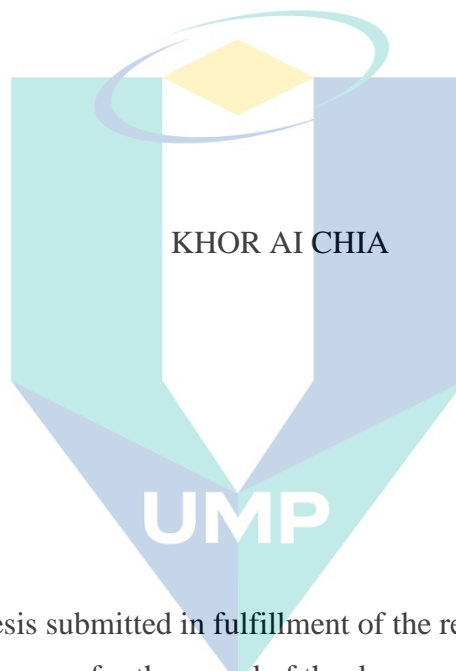
Date : 5/4/2021

UMP

اونيورسيتي ملايسيا قهغ

UNIVERSITI MALAYSIA PAHANG

CHARACTERIZATION OF NEGATIVE ELECTROLYTE– ALIZARIN RED S  
AND POSITIVE ELECTRODE FELT FOR ORGANIC REDOX FLOW BATTERY  
APPLICATION



Thesis submitted in fulfillment of the requirements  
for the award of the degree of

Doctor of Philosophy

اونيورسيتي مليسيا قهغ

UNIVERSITI MALAYSIA PAHANG

College of Engineering

UNIVERSITI MALAYSIA PAHANG

APRIL 2021

## ACKNOWLEDGEMENTS

Years of PhD life at Universiti Malaysia Pahang will be a precious moment that I cherish in my life. Putting an end to this thesis represented a new chapter of research is about to begin soon.

First and foremost, I would like to reserve the most precious appreciation towards my parents and siblings for their support in the matter of physically and mentally throughout these tenure years of studies. I would like to dedicate this work to my late grandparent Mr. Khor Boon Sik and Mrs. Lee Keow Hong who always prayed for my success in life.

Apart from the efforts of mine, the success of any project depends largely on the encouragement and guidelines of many others. I take this opportunity to express my gratitude to the people who have been instrumental in the successful completion of this project. I would like to show my greatest appreciation to Associate Professor Ts. Dr Mohd Rusllim Mohamed as my main supervisor. With his encouragement in research and guidance, I am able to complete the laboratory work and thesis for this project. I feel motivated and encouraged every time I attend his meeting. For the useful comments, remarks, and engagement through the learning process of this thesis, I am so grateful to have him as my supervisor. I am also grateful to have Associate Professor Dr. Chong Kwok Feng as Co-supervisor as I received most of his valuable insight regarding the research outputs and experimental setup with his expertise in material science. Special acknowledgement to Dr. Puiki Leung (Field supervisor) for his coaching in writing paper, data analysis and others lab work related consultation thru email and skype. I cannot say thank you enough for their tremendous support and help. Last and not least, I would like to thank all my lecturers and fellow friends for their teaching and assistance in my studies.

The financial support for this work by the grant from the MyBrain and Fundamental Research Grant Scheme (FRGS) Grant No. 150123 from Ministry of Higher Education Malaysia is grateful acknowledged.

اونيورسيتي ملايسيا قهغ

UNIVERSITI MALAYSIA PAHANG

## ABSTRAK

Bateri aliran redoks organik (ORFB) dianggap sebagai salah satu teknologi lestari yang boleh digunakan untuk penyimpanan tenaga berskala besar. Di antara teknologi bateri aliran redoks organik, pasangan redoks quinone adalah salah satu penyelesaian menarik sebagai elektrolit organik kerana mempunyai bilangan elektron yang banyak, mesra alam dan murah. Bahan redoks kuinon organik seperti alizarin red S yang banyak terdapat dengan tindak balas pengurangan dua elektron dan potensi elektronegatif (kira-kira 0.082 V berbanding elektrod hidrogen standard) sangat sesuai digunakan sebagai elektrolit negatif untuk aplikasi ORFB. Namun, terdapat kekurangan penyelidikan saintifik terhadap alizarin red S (ARS) pada pelbagai kepekatan. Kajian sebelumnya mengenai kepekatan ARS terhadap kepada  $50 \text{ mol dm}^{-3}$  dan  $1 \text{ mol dm}^{-3}$  kepekatan asid sokongan. Oleh itu, kajian ini bertujuan untuk mengkaji ciri-ciri elektrokimia ARS terhadap komposisi kepekatan aktif redoks dan kepekatan asid sulfurik yang berbeza. Oleh yang demikian, bahagian pertama thesis ini meliputi eksperimen untuk mengkaji penggunaan alizarin red S (ARS), salah satu jenis pewarna, sebagai bahan organik kuinon dengan tiga kepekatan berbeza ( $0.05$ ,  $0.10$  dan  $0.15 \text{ mol dm}^{-3}$ ) dan dua jenis kepekatan elektrolit sokongan - asid sulfurik yang  $1 \text{ mol dm}^{-3}$  dan  $2 \text{ mol dm}^{-3}$ . Ringkasnya, kajian mendapati bahawa prestasi ARS adalah terbaik di campuran  $0.05 \text{ mol dm}^{-3}$  dan  $1 \text{ mol dm}^{-3}$  asid sulfurik dengan pekali resapan  $6.424 \times 10^{-4} \text{ cm}^2 \text{ s}^{-1}$ . Serat karbon jenis PAN banyak digunakan sebagai elektrod dalam penggunaan RFB. Namun, serat karbon tanpa rawatan mempunyai masalah sifat permukaan rendah pada elektrod kerana ciri hidrofobik dan kekurangan aktiviti pemangkinan terhadap spesies kuinon. Terdapat kekurangan penyelidikan saintifik mengenai kaedah gabungan rawatan elektrod. Kajian perubahan sifat fisiokimia elektrod dan elektrokimia dalam elektrolit berasaskan kuinon adalah penting dan perlu diselidiki. Kaedah novel rawatan dua peringkat pada permukaan elektrod menggunakan tiga kaedah pengoksidaan yang berbeza (asid, alkali dan hidrogen peroksida) dan termal telah diuji pada serat karbon. Kaedah penyediaannya lebih murah. Kajian ini juga telah diperincikan lagi kepada perbandingan antara karbon yang dirawat oleh alkali dan hidrogen peroksida ke atas elektrolit positif, benzokuinon. Penyelidikan terdahulu menunjukkan bahawa aktiviti redoks terbaik dihasilkan oleh bahan redoks berasaskan kuinon dalam persekitaran berasid. Hasil kajian iaitu pencirian komposisi permukaan, morfologi dan ciri pembasahan berkaitan dengan prestasi elektrokimia seperti kebolehbalian dan penyebaran elektron telah dibentangkan dalam tesis ini. Kajian ini telah berjaya membuktikan dari segi fisiokimia dan elektrokimia, penggunaan rawatan dua peringkat bertujuan untuk meningkatkan tindakan elektrolit positif dalam ORFB. Penyelidikan ini menunjukkan bahawa  $\text{CF}_2\text{H}_2\text{SO}_4$  mempunyai kebolehbalian terbaik berbanding  $\text{CF}_2\text{H}_2\text{O}_2$  dan  $\text{CF}_2\text{NaOH}$  yang menunjukkan jarak antara puncak anodik dan katodik ( $\Delta E$ ) hampir  $59 \text{ mV}$  dan nisbah  $I_{pa}/I_{pc} < 1$ . Seterusnya, pencirian elektrokimia menggunakan teknik imbasan grafik elektron terhadap elektrod terawat menunjukkan pori-pori yang terbentuk pada permukaan alkali dan berasid. Tiada perubahan ketara didapati pada permukaan hidrogen peroksida dengan termal. Di samping itu, fungsi oksigen seperti  $\text{CO}$ ,  $\text{C-OH}$ ,  $\text{C=O}$  dan  $\text{CC=O}$  terbukti hadir pada permukaan karbon yang dirawat hasil yang turut disokong oleh hasil pengukuran sudut daripada penambahbaikan sifat penyerapan serat karbon dirawat dan peningkatan reaksi kinetik dalam larutan BQ. Penyelidikan ini juga mengkaji perbandingan penggunaan serat asid dirawat,  $\text{CF}_2\text{H}_2\text{SO}_4$  terhadap asid sokongan yang lain iaitu asid metanesulfonik dan asid sulfurik. Hasil kajian menunjukkan  $\text{CF}_2\text{H}_2\text{SO}_4$  mempunyai kebolehbalian yang lebih baik dalam asid sulfurik berbanding dengan asid metanesulfonik.

## ABSTRACT

Organic redox flow battery (ORFB) is considered as one of the sustaining technologies for large scale energy storage. Among the organic redox flow battery technology, quinone redox couple is one of the attractive solutions as organic electrolyte because of the low-cost, multiple electron and eco-friendly solution. Organic quinone redox material such as abundantly available alizarin red S with two electron reduction reaction and electronegative potential (c.a. 0.082 V vs. standard hydrogen electrode) is suitable to be applied as negative electrolyte for ORFB application. There is a lack of scientific investigation of alizarin red S (ARS) at various concentration which the previous studies on ARS concentration are limited to 50 mol dm<sup>-3</sup> and 1 mol dm<sup>-3</sup> supporting acid concentration. This work aims to investigate the electrochemical characteristics of ARS with respect to different composition of redox active and sulphuric acid concentration. Consequently, the first part of this work introduces experimental work for alizarin red S (ARS) organic dye with three proposed concentrations of ARS (0.05, 0.10 and 0.15 mol dm<sup>-3</sup>) and two concentration of supporting electrolyte – sulphuric acid which are 1 mol dm<sup>-3</sup> and 2 mol dm<sup>-3</sup>. Electrochemical study such as cyclic voltammetry has been conducted under several operating conditions (i.e., ARS concentration and acid concentration). In summary, the result indicates that ARS highly reversible at 0.05 mol dm<sup>-3</sup> and 1 mol dm<sup>-3</sup> sulphuric acid with calculated diffusion coefficient of 6.424 x 10<sup>-4</sup> cm<sup>2</sup> s<sup>-1</sup>. Another key component that determines the performance of RFB is electrode. In RFB application PAN type carbon felts are widely used as the electrodes, however, pristine carbon felts suffer from low surface properties on electrode due to the hydrophobic characteristics and poor catalytic activity towards quinone species. There is a lack of scientific investigation on combined methods on electrode treatment. Most importantly, the study between the change in electrode physiochemical and electrochemical properties in quinone based electrolyte need to be investigated. A novel of two stage treatment on electrode surface by using three different oxidation methods – acid, alkaline and hydrogen peroxide combined with thermal are carried out on carbon felts. The preparation method is inexpensive, and the study has been extended to the comparison between alkaline and hydrogen peroxide treated carbon felt investigation in selected positive electrolyte, benzoquinone. The results from characterization to identify the surface composition, surface morphology and wetting characteristics that relate to the electrochemical performance such as reversibility and electron diffusion are presented in this work. This study has successfully demonstrated the application of two stage surface treated felt with respect to physiochemical and electrochemical with aims to enhance the positive half-cell of ORFB. The comparison work concludes that CF<sub>H<sub>2</sub>SO<sub>4</sub></sub> presented the best reversibility compared to pristine felt, CF<sub>H<sub>2</sub>O<sub>2</sub></sub> and CF<sub>NaOH</sub> with the difference between the anodic and cathodic peak ( $\Delta E$ ) near to 59mV and  $I_{pa}/I_{pc}$  ratio <1 demonstrated good reversibility. The work reports no significant change on the surface of hydrogen peroxide with thermal. In addition, oxygen functional group such as C-O, C-OH, C=O and C-C=O are successfully introduced onto the surface of treated carbon felt as the result of improved wettability properties of treated carbon felt supported by the finding in contact angle measurement, and it can enhance the kinetics reaction in BQ solution. From previous findings, it has found out that quinone based redox material demonstrates the best redox activity under acidic environment. As a result, this study is extended to investigate the effect of supporting acid (methanesulfonic acid and sulphuric acid). The findings reveal that CF<sub>H<sub>2</sub>SO<sub>4</sub></sub> shows good reversibility in sulphuric acid compared to methanesulfonic acid.



## TABLE OF CONTENT

**DECLARATION**

**TITLE PAGE**

**ACKNOWLEDGEMENTS** **ii**

**ABSTRAK** **iii**

**ABSTRACT** **iv**

**TABLE OF CONTENT** **v**

**LIST OF TABLES** **ix**

**LIST OF FIGURES** **x**

**LIST OF SYMBOLS** **xiii**

**LIST OF ABBREVIATIONS** **xiv**

**CHAPTER 1 INTRODUCTION** **1**

1.1 Background 1

1.2 Problem Statement 3

1.3 Objectives 5

1.4 Scope of Research 6

1.5 Research Contribution 7

1.6 Thesis Outline 8

**CHAPTER 2 LITERATURE REVIEW** **10**

2.1 Introduction 10

2.2 Types of Energy Storage System 11

2.2.1 Mechanical Energy Storage (MES) 12

2.2.2	Electrical Energy Storage (EES)	15
2.2.3	Thermal Energy Storage (TES)	17
2.2.4	Electrochemical Energy Storage (EcES)	18
2.3	Overall Comparison of Energy Storage	23
2.4	Redox Flow Battery Development	30
2.4.1	Iron Chromium	31
2.4.2	Zinc Bromide	32
2.4.3	All Vanadium	34
2.4.4	All Iron	36
2.4.5	Comparison among various redx flow battery technologies	37
2.5	Research Progress in Quinone Based Electrolyte	43
2.5.1	Positive Electrolyte	47
2.5.2	Negative Electrolyte	50
2.6	Electrode Material	53
2.7	Modification/Electrode Activation	54
2.7.1	Thermal Treatment	56
2.7.2	Chemical Treatment	57
2.7.3	Plasma Treatment	58
2.7.4	Carbon Nanotube Based Modification	58
2.7.5	Metal or Metal Oxide Deposition	59
2.8	Surface Morphologies of treated felt	61
2.9	Electrochemical measurement	65
2.9.1	Cyclic Voltammetry	66
2.9.2	Electrochemical Impedance Spectroscopy	66
2.10	Chapter Conclusion	67

**CHAPTER 3 METHODOLOGY** **69**

3.1	Introduction	69
3.2	Materials Preparation	70
3.2.1	Electrode Selection	70
3.2.2	Treatment Reagent Preparation	70
3.2.3	Felt Preparation	71
3.2.4	Electrolyte Preparation	72
3.3	Material Characterisation	73
3.3.1	Scanning Electron Microscope	73
3.3.2	Field Emission Scanning Electron Microscope	73
3.4	Spectroscopy Characterisation	74
3.4.1	X-ray Photoelectron Spectroscopy	74
3.4.2	Contact Angle Measurement	74
3.4.3	BET Surface Area Measurement	75
3.5	Electrochemical Measurement	75
3.5.1	Cyclic Voltammetry	76
3.5.2	Electrochemical Impedance Spectroscopy	78
3.6	Measurement Procedure	79

**CHAPTER 4 RESULTS AND DISCUSSIONS** **81**

4.1	Introduction	81
4.2	Electrochemical Measurement of Potential Negolyte Candidate - Alizarin Red S	81
4.2.1	The effect of ARS Concentration	82
4.2.2	The effect of Sulphuric Acid Concentration	84
4.3	Evaluation of Carbon Felt with Two-Stage Treatment	87

4.3.1	FESEM Surface Topology Analysis	88
4.3.2	X-ray Photoelectron Spectroscopy (XPS) Spectrum Studies	92
4.3.3	Contact Angle Measurement	95
4.4	Electrochemical Investigation for 2D Electrode in Positive Electrolyte	96
4.5	Electrochemical Studies for Modified 3D Electrode	98
4.5.1	Cyclic Voltammetry (CV)	98
4.5.2	Electrochemical Impedance Spectroscopy (EIS)	100
4.6	The Effect of Different Supporting Acid	103
4.6.1	Sulphuric Acid	103
4.6.2	Methanesulfonic Acid	105
4.7	Chapter Conclusion	106
<b>CHAPTER 5 CONCLUSION AND RECOMMENDATION</b>		<b>108</b>
5.1	Future Work	109
<b>REFERENCES</b>		<b>112</b>
<b>LIST OF PUBLICATIONS</b>		<b>129</b>
<b>APPENDIX A</b>		<b>130</b>

اونیورسیتی ملیسیا قهق

UNIVERSITI MALAYSIA PAHANG

## LIST OF TABLES

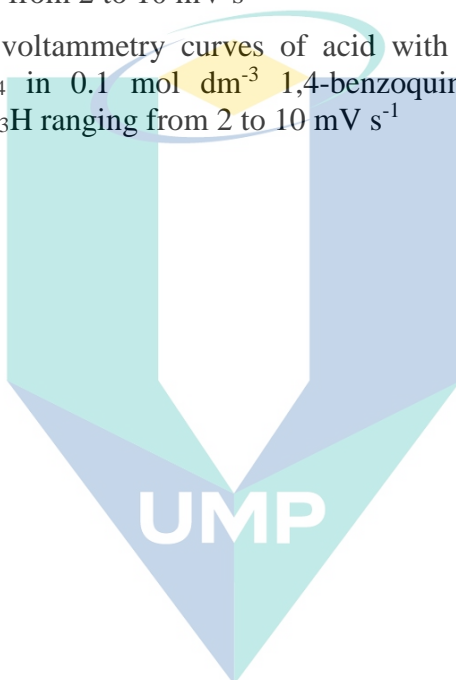
Table 2.1	Energy storage technologies (mechanical, electrical, thermal and electrochemical)	27
Table 2.2	Operational parameters and performance of redox flow batteries or flow-assisted batteries with positive active species in solid, liquid and gaseous phases.	38
Table 2.3	Summary of existing organic couples with respect to the current density, open circuit voltage and no of charge-discharge cycles	45
Table 2.4	Three electrode setups	65
Table 4.1	Measured data for 0.05 mol dm <sup>-3</sup> and 0.15 mol dm <sup>-3</sup> ARS in 1.0 mol dm <sup>-3</sup> and 2.5 mol dm <sup>-3</sup> of H <sub>2</sub> SO <sub>4</sub> in terms of anodic current (I <sub>pa</sub> ), cathodic current (I <sub>pc</sub> ), calculated potential (E <sub>p</sub> ) and diffusion value.	87
Table 4.2	Surface composition CF <sub>H2O2</sub> and CF <sub>NaOH</sub> for from XPS (atomic %).	93
Table 4.3	Element composition ratio of carbon and oxygen functional groups of CF <sub>NaOH</sub> and CF <sub>H2O2</sub> on C1s and O1s XPS curve fitted spectra.	94
Table 4.4	Electrochemical parameters with respect to cathodic and anodic (current, voltage, ratio) of glassy carbon electrode in 0.1 mol dm <sup>-3</sup> 1,4-benzoquinone + 1.0 mol dm <sup>-3</sup> of H <sub>2</sub> SO <sub>4</sub> in terms of anodic current (I <sub>pa</sub> ), cathodic current (I <sub>pc</sub> ) and potential (E <sub>p</sub> )	98
Table 4.5	Electrochemical parameters with respect to cathodic and anodic (current, voltage, ratio) of CF <sub>NaOH</sub> and CF <sub>H2O2</sub> carbon felt.	100
Table 4.6	Electrochemical parameters with respect to cathodic and anodic (current, voltage, ratio) of CF <sub>H2SO4</sub> carbon felt in sulphuric acid.	104
Table 4.7	Electrochemical parameters with respect to cathodic and anodic (current, voltage, ratio) of CF <sub>H2SO4</sub> carbon felt in methanesulfonic acid.	106

## LIST OF FIGURES

Figure 2.1	Classification of energy storage system ESS.	11
Figure 2.2	PHES system layout.	12
Figure 2.3	Schematic for diabatic and adiabatic CAES system.	13
Figure 2.4	Schematic diagram of FES system.	14
Figure 2.5	Schematic diagram for SMES system.	16
Figure 2.6	Schematic diagram for a supercapacitor system.	17
Figure 2.7	Schematic of Ultrabattery by CSIRO Energy Technology and Furukawa Battery Co., Ltd.	19
Figure 2.8	Basic operation of fuel cell (a) charging (b) discharging.	20
Figure 2.9	Detailed schematic diagram of redox flow cell (RFB) consists of (a) outer case (b) bipolar electrodes (c) electrode compartment with porous electrodes (d) ion exchange membrane.	22
Figure 2.10	Energy storage systems according to the form of storage, discharge time and application.	24
Figure 2.11	Review of the zinc-based hybrid flow battery in solid phase, liquid phase and gaseous phase positive reaction configuration.	34
Figure 2.12	Design consideration for organic based RFB.	43
Figure 2.13	Half-cell reduction potential versus SHE for benzoquinones (BQ), naphthoquinones (NQ), anthraquinone (AQ), phenanthroquinones (PQ) in red (calculated) dotted line (experimental).	48
Figure 2.14	Charge-discharge profile (a) 1 M AQS + 2 M H <sub>2</sub> SO <sub>4</sub> / 3 M HBr + 0.5 M Br <sub>2</sub> + 2 M H <sub>2</sub> SO <sub>4</sub> under 0.25 A cm <sup>-2</sup> (b) 2 M HBr + 0.5 M Br <sub>2</sub> /0.1 M AQDS + 2 M H <sub>2</sub> SO <sub>4</sub> under 0.2 A cm <sup>-2</sup> (c) 3 M HBr + 0.5 M Br <sub>2</sub> /1 M AQDS + 1 M H <sub>2</sub> SO <sub>4</sub> under 0.5 A cm <sup>-2</sup> .	49
Figure 2.15	9,10-anthraquinone (AQ) with its derivatives with the functional group	51
Figure 2.16	Process involved in the electrode reaction	54
Figure 2.17	SEM image (a) HNO <sub>3</sub> treated carbon nanoparticles coated felt (b) modified Hummer felt (c) thermal treated felt (NH <sub>3</sub> /O <sub>2</sub> )(d) 98% H <sub>2</sub> SO <sub>4</sub> treated felt (e) N- and WO <sub>3</sub> decorated felt (f) CNF/CNT grown surface	62
Figure 2.18	The morphology of treated felt illustrated by SEM image (a) oxygen plasma (b) nitrogen plasma (c) oxygen plasma	63
Figure 2.19	HRTEM and SEM of metal or metal oxide deposition (a) CuPt <sub>3</sub> (b) Cu <sup>2+</sup> (c) TiC (d) NiO (e) TiN (f) Ir deposition on surface of felt.	64
Figure 3.1	Research flow with highlighted objectives and proposed methodologies.	69

Figure 3.2	Flow for the fabrication of treated felt samples.	71
Figure 3.3	Chemical structure for Alizarin red s.	72
Figure 3.4	Chemical structure for 1,4-benzoquinone.	73
Figure 3.5	Contact angle between water droplet and surface.	75
Figure 3.6	Three electrode system equivalent circuit diagram.	76
Figure 3.7	Cyclic voltammetry example with labels	77
Figure 3.8	Process involved in electrode reaction in three states: bulk solution, electrode surface and electrode.	79
Figure 3.9	Three electrode system.	80
Figure 4.1	Cyclic voltammetry of (a) 0.05 mol dm <sup>-3</sup> ARS (b) 0.10 mol dm <sup>-3</sup> ARS (c) 0.15 mol dm <sup>-3</sup> ARS in 1 mol dm <sup>-3</sup> of H <sub>2</sub> SO <sub>4</sub> with scan rate ranging from 10 mV s <sup>-1</sup> till 25 mV s <sup>-1</sup> .	83
Figure 4.2	Cyclic voltammetry of 0.15 mol dm <sup>-3</sup> ARS in 2.5 mol dm <sup>-3</sup> of H <sub>2</sub> SO <sub>4</sub> with scan rate ranging from 10 mV s <sup>-1</sup> till 25mV s <sup>-1</sup>	85
Figure 4.3	Cyclic voltammetry of 0.05 mol dm <sup>-3</sup> and 0.15 mol dm <sup>-3</sup> ARS in different concentrations (i.e. 1 mol dm <sup>-3</sup> and 2.5 mol dm <sup>-3</sup> ) of H <sub>2</sub> SO <sub>4</sub> with scan rate of 10 mV s <sup>-1</sup>	86
Figure 4.4	Two-stage treated felt (a) hydrogen peroxide with thermal (b) sodium hydroxide with thermal.	88
Figure 4.5	Morphology characterization for SEM image for raw felt with magnification of x500	89
Figure 4.6	FESEM images with magnification x5k for untreated carbon felt.	90
Figure 4.7	FESEM images with magnification x5k and x10k for surface modification (a, b) NaOH with thermal treated felt, (c, d) hydrogen peroxide with thermal treated felt	91
Figure 4.8	FESEM images with magnificant of (a) x5k (b) x15k for surface modification of sulphuric acid with thermal treated felt.	92
Figure 4.9	The XPS wide scan of (a) H <sub>2</sub> O <sub>2</sub> with thermal treatment and (b) NaOH with thermal treatment treated felt.	92
Figure 4.10	XPS curve fitting of (a) C1s spectra and (c) O1s spectra of H <sub>2</sub> O <sub>2</sub> with thermal treatment and (b) C1s spectra and (d) O1s spectra of NaOH with thermal treatment.	94
Figure 4.11	The contact angle measurement using water droplets on (a) pristine carbon felt (b) H <sub>2</sub> O <sub>2</sub> with thermal treatment and (c) NaOH with thermal treatment.	95
Figure 4.12	The experimental CV of glassy carbon electrode in 0.1 mol dm <sup>-3</sup> 1,4-benzoquinone in 1 mol dm <sup>-3</sup> of H <sub>2</sub> SO <sub>4</sub> with range of scan rate from 2 mV s <sup>-1</sup> till 10 mV s <sup>-1</sup>	97

Figure 4.13	Cyclic voltammetry curves of pristine felt, H <sub>2</sub> O <sub>2</sub> with thermal and NaOH with thermal treated felt in 0.1 mol dm <sup>-3</sup> 1,4-benzoquinone + 1 mol dm <sup>-3</sup> H <sub>2</sub> SO <sub>4</sub> at scan rate of 20 mV s <sup>-1</sup> .	99
Figure 4.14	Nyquist plots (a) H <sub>2</sub> O <sub>2</sub> with thermal treatment (b) NaOH with thermal treatment carbon felt in 0.1 mol dm <sup>-3</sup> 1,4-benzoquinone + 1 mol dm <sup>-3</sup> H <sub>2</sub> SO <sub>4</sub> vs. Ag/AgCl fitted to equivalent circuit.	101
Figure 4.15	Fitted data (a) NaOH with thermal treatment (b) H <sub>2</sub> O <sub>2</sub> with thermal treatment carbon felt.	102
Figure 4.16	Cyclic voltammetry curves of acid with thermal treated felt, CF <sub>H<sub>2</sub>SO<sub>4</sub></sub> in 0.1 mol dm <sup>-3</sup> 1,4-benzoquinone + 1 mol dm <sup>-3</sup> H <sub>2</sub> SO <sub>4</sub> ranging from 2 to 10 mV s <sup>-1</sup>	104
Figure 4.17	Cyclic voltammetry curves of acid with thermal treated felt, CF <sub>H<sub>2</sub>SO<sub>4</sub></sub> in 0.1 mol dm <sup>-3</sup> 1,4-benzoquinone + 1 mol dm <sup>-3</sup> CH <sub>3</sub> SO <sub>3</sub> H ranging from 2 to 10 mV s <sup>-1</sup>	105



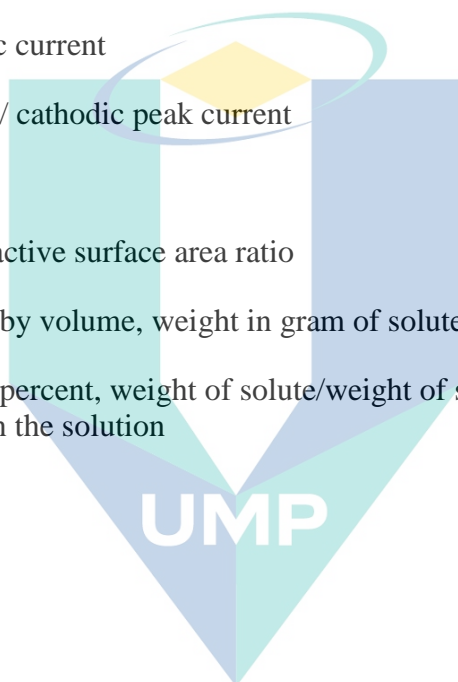
اونيورسيتي مليسيا قهغ

UNIVERSITI MALAYSIA PAHANG



## LIST OF SYMBOLS

$E_{\text{cell}}$	Cell voltage
$\Delta E_p$	Difference between peak potential of anodic and cathodic process
$f$	Frequency
$I_{\text{pa}}$	Anodic peak current
$I_{\text{pc}}$	Cathodic peak current
$I_F$	Faradaic current
$I_{\text{pa}}/I_{\text{pc}}$	Anodic / cathodic peak current
$Q$	Charge
$S_A$	Electroactive surface area ratio
$w/v$	Weight by volume, weight in gram of solute/millilitres of solute
$\text{wt}\%$	Weight percent, weight of solute/weight of solvent*100= percent of solute in the solution



اونيورسيتي ملايسيا قهغ

UNIVERSITI MALAYSIA PAHANG

## LIST OF ABBREVIATIONS

1,8-DHAQ	1, 8 Dihydroanthraquinone
AA-CAES	Advance Adiabatic Compressed Air Energy Storage
AC	Alternating Current
AFC	Alkaline Fuel Cell
AQ	Anthraquinone
AQDS	Anthraquinone-2,6-disulfonic Acid
AQS	Anthraquinone-2-sulfonic Acid
ARS	3,4-dihydroxyl-9,10-anthraquinone-2-sulfonic acid/Alizarin red S
BQ	1,4-benzoquinone
BQDS	1,2-benzoquinone-3,5-disulfonic Acid
CH <sub>3</sub> SO <sub>3</sub> H	Methanesulfonic Acid
CAES	Compressed Air Energy Storage
CF	Carbon Felt
CNT	Carbon Nanotube
CPE	Constant Phase Element
CV	Cyclic Voltammetry
DC	Direct Current
DMFC	Direct Methanol Fuel Cell
DOD	Depth of Discharge
EIS	Electrical Impedance Spectroscopy
EES	Electrical Energy Storage
EcES	Electrochemical Energy Storage
ESS	Energy Storage System
FESEM	Field Scanning Electron Microscopy
GF	Graphite Felt

H <sub>2</sub> SO <sub>4</sub>	Sulphuric Acid
HEV	Hybrid Electric Vehicle
HNO <sub>3</sub>	Nitric Acid
MCFC	Molten Carbonate Fuel Cell
MWCNT	Multi-walled Carbon Nanotube
NASA	National Aeronautics and Space Administration
NQ	Naphthoquinone
ORFB	Organic Redox Flow Battery
PAN	Polyacrylonitrile
PCM	Phase Change Material
PEMFC	Proton Exchange Membrane Fuel Cell
PFC	Phosphoric Fuel Cell
PHES	Pumped Hydro Energy Storage
RE	Renewable Energy
RFB	Redox Flow Battery
SOC	State of Charge
SOFC	Solid Oxide Fuel Cell
SEM	Scanning Electron Microscope
SHE	Standard Hydrogen Electrode
SMES	Superconducting Magnetic Energy Storage
SWCNT	Single-walled Carbon Nanotube
TES	Thermal Energy Storage
UCAES	Underwater Compressed Air Energy Storage
XPS	X-ray Photoelectron Spectroscopy

# CHAPTER 1

## INTRODUCTION

### 1.1 Background

Energy demands are increasing globally with the fact of expanding population, introduction of electric transportation, rapid industrial and economic growth. The major player to support energy demand remain as the traditional fossil fuel generation. Fossil fuel-based generation is currently the main source to support the energy demands but with drawbacks in terms of harmful carbon emission. Nevertheless, the main drawback for fossil fuels generation is environmental problem leads by high carbon emission. There is a great challenge for the nation to support the energy demands while at the same time to achieve low carbon generation. Recently, there is a significant paradigm shift towards incorporating electricity generation with renewable energy resources such as solar, tidal, wind, geothermal etc.

The introduction of renewable energy such as solar, wind, tidal, geothermal, hydro, biofuel and etc. are among the available solutions for zero carbon emission generation. With zero carbon emission generation, renewable energy has been overseen to be beneficial as clean energy generation. In contrast to fossil fuel generation, renewable energy with abundant available resources offers cheaper solution. Nevertheless, the intermittence of renewable energy can easily be abrupt by the weather conditions due to variations for hourly, daily and seasonal of renewable energy require back-up such as energy storage to maintain the security of supply. Without the storing capacity, the demand and intermittent of RE will cause blackouts during the frequency shifting. Therefore, pairing suitable large scale energy storage system (ESS) with renewable energy generation can be the alternative to enable renewable energy (RE) attachment into the grid (Sener, Sharp, & Anctil, 2018).

ESS is a critical part of solution to improve the reliability of RE resource, for example solar and wind system as well as providing stable electricity grid, improving power quality, reducing fossil fuel dependency, lowering carbon emission and increasing the share of variable of RE into electricity generation (Barbour, Wilson, Radcliffe, Ding,

& Li, 2016). ESS can help to balance the viable generation and demand with the handling of excessive electricity into storage. There is a series of methods to store electrical energy by converting into different form of energy, energy storage is categorised according to their storage form which are mechanical, thermal, electrical, and electrochemical.

Referring to the limitation of geographic application of mechanical ESS and complexity installation of electrical ESS, electrochemical energy storage (EcES) happens to be the most widespread electrical energy system. EcES with capability to provide fast response within milliseconds and available in different sizes ranging from kilo to megawatts. The storage principle of EcES is the conversion of electrical energy to kept in chemical form. EcES can be categorized into primary in which the chemical can be consumed only once and secondary battery which is rechargeable. Among available options in primary and secondary EcES, secondary battery redox flow battery (RFB) with advantageous of having unlimited life cycle and flexible design. Different with other rechargeable batteries such as lithium battery that store energy in solid state, RFB has almost similar features as fuel cell that utilized liquid electrolyte except for the exceptional of recycling the similar electrolyte.

Challenges included cost and material toxicity restricted the extension of metal based RFB application. Consequently, achievable approaches by using organic redox couples as electrolyte can penetrated these issues. In norm, any pair of reversible redox couple can be use as electrolytes for RFB application. An ideal redox couple should possess reversibility of multiple electrons and highly soluble where in this case organic material such as quinone offers two electrons redox reactions. Based on the given literature, organic molecules that are abundant, tuneable and two electron process is reported to be the most potential solution to meet the cost effective, eco-friendly and sustainability requirements for EcES. One of the organic molecule-quinone possesses several advantages such as charge capacity of 200-490 Ah kg<sup>-1</sup> and cost about \$10-20 kWh<sup>-1</sup> providing ample opportunities for RFB to achieve the targeted low cost. This necessitates the development of different range of organic redox chemistry as well as the improvement on the selection of redox material and their integration in different composition and electrode material. Exploring and testifying the potential of quinone incorporated with redox material concentration, supporting acid concentration and

electrode material can fasten the development and improvement on ORFB technologies for ESS application.

## 1.2 Problem Statement

The rising demand of the utilization renewable energy sources have gained much attention in recent years due to their contribution of low environmental impact. However, the intermittent nature of renewable energy such as solar and wind power can be unstable. These issues can be solved by utilizing suitable energy storage system. Redox flow battery is one of the most promising electrochemical technology to with the advantages of decoupling of power and energy, long life cycle and safety. Metal based (i.e., vanadium, iron, chromium etc.) or metal complexes technically demonstrated a higher energy density owing to the larger potential difference and higher species concentration per molarity but have significant negative drawbacks such as low ionic conductivities, high solvent price and higher viscosities. The existing conventional RFB involving numerous combinations of metal salts, halogens and low molar mass compound. With the purpose of solve the stated problem, the recent research has focused on organic redox couple. In contrast with metal redox couple which undergo one electron exchange in aqueous form yields low energy density, organic quinone derivatives 3, 4-dihydroxyl-9, 10-anthraquinone-2-sulfonic acid or known as ARS with quasi-reversible two electrons redox reaction can lead to the doubling of energy density.

Previous studies conducted by Zhang *et al.* has focused on the low concentration of ARS and electrolyte based solely on sulphuric acid (S. Zhang, Li, & Chu, 2016). In the reported literature, the anthraquinone based derivative – ARS is characterized via cyclic voltammetry approach at low concentration of  $1\text{m mol dm}^{-3}$  to  $0.1\text{ mol dm}^{-3}$ . The early scientific investigation involving ARS are still limited to  $0.1\text{ mol dm}^{-3}$  (Tabor et al., 2019) whereas the concentration of supporting electrolyte – sulphuric acid is limited to  $1\text{ mol dm}^{-3}$  (Dadpou & Nematollahi, 2016; S. Zhang, Li, & Chu, 2016). Such low concentration of active material is not practical where the energy density of RFB is depending on the concentration of active material. Therefore, investigation on the electrochemical activity of ARS with combination in higher concentration of ARS species and supporting electrolyte are required. Besides, the studies on ARS involving the investigation on related parameters such as active material and supporting acid concentration in the electrochemical still limited. Consequently, further investigation on

ARS potential as electrolyte for RFB with respect to different electrolyte based with different supporting acid concentration are required.

Presently, carbon felt with its ability to resist acidic environment, high surface area, cost effective and good electrical properties. Carbon felt has been found in many electrochemical application like fuel cell, flow battery etc (R. Wang & Li, 2020; Huan Zhang, Chen, Sun, & Luo, 2020). Porous material such as carbon felt with three-dimensional structure is useful as working electrode for RFB. As the critical part that affects the performance of redox flow battery, carbon felt demonstrated good stability during cycling for redox reaction. The electrochemistry properties of carbon, akin to the surface structure and chemical group with respect to active area, which it is directly affected the reaction of electrolyte (R. Wang, Li, & He, 2019). The pristine carbon felt with hydrophobic characteristics exhibits low specific surface area, low electrochemistry performance and weak surface activity for electrolyte transportation (R. Wang & Li, 2020). Due to the hydrophobic properties, surface of carbon felt is subjected to modification to improve the electrochemical properties. Hydrophilic character can be achieved by the insertion of oxygen functional group. Oxygen functional group are formed on the surface of felt treated with oxidizing agent such as acidic, neutral and alkaline oxides.

In previous studies, several surface modification and metal coating process were proposed to catalyse redox reaction, nevertheless, most of the studies employed single stage surface modification, there is a lacking in the investigation for two stages surface modification. Most of the reported treatment applied single treatment method which only serve single modification purpose to the electrode felt. Single treatment namely thermal promote oxidation on the surface but restricted the insertion of another functional group onto the surface. The method limited the finding to further enhance carbon felt surface morphology purpose. Although most of the result shows that acid, alkaline, hydrogen peroxide and thermal treatment can improve the electrochemical properties electrodes, nevertheless, lack of understanding in two stage treated felt in quinone based positive electrolyte are made.

The adsorption and diffusion of redox species on carbon felt is important to study on the charge transfer resistance and electrode/electrolyte (Tamtögl et al., 2018). To enable more functional group such as  $-C-OH$ ,  $-C=O$  and  $-COOH$ , two stage treatment on

felt can be another way for insertion on the surface can generate more electroactive surface area. With the purpose of optimize carbon electrochemistry performance, activation process based on carbon modification through various catalytic material are applied by most researchers (Xu et al., 2020; Huan Zhang et al., 2020), nevertheless, most of the studies focused on vanadium and iron chromium RFB. Despite the large amount of research devoted to the understanding of carbon felt, the extend of felt in organic based electrolytes is still inadequate.

Supporting electrolytes such as ionic salts are added to the electrolyte to improve the conductivity. In general, sulphuric acid is widely used as supporting acid for redox flow application. Methanesulfonic acid is used as supporting electrolyte in zinc based RFB related studies which is less corrosive compared to sulphuric acid. Previous works presented in zinc related investigation concluded that methanesulfonic acid acts as inhibitor to dendrite formation and facilitate redox reaction. The experimental investigation in comparison of different supporting acid involving methanesulfonic acid and sulphuric acid in benzoquinone are still inadequate.

### 1.3 Objectives

For this thesis dissertation, the primary work will focus on the selection of negative electrolyte for organic based (quinone) redox flow battery. Based on the proposed investigation, first methodology is developed to investigate the optimum electrolyte composition of ARS with supporting electrolyte.

1. To investigate the best composition of negative electrolyte that incorporates with ARS in three selected concentrations of 0.05, 0.10 and 0.15 mol dm<sup>-3</sup> and sulphuric acid concentration in two selected concentrations 1.0 mol dm<sup>-3</sup> and 2.5 mol dm<sup>-3</sup> for organic redox flow battery application.

First objective investigates the effect of active material and sulphuric acid concentration in terms of electrochemical studies as current, kinetics and diffusion, the study compared the performance of obtained CV. Next stage for this work involved the improvement of electrode surface for positive redox reaction. Second goal of this work is to characterize porous carbon electrode by introducing functional group onto the surface.



2. To propose, fabricate and evaluate the effect of surface morphology for proposed two-stage (sodium hydroxide with thermal and hydrogen peroxide with thermal) on pristine felt in terms of electrochemical (i.e., electron diffusion, current and reversibility) in cathode side of ORFB by utilised  $0.1 \text{ mol dm}^{-3}$  1,4-benzoquinone in  $1 \text{ mol dm}^{-3}$  sulphuric acid.

The second aims for the present work is to ascertain the surface changes and chemistry with two different activations which are alkaline or hydrogen peroxide with thermal treatment. The samples were prepared by two stage process, pristine felts first treated with oxidation agent then were thermally treated at a temperature of  $450 \text{ }^{\circ}\text{C}$ .

3. To investigate acid treated felt in different positive electrolyte composition with respect to supporting acid (methanesulfonic acid or sulphuric acid) for ORFB application.

Furthermore, the work continued to study on acid with thermal modified porous felt. The study has been conducted to analyse the modified term of electron diffusion, current and reversibility for modified carbon felt in different scan rates. For quinone based ORFB, benzoquinone (BQ) has been selected and proven in most of the organic electrolyte investigations, BQ is selected as positive side due to its higher electropositive potential.

#### 1.4 Scope of Research

As mentions in section 1.3, this PhD research focused on concentration of active material – ARS and concentration of supporting electrolyte – acid sulphuric acid.

Nevertheless, the investigation reported ARS concentration up to  $0.15 \text{ mol dm}^{-3}$  due the solubility limitation. Concentrated sulphuric acid ( $2\text{-}4 \text{ mol dm}^{-3}$ ) usually used as the supporting electrolyte in metal based RFB application (Parasuraman, Lim, & Menictas, 2013), selected concentrations limited to  $2.5 \text{ mol dm}^{-3}$  were utilised for negative electrolyte studies in this work. While to serve the preliminary work for positive felt investigation, the solution in this study was limited to  $1 \text{ mol dm}^{-3}$  of sulphuric acid or methanesulfonic acid concentration and volume of 25 ml for each solution and the investigation of studies focused only on the room temperature of 25-degree Celsius. All the related studies are conducted under room temperature and atmospheric pressure. Spectroscopic measurement such as XPS, SEM, FESEM, CV are under university

responsibility for calibration and handle with laboratory staffs for the investigation. There are several assumptions made for the recorded Nyquist plots of  $CF_{H_2O_2}$  and  $CF_{NaOH}$  treated carbon felts in electrolyte medium. The assumptions are (a) transport properties of electrolyte and felt are constant, (b) current collector and contact resistances are negligible and (c) self-discharge is ignored.

### 1.5 Research Contribution

This thesis focuses on the development of quinone based redox flow battery, an organic type of negative electrolyte selection, supporting electrolyte composition in negative electrolyte, investigation of two stages treated felt in selected positive electrolyte and different supporting electrolyte in positive electrolyte.

The contributions for this work are listed as follow:

1. Experimental study of reduction and oxidation of alizarin red S in the effect of ARS and supporting acid concentration.

Half-cell potential measurements by varying the concentration for active redox material and supporting acids allow investigation on revealing the potential of ARS as negative electrolyte in ORFB application. Previous studies as mentioned in section 0 discloses the limitation of studies. In this study, extension works were performed at higher concentration of active material and supporting acid.

2. Development of two stage surface treatment onto the surface of carbon felt to enhance the performance of a positive half-cell of organic RFB

Two stage surface treatment on the surface of electrode increase the performance of ORFB. The proposed method is more effective than single surface treatment, cheaper and less corrosive compared to metal deposition and reduce the performance loss due to the possibility of the formation of metal complexes. A novel of two-stage method for the preparation of treated on carbon felts for the use in ORFB is presented. The method of preparation is inexpensive and simple.

3. Development of experimental setup for the comparison studies for treated felt between hydrogen peroxide with thermal and alkaline with thermal

In this study, a comparison studies for treated PAN based carbon felts as positive electrode of ORFB has been performed. In the previous studies, most of the activation of electrode is investigated in the medium of vanadium. The lack of investigation on treated surface for benzoquinone (BQ) which has limited the understanding of electrode properties such as electrochemical, physical changes and contribution towards the performance of electrode. In this study, two stage treated carbon felt hydrogen peroxide with thermal and alkaline with thermal were selected. Out of the investigation, it has been found out that CF<sub>NaOH</sub> showed the most favourable effect.

4. Experimental investigation of the effect of supporting acid for acid with thermal treated felt in positive half-cell for ORFB

Supporting acid which included methanesulfonic acid and sulphuric acid were performed in half cell potential measurement in benzoquinone allow further understanding the supporting acid.

## 1.6 Thesis Outline

This thesis aims to identify the key parameters that affected electro kinetics of organic RFBs to explore excessive area for improvement. As presented in five chapters, this thesis is organized as follows:

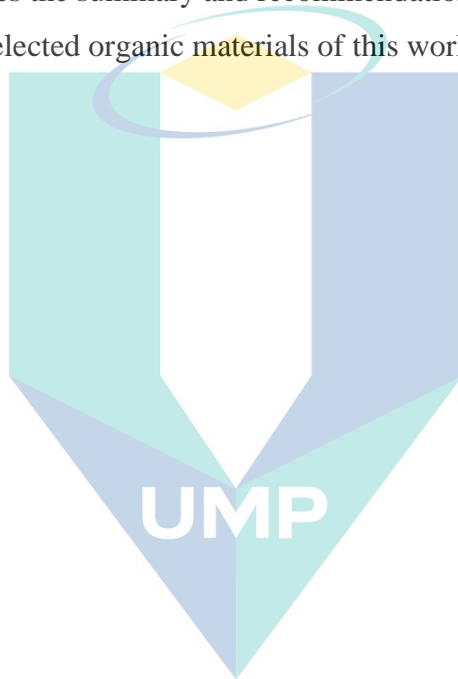
**Chapter 1** explains an overview of the study background for energy storage technology, problem statement, scope of studies, objectives, and the novelty of work of this project.

**Chapter 2** presents a comprehensive literature review on the development concerning the research interest including research relates to various energy storage system, redox flow battery configuration, overview of inorganic and organic RFBs. The thesis continued with the highlight on potential organic based negolyte screening for aqueous organic redox flow battery application. Literature on previous surface characterization for porous electrode also included in this thesis.

**Chapter 3** describes the methodologies for negolyte and felt characterization. This section further elaborates the methodology part starting with experimental flow chart, list of materials, negolyte experimental setup and surface characterisation steps for carbon felt.

**Chapter 4** discusses on fundamental findings of selected negative electrolyte candidate – alizarin red s related to active material and supporting acid concentration for redox flow battery application. The investigation on the potential negative electrolyte in terms of kinetics ability and redox potential explains the ARS as potential replacement for RFB. Porous electrode with surface modification also part of the discussion. The effect of two stage surface modification in selected organic positive electrolyte are also included in this thesis.

**Chapter 5** gives the summary and recommendation for future work. In appendix A, the details on the selected organic materials of this work are gathered.



اونيورسيتي مليسيا قهغ

UNIVERSITI MALAYSIA PAHANG

## CHAPTER 2

### LITERATURE REVIEW

#### 2.1 Introduction

Global industrial development is constantly expanding over years along with the rapid growth of global human population, these problems have caused a drastic increase in energy demand (Agency, 2016). To date, conventional fossil energy generation is still the main source to accommodate the increased energy demand. For environmental impacts and depletion of fossil fuel, there is an obvious trend of shifting of fossil generation towards renewable energy generation. Despite that, the recent scenario elevated the exploration of intermittently available renewable energy such as wind, tidal and solar energy. However, there are several challenges such as unpredictable and variability of nature (wind) that resulting fluctuate dynamic response for frequency variation in electricity generation.

To solve the fluctuation issue of intermittency for renewable energy in electricity grid, a low cost, stable and efficiency solution of energy storage with rapid response capability is essential to tackle the technical barriers of renewable resources adaptation to electricity grid. Therefore, the installation of energy storage system (ESS) is considered as one of the economical solutions that can manage the integration of intermittent renewable energy sources. The energy generated from renewable energy during off-peak can be retained and reserve in ESS in various media and converted to electrical energy when required. The variant of application defined the suitable ESS. Peak demand and grid reliability can be achieved from the decoupling of electricity generation, ESS and electrical grids.

This section, a comparative overview of state of the art for existing energy storage systems with previous review articles for recent years is conducted. Different types of ESS with respect to storage types, operation principles, technical, current research and development for respective technologies are discussed. In addition, the advantages, disadvantages, and application of these ESS technologies have been developed and compared in Table 2.1 under section 2.3. The historical development of RFB is also part of the discussion with the work extended to review metal based RFB. Section 2.6 concerns the current research progress for quinone-based electrolyte, whereas positive

and negative electrolyte are presented. Part of the previous investigation for electrode surface modification and treatment is discussed in section 2.7. This work is continued with the introduction of electrochemical measurement methods (cyclic voltammetry and electrochemical impedance spectroscopy). Finally, chapter conclusions are summarized in section 2.9.

## 2.2 Types of Energy Storage System

Multiple ways can be used to store energy. ESS technologies can be classified into 4 major groups: mechanical (i.e., pumped hydro, flywheel, compressed air, electrical (i.e., supercapacitor and superconducting magnetic energy storage), thermal, electrochemical (i.e., rechargeable batteries, redox flow battery and fuel cells) (Cavazzini, Houdeline, Pavesi, Teller, & Ardizzon, 2018). Classification of energy storage system is illustrated in Figure 2.1, where the system is categorised depending on the conversion process and form of storage.

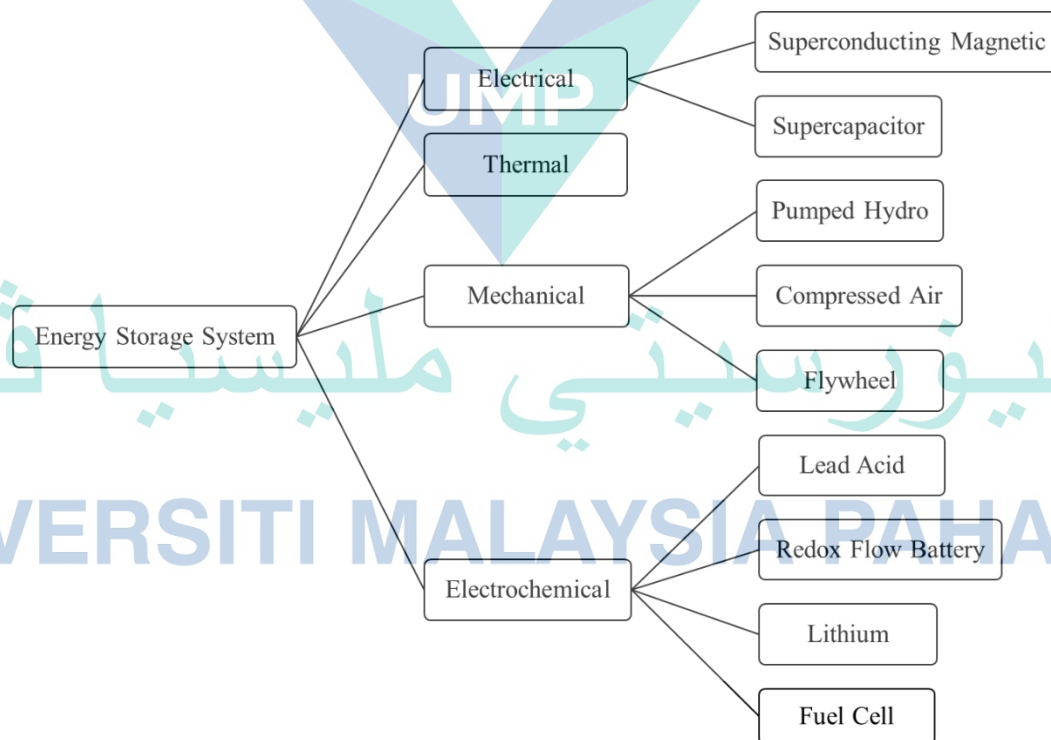


Figure 2.1 Classification of energy storage system ESS.

## 2.2.1 Mechanical Energy Storage (MES)

Mechanical energy storage store energy in kinetic ways or potential with different storage mechanism. Examples of mechanical energy storage are pumped hydro, compressed air energy storage and flywheel (Faraji, Majazi, Al-Haddad, & others, 2017). This section discussed the principles of MES, advantages, disadvantages, and recent advancement on the related technologies.

### 2.2.1.1 Pumped Hydro Energy Storage (PHES)

Storage mechanism for pumped hydro energy storage (PHES) used two water reservoirs separately located at different elevations. The operation of PHES is the translation of the gravitational potential energy to mechanical energy then stored in the form of electrical energy. Gravitational potential energy is in the form of the energy stored in the difference of height or vertical position and the amount of energy depends on the mass and height. During charging operation, energy is stored in terms of gravitational potential energy by pumping water from low to high reservoirs. In discharging operation, the potential energy of the water flow from the upper reservoir to lower reservoir and mechanically turn the turbine that drives a generator to produce electrical energy. Total energy stored is depending on the volume of water and reservoir size, rated power depends on the flow rates of water, ratio rated power/turbine and generator/motor (Luo, Wang, Dooner, & Clarke, 2015a).

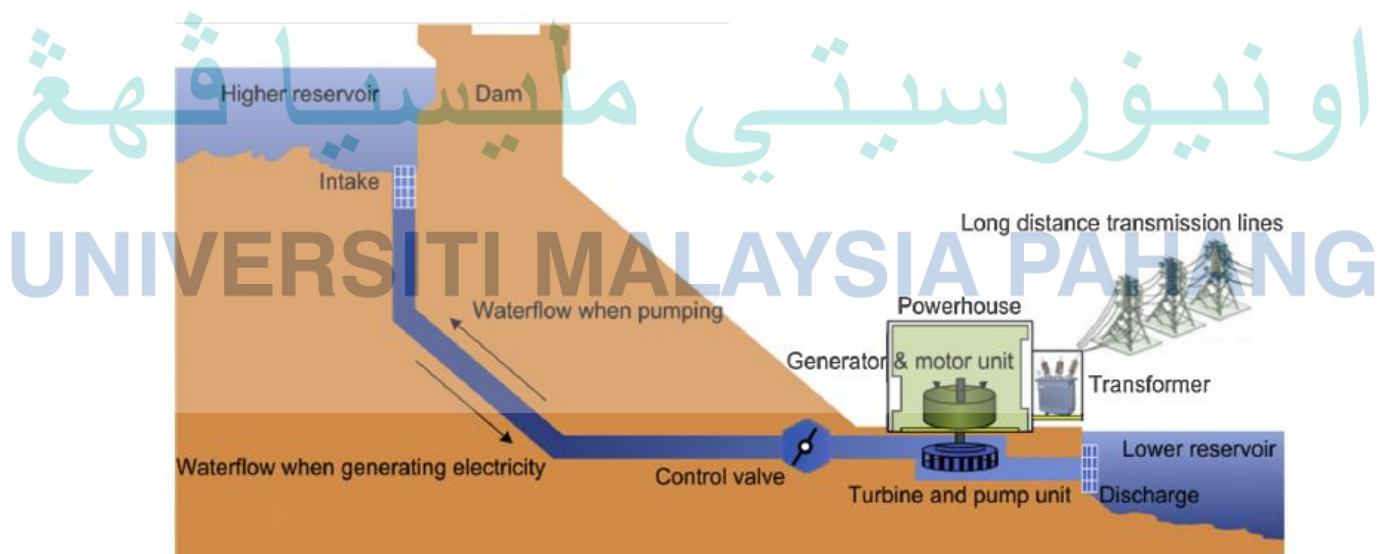


Figure 2.2 PHES system layout.  
Source: Luo, Wang, Dooner, & Clarke, (2015b)

To date, there are several potential PHES technologies reported which are underground PHES, seawater PHES, seasonal PHES and variable speed PHES (Albadi, Al-Busaidi, & El-Saadany, 2017; Hunt et al., 2020). Worth to mentioning that the construction of underground PHES is more environmentally friendly compared to conventional PHES where it reutilized the disused mining facility (Lalanne & Byrne, 2019; Menéndez, Fernández-Oro, Galdo, & Loredó, 2019; Menéndez & Loredó, n.d.). Without required to construct in different elevations, underground PHES can adapt the flat surface of can be utilised as upper while the lower is underground. Although the capital cost of PHES can be reduced using abandoned infrastructure, however, the construction stability and complexity of mines geometry design should be considered for implementation.

### 2.2.1.2 Compressed Air Energy Storage (CAES)

Compressed air energy storage (CAES) comprised compressor, motor/generator, gas turbine and recuperator. In storage mode, electricity energy is converted to mechanical energy by using motor. The energy is stored in compressed air under high pressure (up to 100 Bar) in underground reservoir. For the discharge mode, the pressurized air is mixed with fuel and burned in a gas turbine and turned to the generator for electricity generation. Recuperator is used to heat the gas before release in turbine to get higher efficiency. The power of CAES depends on the number and power of the compressor and turbine, the storage capacity can be defined by the volume of compressed air and the pressure level.

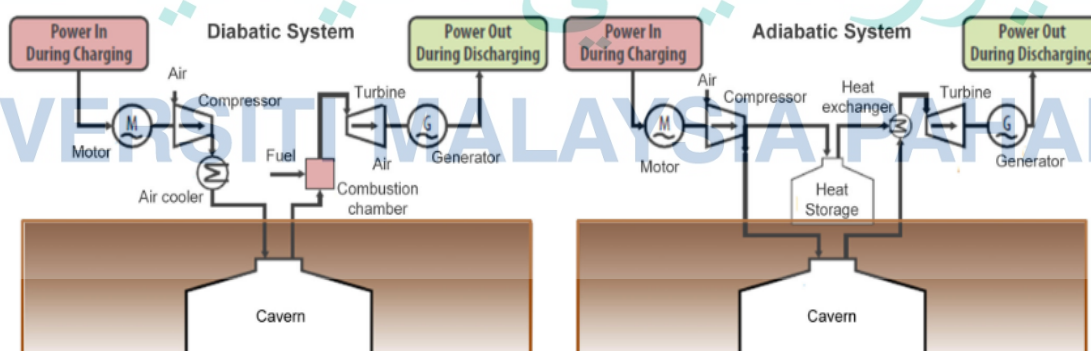


Figure 2.3 Schematic for diabatic and adiabatic CAES system.

Source: N. Khan, Dilshad, Khalid, Kalair, & Abas, (2019)



There are two types of CAES as illustrated in Figure 2.3 that are diabatic system and adiabatic system, the main difference is the air in an adiabatic is compressed without gain and loss of heat while diabatic system stored after passing the cooler (N. Khan et al., 2019). Up to recent, new developments such as underwater CAES (UCAES) and advanced adiabatic CAES (AA-CAES) have been reported. AA-CAES integrated with thermal energy storage require no fossil based thermal system to restore the energy, the system reported zero carbon emissions.

### 2.2.1.3 Flywheel Energy Storage (FES)

Flywheel energy storage (FES) mechanism is by angular momentum of spinning mass in vacuum chamber (Cho, Jeong, & Kim, 2015). As shown in Figure 2.4, the basic component for FES consists of four components, which are electric motor, magnetic bearing, flywheel rotor and AC/DC converter. The charging operation of flywheel, which is the flywheel rotor, is by rotating the shaft around the centre axis and store the kinetic energy in electric motor. For discharging, the electric motor acts as the generator (power source) to the electric grid. The energy generation for FES depends on the cylinder radius, rotational and material density, while power relies on the electrical motor and shaft between motor and cylinder.

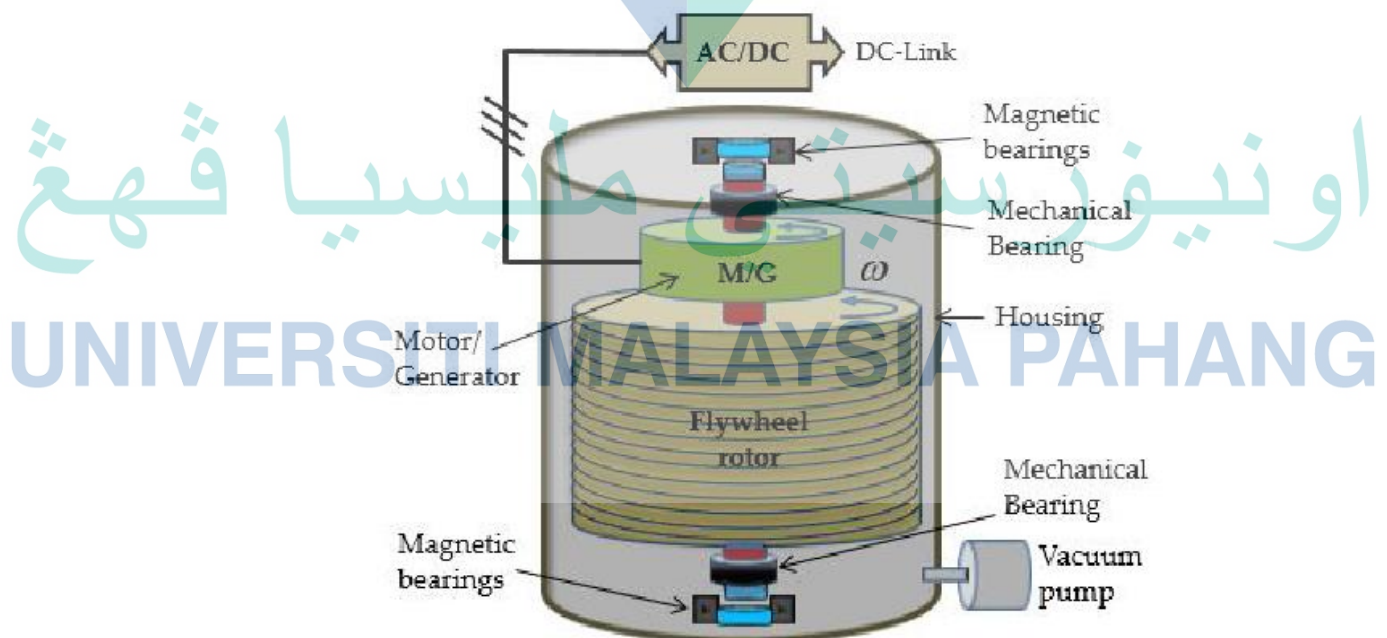


Figure 2.4 Schematic diagram of FES system.

Source: Amiryar & Pullen, (2020)

Due to the advantage of being fast response time, FES is the most suitable in frequency regulation for electricity grid. Nevertheless, FES suffers from loss such as friction and magnetic forces, tricky design feature with vacuum operation setting, less energy stored per volume and limited speed (Burheim, 2017; Krishan & Suhag, 2019). To handle the current limitation of FES speed (100,000 rpm), permanent magnet synchronous machine (1,000,000 rpm), induction motor (>100,000 rpm) and bearingless machine are proposed.

## **2.2.2 Electrical Energy Storage (EES)**

Electrical or electromagnetic energy storage store electricity in terms of electromagnetic fields. Two types of available EES technologies that are superconducting magnetic energy storage (SMES) and supercapacitor.

### **2.2.2.1 Superconducting Magnetic Energy Storage (SMES)**

Superconducting magnetic energy storage (SMES) is an electrical storage technology that stored potential energy in the magnetic field and converted the energy within a fraction of a cycle to replace a sudden loss in line power. It stores energy in the magnetic field created by the flow of direct current (DC) power in a coil of superconducting material that has been cryogenically cooled with ideally no resistive losses. The main components for SMES consist of conducting coil, cryogenics, vacuum vessel, and electronics system (Zach, Aeur, & Lettner, 2012). During off-peak, electrical energy in the form of alternating current (AC) is stored in direct current produced by the superconducting coil. The system is capable of releasing megawatts of power traveling through a superconducting magnet during load peak. The superconducting coil should be kept in a refrigeration system under low temperature of  $-270\text{ }^{\circ}\text{C}$  to maintain the superconducting state (Luo et al., 2015; Mukherjee & Rao, 2019). Energy capacity of SMES depends on the inductance and the total amount of DC current flow across the superconducting coil. Consequently, the system is highly dependent on the temperature which technically difficult to maintain.

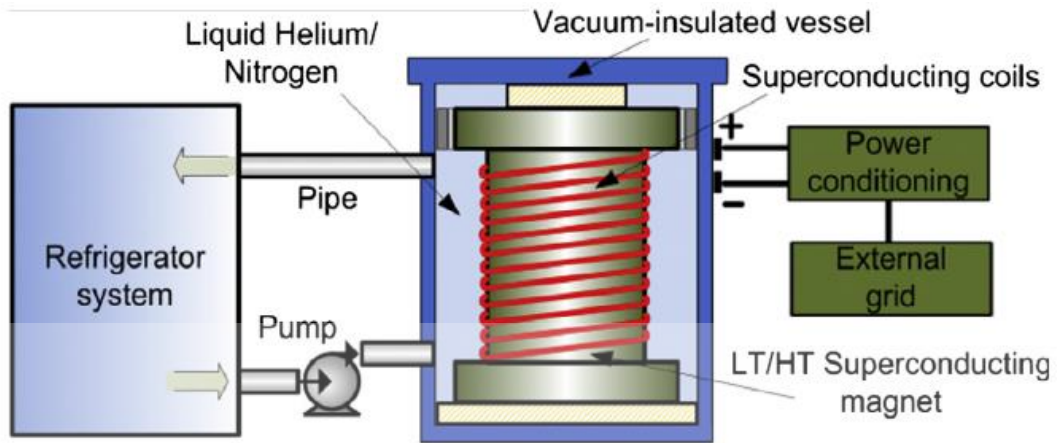


Figure 2.5 Schematic diagram for SMES system.

Source: Luo et al., (2015b)

SMES has high charge/discharge cycle, fast charge/discharge response and no resistive loss (under the superconducting state). SMES is suitable for energy stability and voltage compensation due to the large power transfer and absorption capability. Drawbacks for SMES are temperature dependence and cost (Dekka, Ghaffari, Venkatesh, & Wu, 2015). For example, a slight change of temperature will cost the coil to become unstable and lose energy, as a result additional cost is required for refrigeration.

### 2.2.2.2 Supercapacitor

The operation of supercapacitor is based on the capacitive energy stored between positive and negative electrical charge carrier as demonstrated in Figure 2.6. Similar to batteries, supercapacitor consists of two conductive plates and electrolyte separated by porous membrane (Chan et al., 2018). During the charging operation, ion in the electrolyte move to electrodes and form a double layer on the surface of each electrode. The ions are stored in between electric double layer (Zach, Aeur, & Lettner, 2012). Energy for supercapacitor storage depends on the gap between the two electrode plates and material selection for electrolyte and separator (A. González, Goikolea, Barrena, & Mysyk, 2016).

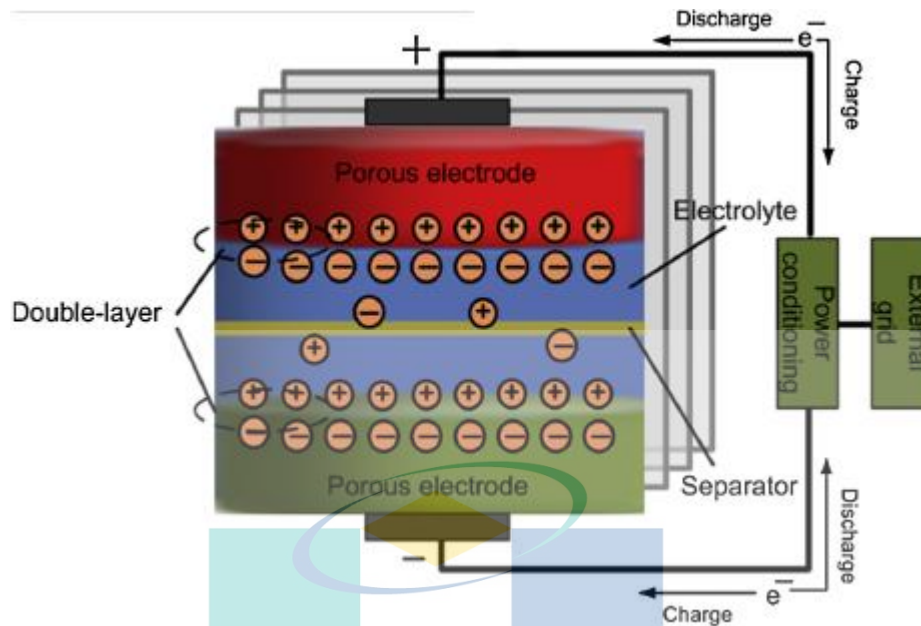


Figure 2.6 Schematic diagram for a supercapacitor system.  
Source: Luo et al., (2015a)

### 2.2.3 Thermal Energy Storage (TES)

Thermal energy storage (TES) can be driven by different sources of heat such as solar, geothermal, industrial waste, geothermal, nuclear power plant, fossil fuel, biomass, etc. TES provide economic and environmentally friendly solution by reducing the fossil fuel utilization. The heat generated from daily social and industry activities can be collected with suitable TES system. Thermo-physical material with high specific heat, chemical stability, thermal stability, and high thermal conductivity materials. The specific heat capacity for TES depends on the density, volume, specific heat, and temperature variant of storage material. TES can work in a broad range of temperatures between  $-40^{\circ}\text{C}$  and  $600^{\circ}\text{C}$  referring to the selection of heat storage material. TES systems can be differentiate based on heat storage material, mechanism, delivery scheme, storage cycle frequency and operating temperature range (Alva, Lin & Fang, 2018).

TES can be categorised into three major types included sensible heat storage, latent heat storage and thermochemical heat storage. Sensible thermal storage is the simplest among available thermal energy storages that store energy in terms of heat. In sensible, thermal energy stored in the heat capacity of the material (i.e., rock, oil, water, brick, etc.). The volume of selected medium and temperature defined the storage capacity of sensible heat (Kocak, Fernandez, & Paksoy, 2020). Latent heat is different from the sensible heat regarding storage, thermal energy is stored through the process of phase

change. At a certain temperature with the principle of enthalpy of melting, evaporation, and sublimation. Compared to the sensible and latent, thermochemical stored based on the principle of physical and chemical bonding (Mehari, Xu, & Wang, 2020).

#### **2.2.4 Electrochemical Energy Storage (EcES)**

The electrochemical energy storage system has been recognized as potential technology in terms of enhancing the output from unsteady renewable resources and maintaining grid stability associated with distributed generation. Electrochemical energy storage used the principle of storing electrical energy into electrochemical energy using the chemical reaction.

##### **2.2.4.1 Lead Acid**

Lead acid battery is the oldest electrochemical battery that consist of lead dioxide and spongy lead as electrodes and sulphuric acid as the supporting electrolyte. The mature technology of lead acid battery has dominated the automotive industries for years. Thanks to the advantages of relatively-low production cost , recyclable and ease of manufacture (Cho et al., 2015; Z. Wu et al., 2020; C. Zhang, Wei, Cao, & Lin, 2017). Nevertheless, lead acid battery is less favoured in utility-based energy storage systems because of the technical challenges of relatively low cycling times, sulphation issue and required periodic water replacement (B. Li & Liu, 2017). In addition, limitations on working temperature, especially low temperature required thermal activation system (Luo et al., 2015a).

The disadvantage of lead acid battery is a short life span. Conventional lead acid battery was reported to have a heavy weight, limited cycle, sulphation, and long charge time unable to meet the requirement for HEV application. The limitation of the depth of discharge of lead acid battery, whereas the working operation of lead acid battery is within 30%-70% state of charge (SOC). As a result, lead acid battery unable to deliver cranking current when the depth of discharge (DOD) is below 30% (Cooper, Furakawa, Lam, & Kellaway, 2009).

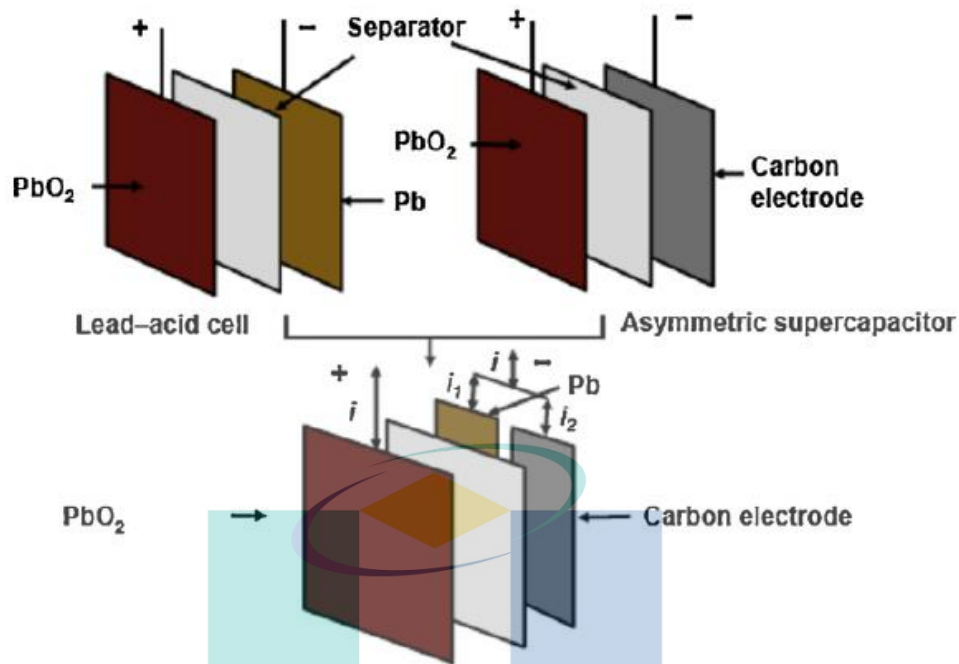


Figure 2.7 Schematic of Ultrabattery by CSIRO Energy Technology and Furukawa Battery Co., Ltd.

Source: Cooper et al., (2009)

A recent advancement in lead acid battery to improve high-rate charge acceptance is by composite negative electrode with carbon-based supercapacitor and use with standard positive electrode as illustrated in Figure 2.7. This lead acid battery is known as Ultrabattery, the new added feature with installed capacitor electrode acts as buffer for high-rate discharge and charging that allows rapid charge absorption under acceleration and braking condition.

#### 2.2.4.2 Lithium Ion

Lithium-ion battery operates using lithium-ion intercalation between positive (i.e., lithium metal oxide) and negative (i.e., graphite) electrodes that are separated by microporous plastic film (Soloveichik, 2011). Compared to other emerging electrochemical energy storage, lithium is the most electropositive element in the periodic table.  $\text{Li}/\text{Li}^+$  with redox potential of -3.04 V vs SHE and high specific capacity of 3860 mAh  $\text{g}^{-1}$  offering high energy density (up to 10,000 Wh/L), as well as high specific energy up to 200 Wh  $\text{kg}^{-1}$  (Luo et al., 2015a). The characteristics of having high specific energy

enabled lithium-ion batteries to dominate electronic market for mobile phones, laptop and electric vehicle applications (Scrosati & Garche, 2010).

Like lead, elemental lithium anodes tend to grow dendrites during charge and discharge cycling due to the deposition of Li. The dendrite formation on the surface of the anode causes a short circuit, consequently leading to an explosion. Other several major issues include thermal runaway, high material and manufacturing cost and safety (J. G. Kim et al., 2015). Safety with respect to thermal stability is the main concern for lithium-based battery where the material for lithium battery involved high energy density and highly flammable. The long charging period has restricted the extension of energy efficient vehicle in automotive compared with fossil fuels.

### 2.2.4.3 Fuel Cell

Electrochemical energy storage, such as fuel cell convert chemical energy (hydrogen fuel) into electricity and heat release for the process. The fuel cell configuration illustrated in Figure 2.8 comprises positive, negative bipolar plates, electrolyte, and ion exchange membrane. Electric power is used to produce fuel B via the electrolysis process for storage mode while for supply mode fuel B with an oxidant agent A generate electricity to meet the demand.

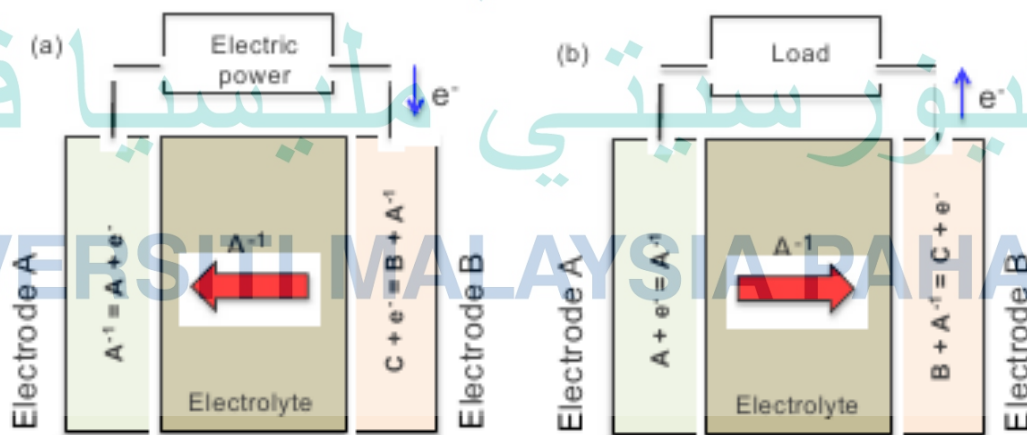


Figure 2.8 Basic operation of fuel cell (a) charging (b) discharging.

Source: Gür, (2018)

Fuel cells can be further classified into 6 types depending on the electrolytes/fuel selection, which are solid oxide fuel cell (SOFC)(R. Raza, Zhu, Rafique, Naqvi, & Lund, 2020), proton exchange membrane fuel cell (PEMFC)(Pivac & Barbir, 2016), alkaline fuel cell (AFC)(Sheng et al., 2020), direct methanol fuel cell (DMFC)(Alias, Kamarudin, Zainoodin, & Masdar, 2020; Kumaresan et al., 2020), molten carbonate fuel cell (MCFC) and phosphoric fuel cell (PFC).

#### 2.2.4.4 Redox Flow Battery

In redox flow battery, electrical energy is stored in the electrolyte and can be instantly released into electrical energy. Three main components of RFB are unit cell, external electrolyte tank and flowing system. The configuration of RFB illustrated in Figure 2.9 consists of two external electrolytes reservoir, cell frame, bipolar electrode, membrane, and porous electrode. In RFB cells, ion exchange membrane separated positive and negative electrolytes. The exchange of reduction and oxidation reaction happen between the compartments that are separated by a membrane. Redox reaction happens in the active area of carbon felt, the electron is then collected by carbon electrode and then to the copper terminal. Thin membrane prevents the electrolyte to cross over into another compartment.

The electrolyte with redox active material is circulated by using a peristaltic pump for each positive/negative compartment of the cell. Redox term originated from two terms, that are reduction and oxidation, one type of chemical reaction in which atom or molecule gains or loses electrons. According to redox reaction equation as follows, where Ox defined oxidised species, n represents the number of electrons and Re was reduced species.



2.1



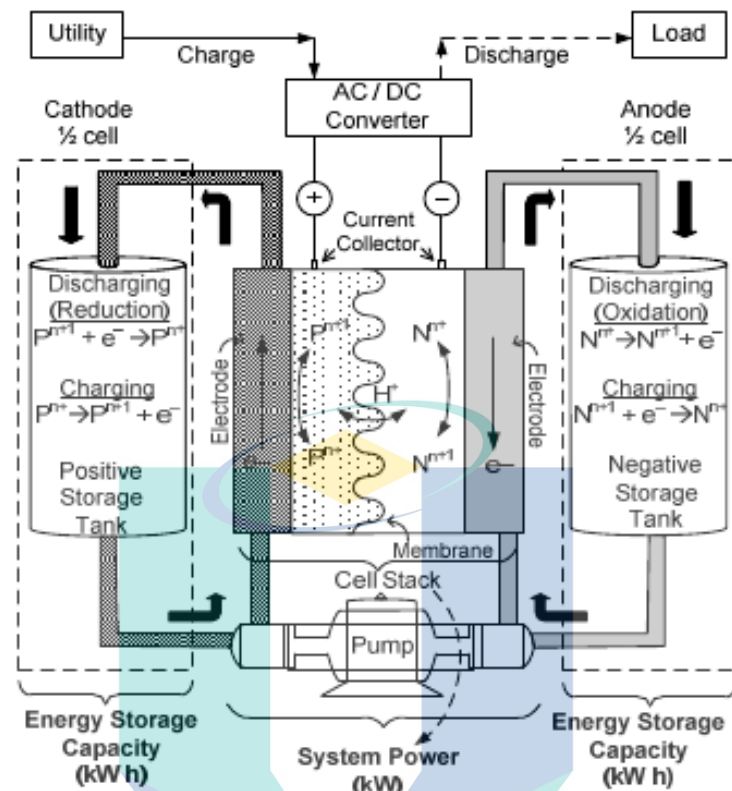


Figure 2.9 Detailed schematic diagram of redox flow cell (RFB) consists of (a) outer case (b) bipolar electrodes (c) electrode compartment with porous electrodes (d) ion exchange membrane.

Source: M. R. Mohamed, Sharkh, & Walsh, (2009)

Similar to fuel cell, RFB has a similar configuration except for the circulated electrolytes. Different with a fuel cell used the reactant (i.e., gas or liquid fuel) to release energy, RFB stored electrolyte in separate liquid reservoirs. From the review, it has been discovered that the advantages of recycling give thermal cooling in contrast with the conventional type of secondary battery with solid polymer. The circulation of electrolyte in redox flow battery provides a cooling effect by enabling heat exchange from the internal cell to external tank (Z. Wei, Zhao, Skyllas-Kazacos, & Xiong, 2014; Z. Wei, Zhao, & Xiong, 2014).

The decouple energy and power offering flexible design for RFB, for example energy capacity can be modulated by varying the amount of electrolyte or active species concentration. The power output can be varied with the definition of the number for RFB cell stack. Emphasising the advantage of being decoupled of energy and power, RFBs

pledged a tremendous design flexibility to fit the energy and power criterion over other types of electrochemical energy storage, this feature making it well suited for applications such as remote area supplier. This feature offers a wider option for the customization of RFB in the range kilowatt to Megawatt applications such as backup power supplier (Miyake & Industries, 2001), generation and distribution (Barote, 2009), power quality optimisation and in the future for hybrid electric vehicle applications (M. R. Mohamed et al., 2009). Nevertheless, bulky, and complex design makes RFB not suitable for portable applications such as mobile phones and laptop.

### 2.3 Overall Comparison of Energy Storage

Various types of energy storage systems, such as mechanical, electrical, thermal and electrochemical with examples are illustrated in Figure 2.5. The presented work included detailed information such as storage capacity, life span, response time, efficiency, cost and densities, discharge time at rated power, system power rating and module size. These are the critical parameters that govern the suitability of energy storage to serve for any specific application either mobile or stationary.

In terms of working temperature, the supercapacitor outranked most if the energy storage system (i.e., batteries) where it operates in wider temperature ranges of  $-40^{\circ}\text{C}$  and  $100^{\circ}\text{C}$  compared to EcSS such as battery that limited between  $-20^{\circ}\text{C}$  and  $60^{\circ}\text{C}$ . The advantage of low temperature operation allows supercapacitor to operate between  $-40^{\circ}\text{C}$  and  $100^{\circ}\text{C}$ . The working temperature for most mechanical based ESS is independent of the efficiency of system. Besides, supercapacitor-stored charge electrostatically allows fast response between 1 and 10s for charge and discharge (Devillers, Jemei, Péra, Bienaimé, & Gustin, 2014). Although a supercapacitor is more capable of storing large amounts of energy and charged discharged in a short period, the power density is low due to the storage mechanism (A. González et al., 2016). These criteria make supercapacitors more suitable to handle high power and short period application or pairing with other ESS (i.e., batteries) in hybrid approach (ud din Mufti, Lone, Iqbal, Ahmad, & Ismail, 2009).

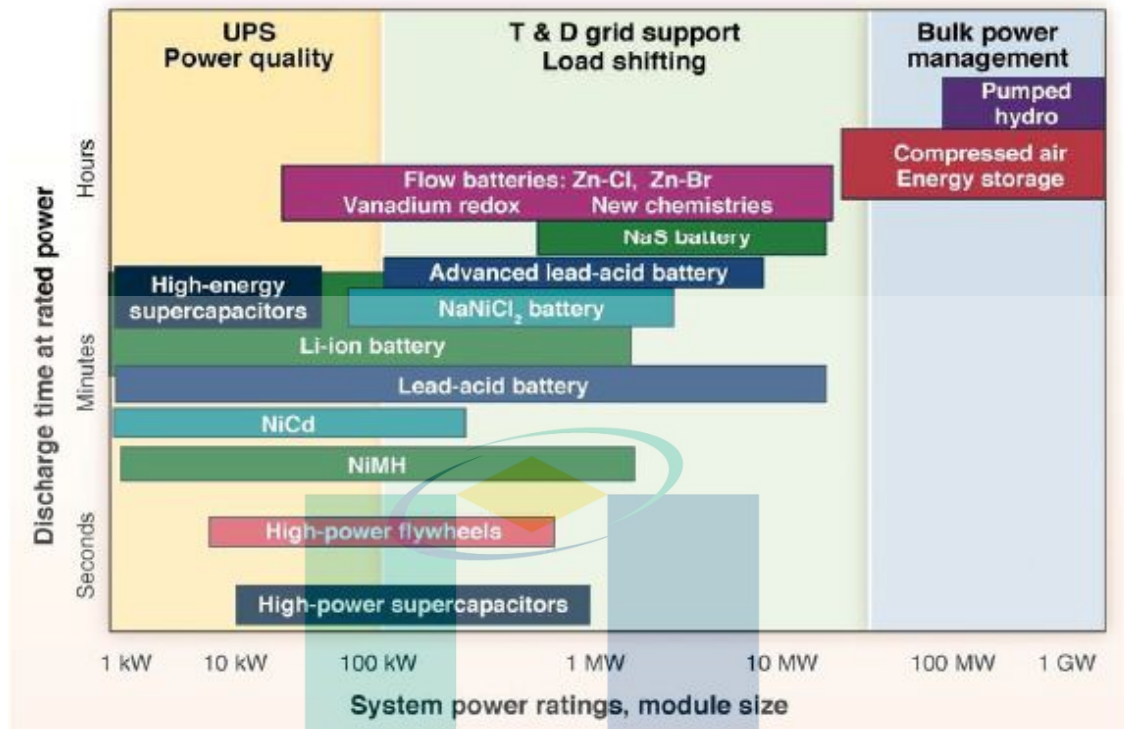


Figure 2.10 Energy storage systems according to the form of storage, discharge time and application.

Source: Gür, (2018)

UMP

The advantage of sensible heat is low-cost material among other TES and types of energy storage systems. The disadvantages of sensible heat storage are low temperature compared to latent heat and temperature stability during the discharge process. Low thermal conductivity (between 0.2 and 0.8 W/mK) is one of the disadvantages for PCM storage (Huili Zhang, Baeyens, Caceres, Degreve, & Lv, 2016). TES suffer from the technical operational problem, poor heat transfer, phase change leakage control, heat loss, phase separation, supercooling, container corrosion, vapour pressure, volume changes, safety, and toxicity (formaldehyde and thermal oil).

In comparison with pumped hydro, compressed air energy storage (CAES) employed medium of air instead of pumping water. Like pumped hydro, CAES is contributed to environmental destruction and land loss, whereas both systems are in an isolated and mountainous region. Another disadvantage is conventional CAES required gas air turbine with fossil combustion to restore the stored energy results carbon emission. All the mentioned energy storage systems differ in response time. Mechanical energy

storage systems are limited by geographical restriction, design, and high cost. Another option for mechanical storage, FES has favourable features such as environmental friendly, high energy efficiency of 95%, low maintenance with fast charge/discharge and high-power density (Samineni, Johnson, Hess, & Law, 2006; Wicki & Hansen, 2017).

Compared with capacity output, three examples for low storages with high output energy are superconducting magnetic energy storage (SMES), flywheel and supercapacitor. Most of electrochemical storage systems such as lead acid, fuel cell, lithium-ion battery and redox flow battery are suitable for medium range storage applications. For higher capacity ranges up to GW scale, pumped hydro energy system (PHES), compressed air energy storage (CAES) and thermal energy system. CAES is another type of mechanical storage system that can provide power output scale up to MWh with long storage period (>1 year). Also, CAES produced the same amount of electricity with 40% lower fuel consumption compared to conventional gas turbine system (Zach et al., 2012).

From the discussion presented in the previous section, it is observed that each ESS has exceptional characteristics with its suitability for power application (peak shaving, sag compensation and load levelling). For example, electrical ESS can provide high efficiency with fast response times that can respond to the demand peak in electricity grid, whereas batteries offer high energy densities. Pumped hydroelectricity production capacity can reach up to GWh scale with high round trip efficiency of approximately 85%, and long-life cycle up to 60 years (H. Lee, Jung, Cho, Yoon, & Jang, 2013). PHES serves as the cheapest solution with the highest life span for large capacity storage. Despite the stated advantages, PHES that include reservoirs, turbine and dam encountered social implications (i.e., landslides, water quality and wildlife migration) and geographical limitation whereas the installation required specific site conditions for water storage (Ardizzon, Cavazzini, & Pavesi, 2014). Slow switching during the changes between pumping and generating modes is affecting the efficiency of PHES. The slow switching and response time has restricted PHES as support for reserve, response services, transmission and distribution grid support.

The comparison shows electrochemical ESS have advantages over other ESS in terms of customisation flexibility, advantages. Electrochemical ESS has outraged electrical and mechanical due to their robust characteristics, shorter response time and the most important thing is that it can be applied in anyplace free from geographical consideration. It offers a lower environmental impact for user especially if being compared to mechanical storage systems (pumped water, compressed water, flywheel etc.), as it can be sited nearer to the consumer area. Lithium-ion battery is widely deemed the most suitable solution for electrified mobility due to the high energy densities, however, less preferable for stationary applications dealing with the disadvantages of lithium resources, safety issues dealing with thermal, cost and battery management system.



اونيورسيتي مليسيا قهغ

UNIVERSITI MALAYSIA PAHANG

Table 2.1 Energy storage technologies (mechanical, electrical, thermal and electrochemical)

Types		Capacity	Response time	Efficiency	Life Span	Application	References
Mechanical	Pumped Hydro Energy System (PHES)	3 GW	min to hour	85%	>60 years	<ol style="list-style-type: none"> <li>1. Long time scale grid energy storage</li> <li>2. Non spinning reserve</li> <li>3. Supply reserve</li> </ol>	(Rehman, Al-Hadhrami, & Alam, 2015)
	Compressed Air Energy Storage (CAES)	3 GW	min	80%	20-40 years	<ol style="list-style-type: none"> <li>1. Long time scale grid energy storage</li> <li>2. Peak shaving</li> <li>3. Spinning reserve</li> <li>4. VAR support</li> <li>5. Arbitrage</li> </ol>	(Krishan & Suhag, 2019; Menéndez & Loredó, n.d.; Olabi, Wilberforce, Ramadan, Abdelkareem, & Alami, 2020)
	Flywheel	1 MW	milisec	>80%	20 years	<ol style="list-style-type: none"> <li>1. Power quality (low speed)</li> <li>2. Traction and aerospace (high speed)</li> <li>3. Short time periods (mainly in seconds minutes)</li> <li>4. High energy and power application</li> </ol>	(Faraji et al., 2017)
Thermal	Thermal Energy System (TES)	Up to GW	sec to min	80-100%	N/A	<ol style="list-style-type: none"> <li>1. Thermal building processes,</li> <li>2. Solar tower power plants</li> </ol>	(Alva, Lin & Fang, 2018, Huili Zhang, Baeyens, Caceres, Degreve, & Lv, 2016)
Electrical	Supercapacitor	Limited to 150kW	sec to min	>90%	>500,000 cycles	<ol style="list-style-type: none"> <li>1. Remote area where battery maintenance is impractical</li> <li>2. Short backup application</li> <li>3. Peak load shaving</li> </ol>	(Najib & Erdem, 2019; W. Raza et al., 2018)
	Superconducting magnetic energy storage (SMES)	1MW	milisec	95%	20 years	<ol style="list-style-type: none"> <li>1. large systems are used in particle detector for nuclear fusion and high-energy physics experiments</li> <li>2. Small system are used for power quality control</li> </ol>	(Mukherjee & Rao, 2019)

Table 2.1 Continued

Types	Capacity	Response time	Efficiency	Life Span	Application	References	
Electrochemical	Lead acid	10MW	min	85%	15 years	1. Automotive application 2. UPS	(May, Davidson, & Monahov, 2018)
	Lithium battery	15-50MW	min	85-95%	2-20 years	1.Ramping 2.Frequency regulation 3.Capacity resource 4.Spinning reserve 5. Energy reserve 6. Portable devices 7. Automotive	(Killer, Farrokhsersht, & Paterakis, 2020; Pellow, Ambrose, Mulvaney, Betita, & Shaw, 2020)
	Fuel cell	>1MW	min	40-70%	3-20 years	1. Rural and remote areas 2. combined heat and power system 3. UPS 4. Automotive	(Killer et al., 2020)
	Redox Flow Battery	>10MW	min	60-88%	>20 years	1. Load levelling 2. Peak shaving 3. Voltage sag compensation 4. Emergency power supply	(Killer et al., 2020)

اونیورسیتی ملیسیا قهق

UNIVERSITI MALAYSIA PAHANG

For fuel powered mobility, lead acid batteries with the advantages of simple yet mature manufacturing processes and low self-discharge, but lead acid batteries have low life span, low energy densities and toxicity materials that are not suitable to be applied as a stationary application. From the review, the fuel cell is also being considered as one of the potential solutions for stationary application that it is environmentally friendly with zero carbon emissions and quick start-up capabilities compared to fossil fuel based ESS (Song et al., 2019). With the benefits of non-exhausted and circulated electrolyte, RFB is more cost effective than fuel cell. The external electrolyte tank with unlimited fuel is another key difference in RFB that offered a longer life cycle (Perry & Weber, 2016). Furthermore, fuel cell suffers from several drawbacks such as expensive catalyst, high manufacturing costs and expensive hydrogen fuel.

Among electrochemical ESS, RFB represents a promising solution for a large energy storage system. Unlike the dependent capacity of lithium-ion battery, energy, and power capacity of RFBs are independently scalable. In comparison, fuel cell and RFB share similar configuration except for the fuel. For fuel cell, hydrogen fuel is converted to electrical energy. Meanwhile, the electrolyte is pumped and circulated from external tank to internal for charging and discharging operation for RFB. The flow feature enables better thermal cycling in RFB. In contrast to other ESS, RFB has lower efficiency range, the identified major key factors for designing RFB efficiency are conversion loss and pumping power loss. To optimize the efficiency for RFB, appropriate research extension in control the flow rate of the electrolyte and enhance the cell stack design.

From the review, it has been found that RFB is one of the promising solutions for medium which can be extended to large energy storage. Arguably, the most important advantage for RFB is the flexibility towards power and energy, these attributes make it can be further customise as large capacity storage for stationary application. Compared to other available electrochemical energy storages, RFB serves longer life time for more than 20 years because the electrical energy stored in aqueous electrolyte and did not undergo phase transitions that lead to irreversible losses (Derr, 2017). Types of available redox flow battery based the material selection, namely, metal based and organic based, the findings for each type are discussed in the next sections.



## 2.4 Redox Flow Battery Development

The historical of RFBs invention was firstly applied by French scientist Charles Renard and Arthur Krebs to power up the army airship “La France” in year of 1884 (Z. Yang et al., 2011). In early 50s, German scientist Walter Kangro presented a concept patent on storing electron in terms of chromium, chloride, iron, and titanium redox couples.

The earliest work on RFB was by Thaller from NASA (Thaller, 1976) developed Fe/Cr based RFB system in the early 1970s. Fe/Cr RFB research was then continued and built in big scale prototype by Japanese companies such as Mitsui Engineering, Kansai Electric Power Co. Inc. and Sumitomo Electric Industries Ltd in the year of 1980s (Shigematsu & others, 2011). In the same period, Posner has published the finding in  $\text{Sn}^{2+}/\text{Sn}^{4+}$  in combination of  $\text{Br}^-/\text{Br}^2$  or  $\text{Fe}^{2+}/\text{Fe}^{3+}$  RFBs (Soloveichik, 2015). Since then, a diverse range of metal ions such as zinc, copper, etc with combination of different has been reported.

During the 1980s, the research has shifted towards zinc bromine, which most of the multi-national companies Exxon, Johnson Control Inc. (USA), Toyota motor (Japan), Meidensha (Japan), Sherwood Industries (Australia) and ZBB Energy (USA) are involved. The success of Zn/Br installation in several countries including Japan, Australia and US has been reported and most of the systems are currently operating by ZBB Energy, REDflow Ltd. and Primus Power (Bender, Byrne, & Borneo, 2015). Nevertheless, zinc-based, and iron-based system suffered from massive electrolyte crossover and contamination in a long cycling period.

The investigation employed the same electrolytes (iron based) to overcome electrolyte crossover issue is first reported by L.W. Hruska and R. Savinell in 1981 (Hruska & Savinell, 1981). Anyhow, this system suffers from the uneven passivation of iron metal that required the addition of additive and pH control to the plating problem. A similar effort was made by Kazakos et al. with the introduction of vanadium to both sides of RFB in the year of 1985 with aims to solve the cross-contamination problem faced by most of the conventional RFBs (Maria Skyllas-Kazacos, Kazacos, & Mousa, 2003).

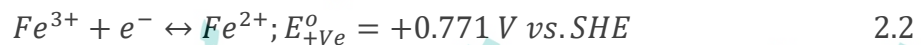
Over the past 40 years, various redox couples, such as iron chromium, zinc bromide, all vanadium and all iron have been investigated and demonstrated in prototypes

and even commercial scales. Early investigations on electrolytes for RFB are limited to inorganic material, especially metal-based redox couples (i.e., vanadium (Maria Skyllas-Kazacos, 2004), zinc (Lim, Lackner, & Knechtli, 1977) and iron (Savinell & Wainright, 2012; Selverston, Savinell, & Wainright, 2017; Zeng, Zhou, An, Wei, & Zhao, 2016)). After almost 40 years of research and development, vanadium RFBs have been widely adopted in Japan, Thailand, China, Austria, Canada, USA, Australia, South Africa and Germany in stationary application (Bender et al., 2015; Craig, Ron, Taylor, & Bret, 2014).

#### 2.4.1 Iron Chromium

In the early stage, iron ( $Fe^{2+}/Fe^{3+}$ ) chromium ( $Cr^{2+}/Cr^{3+}$ ) in hydrochloric acid is used as positive and negative reactants with reported energy density of only  $15 \text{ Wh kg}^{-1}$  (Thaller, 1976). With a standard electrode potential ( $E^0$ ) of  $0.771 \text{ V}$  versus the standard hydrogen electrode (SHE) of the ferrous/ferric ( $Fe^{2+}/Fe^{3+}$ ), and the reversible reaction at the negative electrode involves the kinetics of the chromous/chromic ( $Cr^{2+}/Cr^{3+}$ ) has a standard potential of  $-0.407 \text{ V}$  versus SHE. Open circuit voltage of the system ranges from  $0.90$  to  $1.20 \text{ V}$  depending on the state of charge (Q. Huang & Wang, 2015). The reactions are as follows:

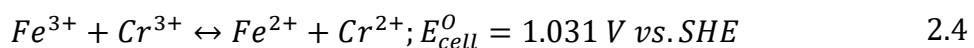
Positive electrode:



Negative electrode:



Overall reaction:



One of the main problems is a slow reduction of chromium on negative side, which is associated with hydrogen evolution reaction (P. K. Leung, 2011). To encounter

this issue, the introduction of electrocatalyst (Bi (Gahn & Hagedorn, 1985), Au-Ti (Heinzel, 1989) and etc.(J. Giner & Cahill, 1980; J. D. Giner, Cahill, & others, 1980; Jalan, Reid, & Charleston, 1984)) that has a higher hydrogen potential must enhance the electrochemical kinetics activity of  $\text{Cr}^{2+}/\text{Cr}^{3+}$  redox reaction and hindered the formation of hydrogen and chromium complexes.

Moreover, other solutions such as hydrogen rebalance cell that manages hydrogen formation and state of charge of both electrodes were installed. Studies showed that the efficiency of Fe/Cr RFBs reported to decrease over a long cycling period owing to high crossover of positive and negative ions by fouling mechanism of membranes (Assink, 1984). The membrane is permeable towards charge-carrier ion, Fe and Cr ion caused the ion or electron migrated and diffused between electrode compartment, whereas it failed to achieve equilibrium (Assink, 1984; Zeng, Zhao, An, Zhou, & Wei, 2015). Nonetheless, iron chromium RFB suffered from slow Cr ion reaction and cell degradation due to cross contamination.

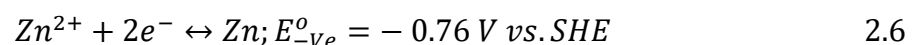
#### 2.4.2 Zinc Bromide

Zinc bromide RFB has intrinsic advantages for its rich and low-priced reactant with high energy density ( $70 \text{ W h kg}^{-1}$ ) over other metal types of RFB. At discharging mode, the zinc ion is reduced into zinc metal while the bromide ion is oxidized to bromine during charging (H. S. Yang, Park, Ra, Jin, & Yang, 2016). The electrolyte is zinc bromide water solution and quaternary ammonium salt. The zinc/bromine redox flow battery received much interest because of its good energy density, high cell voltage, high degree of reversibility, abundant and low-cost.

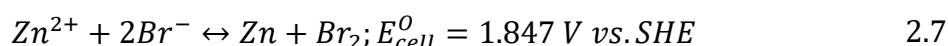
Positive electrode:



Negative electrode:



Overall reaction:



Nevertheless, problems with Zn/Br<sup>2</sup> battery including expensive electrode, material corrosion, dendrite formation during zinc deposition on charge, bromine gas production, low current densities, high self-charge rates and Zn/Zn<sup>2+</sup> couple react faster than bromine/bromide couple. The coulombic efficiency dropped (86.8% to 29.7%) after the zinc dendrite grow leading to self-discharge (H. S. Yang et al., 2016). Furthermore, acidic bromine is corrosive towards most metals that it will degrade carbon or polymer electrodes and cause crossover that leads to a deficiency of battery.

In the meantime, bromine gas is toxicity towards health and environment. Extra cost is needed to handle the leakage or by product from chemical reaction between zinc and bromine. Several challenges have been reported such as electrode corrosion, mossy morphology formation under low acidic condition, dendrite formation during frequent mid-range charge/discharge cycle, short life cycle and high operation and maintenance (O&M) cost (Khor et al., 2018; B. Li & Liu, 2017).

اونيورسيتي ملايسيا قهغ

UNIVERSITI MALAYSIA PAHANG

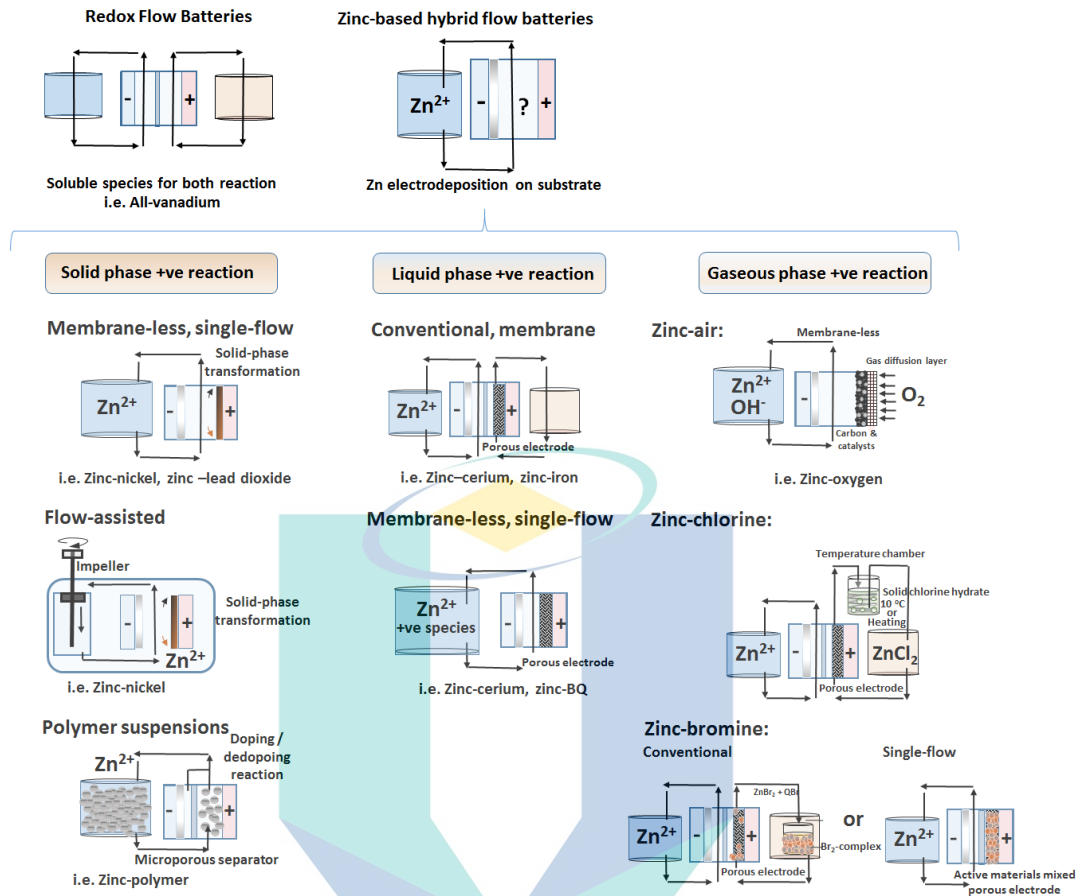


Figure 2.11 Review of the zinc-based hybrid flow battery in solid phase, liquid phase and gaseous phase positive reaction configuration.

Source: Khor et al., (2018)

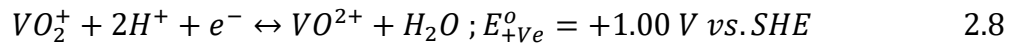
### 2.4.3 All Vanadium

By employing a similar redox couple in different states of oxidation that are  $\text{VO}^{2+}/\text{VO}^{2+}$  and  $\text{V}^{3+}/\text{V}^{2+}$  as catholyte and anolyte in sulphuric acid, the main issue for conventional RFB, cross contamination between the two compartments can be prevented (M Skyllas-Kazacos, Chakrabarti, Hajimolana, Mjalli, & Saleem, 2011; Maria Skyllas-Kazacos, Kazacos, Poon, & Verseema, 2010; Maria Skyllas-Kazacos, Rychick, & Robins, 1988; Maria Skyllas-Kazacos, 2004). This feature making it is the most significant and developed RFBs with 1.6 V with an energy density  $40 \text{ Wh L}^{-1}$  and a specific energy of  $25 \text{ Wh kg}^{-1}$  using a chloride supporting electrolyte (Q. Huang & Wang, 2015).

At positive electrode, V (IV)/ V (V) redox couple tends to generate  $\text{VO}^{2+}$  during charging and discharging processes. Conversely, at the negative side, vanadium (II) ion

and vanadium (III) ion were produced during the redox process. The reactions of vanadium are shown as follows (Maria Skyllas-Kazacos et al., 1988):

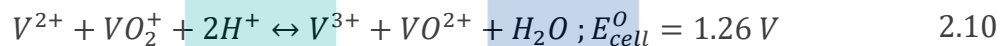
Positive electrode:



Negative electrode:



Overall reaction:



Vanadium based system exhibit good kinetics transfer and performance, but issues are reported that related to membrane, electrolyte, and electrode. The implementation suffers from the economic impact affected by the high cost of vanadium, high and variable price vanadium (approximate of \$40 per kg) with the safety and toxic issue limited their widespread deployment for wide scale commercialisation (Al-Yasiri & Park, 2018; Ito et al., 2011; P. K. Leung, 2011; M. Mohamed, Leung, & Sulaiman, 2015; Zeng, Zhao, Zhou, Zeng, et al., 2016). One of the main issues is related to the high capital cost associate to three listed components. 53% of total cost \$ 229 K Wh<sup>-1</sup> accounted for high electrolyte cost ,whereas membrane consume 19% of the total cost (Zeng et al., 2015).

However, vanadium redox flow battery (VRFB) suffers from low energy density due to the low solubility of vanadium (0.26M vanadium in 9M H<sub>2</sub>SO<sub>4</sub>). The solubility and concentration of vanadium in base acid defined/determined the energy density of the system. Necessary to highlight that the solubility, the cost of vanadium and narrow temperature operating remain challenging to expand for massive production (Liu, Sleightholme, Shinkle, Li, & Thompson, 2009). Energy density is limited to the precipitates of vanadium, which is mainly caused by the solubility of vanadium. This

problem is tackled by introducing additive such as mixed acids such as sulphate chloride (up to 2.5 M). Instead of improving the solubility, mixed sulphuric acid and hydrochloric has provided a broader temperature for VRFB operation ranging from -5 to 50°C.

#### 2.4.4 All Iron

All iron chemistry utilise a single element in oxidation and reduction states for both anode and cathode, similar to vanadium (Hawthorne, 2014; Petek, 2015). The cost of iron is lower than vanadium, low chemical toxicity and abundantly available. The positive reaction is electrochemical oxidation of ferrous ions ( $Fe^{2+}$ ) to ferric ions ( $Fe^{3+}$ ) whereas the negative reaction reduction of ferrous ions to iron metal as described in equation 2.11 during charging (Savinell & Wainright, 2012). The net battery operation is demonstrated in equation 2.13 with standard voltage of 1.21 V.

Positive electrode:



Negative electrode:



Overall reaction:

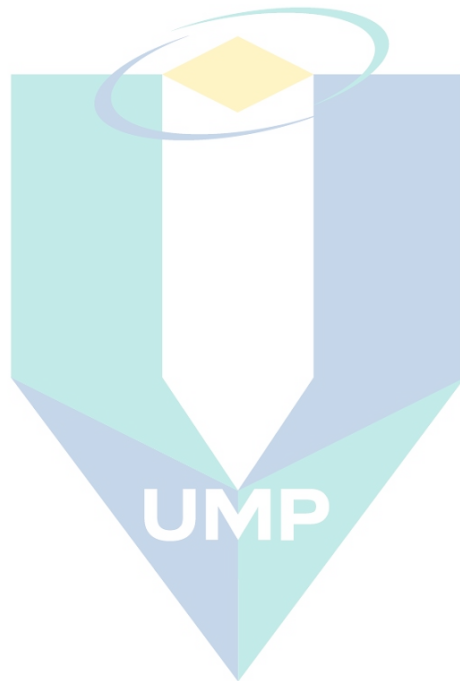


اونيور سیتی ملیسیا قهغ  
UNIVERSITI MALAYSIA PAHANG

It was found that the hydrogen evolution happens in negative electrode, pH needs to be maintained between 2 and 3 to avoid hydrogen evolution. The raise in pH will affect positive side causing precipitation of ferrous species and the corrosion of iron plate was also noted (Petek, 2015).

#### 2.4.5 Comparison among various redox flow battery technologies

This section introduces the characteristics for metal-based RFBs types of cell configuration, positive active species in either solid, liquid, or gaseous phase, operational performance for metal-based batteries. Electrode material and electrolyte composition for different type of RFB are also included and summarised in Table 2.2.



اونيورسيتي ملايسيا قهغ

UNIVERSITI MALAYSIA PAHANG



Table 2.2 Operational parameters and performance of redox flow batteries or flow-assisted batteries with positive active species in solid, liquid and gaseous phases.

Flow Battery Chemistries	Cell Configuration	Electrode Materials	Negative Electrolyte Compositions	Positive Electrolyte Compositions	Exp. OCV/V	% System Eff.	No. of Cycles	References
<b>Both Redox Couples involving Liquid Phase Active Materials</b>								
All Vanadium	Flow - through	Positive and negative electrode: carbon felt	1.6 M $V^{3+}/V^{4+}$ in 1 M $H_2SO_4$		1.5	Energy: 80 Coulombic: 98	>5	(Monteiro, Leirós, Boaventura, & Mendes, 2018; Maria Skyllas-Kazacos, 2004)
Iron-Cadmium	Flow-through	Positive and negative electrode: carbon paper	0.15M $CdSO_4$ +3M HCl	0.3M $FeCl_2$ + 3M HCl	1.05	Energy: 80 Coulombic: 98.7	Nil	(Zeng, Zhao, Zhou, Wei, & Jiang, 2016)
Iron-Vanadium	Flow through	Positive and negative electrode: pre-treat graphite-felt	1.5 M $FeCl_2$ +1.5 M $VOSO_4$ in 3 M HCl		0.5-1.35	Energy: 70 Coulombic 85	30	(B. Li et al., 2013)
Iron-Lead	Flow through	Positive: two-layer carbon cloth negative: pre-treat-carbon cloth + polyacrylonitrile felt	0.6 M $Fe(SO_3CH_3)_2$ + 0.3 M $Pb(SO_3CH_3)_2$ + 2.0 M $HSO_3CH_3$		0.97	Energy: 86.2 Coulombic: 96.2	26	(Zeng, Zhao, Zhou, Wei, & Ren, 2017)
<b>Positive Redox Couples involving Solid Phase Active Materials</b>								
Iron-Chromium	Flow field structure	Negative and positive: serpentine carbon plate Separator: Nafion® NR-212	Common electrolyte: 1.0 M $FeCl_2$ + 1.0 M $CrCl_3$ + 3.0M HCl + 0.005 M $Bi^{3+}$		1.25	Energy: ~ 85 Coulombic: ~96 (80 mA $cm^2$ )		(Zeng, Zhao, Zhou, Zeng, & Wei, 2016; Zeng, Zhou, et al., 2016)

Table 2.2 Continued

Flow Battery Chemistries	Cell Configuration	Electrode Materials	Negative Electrolyte Compositions	Positive Electrolyte Compositions	Exp. OCV/V	% System Eff.	No. of Cycles	References
<b>Positive Redox Couples involving Solid Phase Active Materials</b>								
Zinc-nickel	Single flow, membraneless	Negative: cadmium plated nickel foil Positive: sintered nickel hydroxide	Common electrolyte: 1M ZnO in 10 M KOH		1.6	Energy: 86 Coulombic: 96 (20 mA cm <sup>2</sup> )	1000	(Cheng et al., 2007)
	Flow-assisted, membraneless	Negative: zinc deposited copper plate Positive: sintered nickel oxide	Common electrolyte: ZnO in wt. 45 % KOH		1.5	Energy: > 80 Coulombic: >90 (> 10 mA cm <sup>2</sup> )	1500	(Ito et al., 2011)
Zinc-lead-dioxide	Single-flow, membraneless (static but flow available)	Negative: carbon polymer Positive: lead-sulphate paste	Common electrolyte: 1.5 M ZnSO <sub>4</sub> + 0.5 M Na <sub>2</sub> SO <sub>4</sub> + 0.5 M H <sub>2</sub> SO <sub>4</sub>		2.4	Energy: > 65 Coulombic: > 80 (20 mA cm <sup>2</sup> using static cell)	90	(P. K. Leung, Xu, & Zhao, 2012)
Zinc-polymer	Single-flow, separator	Negative: zinc plate Positive: carbon plate Separator: microporous membrane	Common electrolyte: PANI particles + 2.0 M ZnCl <sub>2</sub> + 2.0 M NH <sub>4</sub> Cl		1.1	Coulombic: 97 (20 mA cm <sup>2</sup> )	32	(Y. Zhao, Si, & Liao, 2013)

اونيور سيني مليسيا قهغ

UNIVERSITI MALAYSIA PAHANG

Table 2.2 Continued

Flow Battery Chemistries	Cell Configuration	Electrode Materials	Negative Electrolyte Compositions	Positive Electrolyte Compositions	Exp. OCV/V	% System Eff.	No. of Cycles	References
<b>Positive Redox Couples involving Liquid Phase Active Materials</b>								
Zinc-iron	Divided, membrane (alkaline)	Negative: silver plated iron Positive: porous nickel Separator: Nafion® XR 475	ZnO at 5M NaOH	K <sub>4</sub> Fe (CN) <sub>6</sub> at 5M NaOH	1.8	Energy: 73 Coulombic: 98 (mA cm <sup>2</sup> )	222	(Adam, 1979)
	Divided, membrane	Negative: carbon plate Positive: carbon felt Separator: Daramic® 175	1.1 M ZnCl <sub>2</sub> + 0.8 M FeCl <sub>2</sub> + 2 M NH <sub>4</sub> Cl + 2 g L <sup>-1</sup> PEG <sub>8000</sub>	1.6 M ZnCl <sub>2</sub> + 0.6 M FeCl <sub>2</sub> + 0.2 M FeCl <sub>3</sub> + 2 M NH <sub>4</sub> Cl + 2 g L <sup>-1</sup> PEG <sub>8000</sub>	1.5	Energy: 70 Coulombic: >60 (25 mA cm <sup>2</sup> )	127	(Selverston et al., 2017)
	Divided, double membranes	Negative: copper mesh Positive: carbon felt Separator: Nafion® 212/211; Fumatech FAA-3	0.5 M Na <sub>2</sub> [Zn(OH) <sub>4</sub> ]	1M FeCl <sub>2</sub> + 1 M HCl	2.0	Energy: 74 Coulombic: 99 (40 mA cm <sup>2</sup> )	>20	(Gong et al., 2015)
Zinc-cerium	Divided, membrane	Negative: carbon polymer plate Positive: platinized titanium mesh stack / carbon felt Separator: Nafon® 117	1.5 M Zn (CH <sub>3</sub> SO <sub>3</sub> ) <sub>2</sub> + 1.0 M CH <sub>3</sub> SO <sub>3</sub> H	0.8 M Ce (CH <sub>3</sub> SO <sub>3</sub> ) <sub>3</sub> + 4.0 M CH <sub>3</sub> SO <sub>3</sub> H	2.3	Energy: 46 Coulombic: 84 (50 mA cm <sup>2</sup> )	57	(P. K. Leung, Ponce de leon, Low, & Walsh, 2011)
	Single flow, membraneless	Negative: planar carbon polymer Positive: carbon felt	Common electrolyte: 1.5 M Zn (CH <sub>3</sub> SO <sub>3</sub> ) <sub>2</sub> + 0.2 M Ce (CH <sub>3</sub> SO <sub>3</sub> ) <sub>3</sub> + 0.5 M CH <sub>3</sub> SO <sub>3</sub> H		2.3	Energy: 76 Coulombic: 90 (20 mA cm <sup>2</sup> )	10	(P. K. Leung, Ponce de Leon, & Walsh, 2012)

Table 2.2 Continued

Flow Battery Chemistries	Cell Configuration	Electrode Materials	Negative Electrolyte Compositions	Positive Electrolyte Compositions	Exp. OCV/V	% System Eff.	No. of Cycles	References
<b>Positive Redox Couples involving Liquid Phase Active Materials</b>								
Zinc-iodine	Divided, membrane	Negative: carbon felt Positive: carbon felt Separator: Nafon® 115	Common electrolyte: 5.0 M ZnI <sub>2</sub>		1.2 – 1.4	Energy: 67 Coulombic: 96 (20 mA cm <sup>2</sup> )	40	(B. Li et al., 2015)
Zinc-polymeric TEMPO	Divided, Membrane	Negative: zinc or carbon plate Positive: carbon felt Separator: size exclusion dialysis membrane	1.0 M ZnCl <sub>2</sub> , 1.0 M NH <sub>4</sub> Cl	Polymeric TEMPO in 1.0 M ZnCl <sub>2</sub> , 1.0 M NH <sub>4</sub> Cl	1.7	Energy: 80 Coulombic: > 90 (20 mA cm <sup>2</sup> )	500	(Winsberg et al., 2016)
Zinc-TEMPO	Divided, membrane	Negative: zinc foil Positive: carbon felts Separator: Nafon® 212	1 M ZnAc + 2 M NaCl + Na <sub>2</sub> SO <sub>4</sub>	1M hydroxyl- TEMPO + 2.0 M NaCl + Na <sub>2</sub> SO <sub>4</sub>	1.7	Energy: 74.0 Coulombic: 88 (10 mA cm <sup>2</sup> )	50	(Orita, Verde, Sakai, & Meng, 2016)
Zinc-benzoquinone	Single flow, membraneless	Negative: planar carbon Positive: carbon felt	Common electrolyte: 1 M ZnCl <sub>2</sub> + 50mM 1,2-BQDS		1.5	Energy :73 Coulombic: 74 (30 mA cm <sup>2</sup> )	12	(P. K. Leung et al., 2017; PK Leung, Martin, Shah, Anderson, & Palma, 2016)

اونيورسيتي ملايسيا قهق

UNIVERSITI MALAYSIA PAHANG

Table 2.2 Continued

Flow Battery Chemistries	Cell Configuration	Electrode Materials	Negative Electrolyte Compositions	Positive Electrolyte Compositions	Exp. OCV/V	% System Eff.	No. of Cycles	References
<b>Positive Redox Couples involving Gaseous Phase Active Materials</b>								
Zinc-air	Single flow, membraneless	Negative: zinc plated copper plate Positive: oxygen composite electrode: Ni(OH) <sub>2</sub> +EMD+NaBiO <sub>3</sub>	Common electrolyte: 0.7M K <sub>2</sub> [Zn(OH) <sub>4</sub> ] + 7M KOH+ 0.7 M LiOH		> 1.6	Energy: 72 Coulombic: 97 (20 mA cm <sup>2</sup> )	150	(Pan et al., 2009)
Vanadium-Air	Nil	Negative: serpentine carbon plate Positive: Sintered Ti Separator: Nafion® 117	2 M V <sup>2+</sup> /V <sup>3+</sup> in 3M H <sub>2</sub> SO <sub>4</sub>	H <sub>2</sub> O/O <sub>2</sub>	1.56	Energy: 45.7	Nil	(Hosseiny, Saakes, & Wessling, 2011)
Zinc-bromine	Divided, membrane	Negative: carbon-based electrode Positive: carbon-based electrode Separator: Nafon® 125 or Celgard 3400	Common electrolyte: 2M ZnBr <sub>2</sub> + KCl + NaCl		>1.5	Energy: > 80 Coulombic: 95 (20 mA cm <sup>2</sup> )	6	(Lim et al., 1977)
	Single flow, membrane	Negative: carbon polymer electrode Positive: carbon felt mixed with active materials and complexing agent Separator: Nafon® 115	Common electrolyte: 2.0 M ZnBr <sub>2</sub>		>1.7	Energy: 82 Coulombic: 92 (20 mA cm <sup>2</sup> )	70	(Lai, Zhang, Li, Zhang, & Cheng, 2013)
Zinc-chlorine	Single flow, membraneless	Negative: carbon plate Positive: porous graphite electrode	Common electrolyte: 2.0 M ZnCl <sub>2</sub> + 4.0 M KCl		c.a. 2.0	Energy: 66 Coulombic: 84 (22 mA cm <sup>2</sup> )	Nil	(Jorné, Kim, & Kralik, 1979)

## 2.5 Research Progress in Quinone Based Electrolyte

Since most considered vanadium electrolyte faced problems on the electrolyte issue in terms of cost and narrow operational temperature range behind the working principle of RFB, replacement of suitable organic electrolyte seems to be a fair solution. Organic active materials with abundant resources, low cost, and availability of modification space (Brushett, Vaughey, & Jansen, 2012; Wedege, Drazevic, Konya, & Bontien, 2016). Furthermore, molecular engineering on carbonyl organic delivers good opportunities for tunability through functional group modification to lower or increase the reduction and oxidation potential for RFB application. A lot of design aspect need to be considered for high density organic RFB that are multiple electrons, concentration, cell voltage, material cost and stability as listed in Figure 2.12. The relationship of multiple electrons in energy density and standard electrode potential is discussed under equation 2.14 and 2.15.

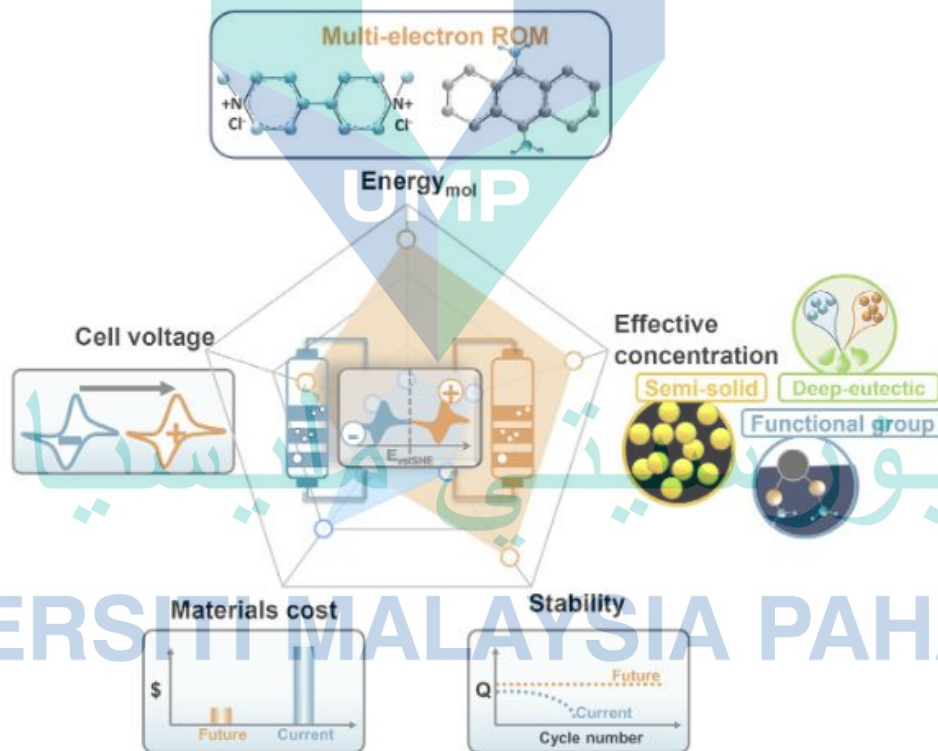


Figure 2.12 Design consideration for organic based RFB.

Source: Li et al., (2018)

Chemistry for selected electroactive species for RFB application reversible, where this reaction can be explained by the Nernst equation. Noted that, before conducting the investigation, the theoretical background must be electrochemically balance for redox to occur and achieve equilibrium. Nernst equation in 2.14 where  $E^0$  represent the standard electrode potential for selected electroactive species,  $C_{Ox}^*$  and  $C_{Re}^*$  are bulk concentration for selected electroactive species (Ox represent oxidised and Re represent reduced).

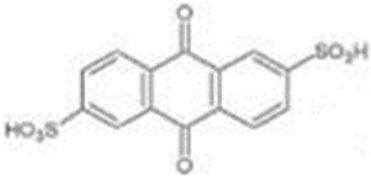
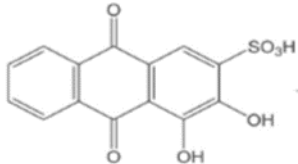
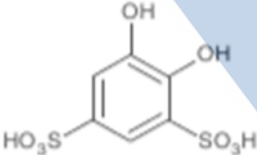
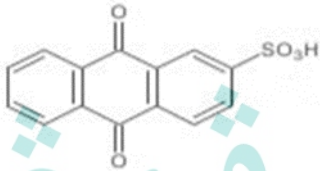
$$E = E^0 + \frac{RT}{nF} \ln \frac{C_{Ox}^*}{C_{Re}^*} \quad 2.14$$

Nernst equation is applicable at all range of temperature. Commonly, the Nernst equation is written under standard conditions in which temperature = 25 °C (298 K), pressure = 1 atm, R is defined as the ideal gas constant (8.314 J mol<sup>-k</sup>) and F is the Faraday's constant (95484.56 C mol<sup>-1</sup>) is predefined. Higher cell voltage can be obtained by pairing the highest electronegative with electropositive material to yield larger potential for the system. According to the equation given in equation 2.15, energy density can be increased by the number of electrons, n. The relationship between the energy density of RFB with organic redox active species concentration can be further defined by the equation below, where n is the number of electrons involved in the redox process, F is the Faraday constant,  $V_{ocv}$  is the open circuit voltage, C is the redox active species concentration. For example, reducing anthraquinone based organic material.

$$\text{Energy density} = \frac{1}{2} n F V_{ocv} C \quad 2.15$$

UNIVERSITI MALAYSIA PAHANG

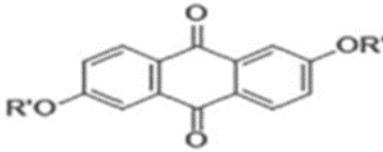
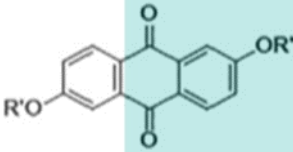
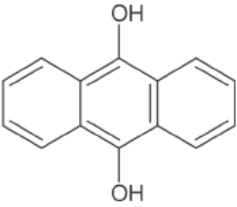
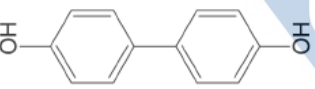
Table 2.3 Summary of existing organic couples with respect to the current density, open circuit voltage and no of charge-discharge cycles

Negolyte	Posolyte	Current Density, A cm <sup>-2</sup>	OCV, V	No of Cycles	Ref
	HBr	0.5	1.5	>15	(Huskinson et al., 2015, 2014)
		0.3	0.7-0.9	100	(B. Yang et al., 2016)
		0.06	0.83	3	(S. Zhang et al., 2016)
		0.01	1.23	>10	(B. Yang, Hooper-Burkhardt, Wang, Prakash, & Narayanan, 2014)

اوتیورسیٹی ملیسیا قہق



Table 2.3 Continued

Negolyte	Posolyte	Current Density, A cm <sup>-2</sup>	OCV, V	No of Cycles	Ref
 <p>2,6-DBEAQ (Alkaline)</p>	 <p>2,6-DBEAQ (Alkaline)</p>	0.002	1.05	>20	(Kwabi et al., 2018)
 <p>0.5 mol dm<sup>-3</sup> 2,7 AQDS</p>	 <p>1.0 mol dm<sup>-3</sup> VOSO<sub>4</sub></p>	0.04	>1.2	>100	(Lantz, Shavaliar, Schroeder, & Rasmussen, 2019)
		0.12	0.9	200	(W. Lee, Park, Kim, Chang, & Kwon, 2020)

اونيور سيئي ملايسيا قهغ

Most of the research focused on the exploration of the potential of quinone derivative electroactive material (i.e. anthraquinone, hydroquinone and benzoquinone) as electrolyte candidates for organic RFB (Bachman, Curtiss, & Assary, 2014; Er, Suh, Marshak, & Aspuru-Guzik, 2015). Quinone has presented viable potential for the application of RFB, with stable and electronics structure is observed to capable of having reversible two-electron reduction and two-proton oxidation devoted to acidic conditions, which leads to an increase in energy densities (Guin, Das, & Mandal, 2011). The two-step electron transfer of quinone is where semiquinone is formed in the first step, then further reduced to quinone dianion generating two electrons, which the process is quasi-reversible during charging and discharging processes. A wide variety of electrolyte employed in quinone based RFB research and development are reviewed in the following section.

### 2.5.1 Positive Electrolyte

Alternatively, various of potential organic materials (composed of natural elements e.g. as C, O, N, H and S) such as nitronyl, quinoxaline (Milshtein, Su, Liou, Badel, & Brushett, 2015), alloxazine (Lin et al., 2016), quinone (Hofmann et al., 2018; Pineda Flores, Martin-Noble, Phillips, & Schrier, 2015) has been investigated as positive charge storing materials for RFB. The early development to incorporate quinone in RFB application was initiated as early as 2009, quinone redox active material benzoquinone has been used as positive electrode pairing with lead/lead sulphate (Xu et al. 2009). The study reported a coulombic efficiency of 99% after 50 cycles were obtained.

As reported in Figure 2.13, large window between oxidation and reduction potential quinone (i.e., difference between 9,10-anthraquinone and 1,2-benzoquinone-3,5-disulfonic acid approximately 1 V) displayed a possibility to be implement as redox couples for ORFB. From the previous studies (Xu, Wen, Cheng, Cao, & Yang, 2012; B. Yang, Hooper-Burkhardt, Wang, Prakash, & Narayanan, 2014), benzoquinone has been selected as the most suitable polysolite due to the highest electrode potential (0.85 V) for ORFB (Isikli, 2013).

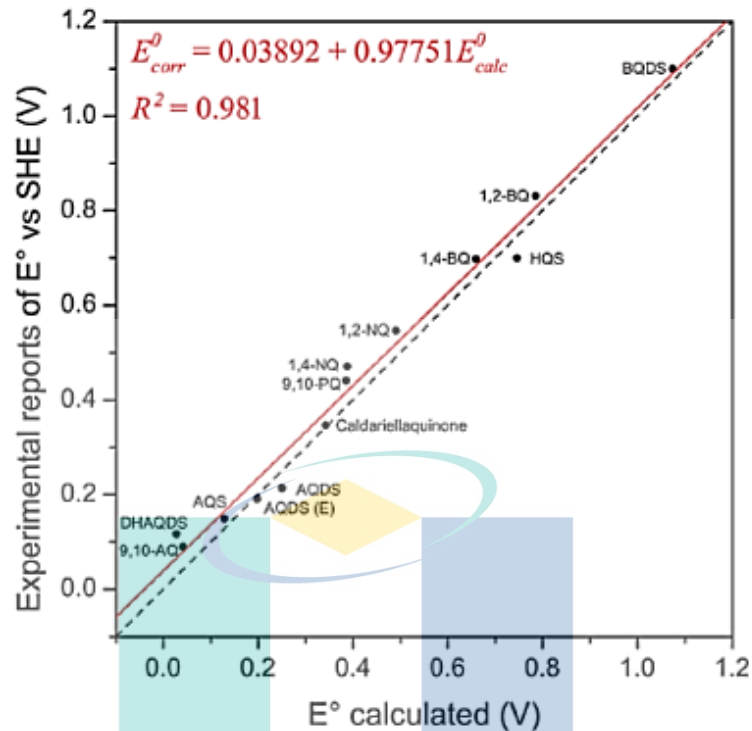


Figure 2.13 Half-cell reduction potential versus SHE for benzoquinones (BQ), naphthoquinones (NQ), anthraquinone (AQ), phenanthraquinones (PQ) in red (calculated) dotted line (experimental).

Source: Pineda Flores et al., (2015)

Huskinson's study on quinone based RFB utilised 2, 7 anthraquinone (2, 7-AQDS) pairing with  $Br^2/Br^-$  redox couple demonstrated a cell voltage of 0.858 V with good and recyclability up to 100th as presented in Figure 2.14 (Huskinson et al., 2014). This study yielded a peak galvanic power density of  $0.6 \text{ W cm}^{-2}$  at a current density of  $1.3 \text{ A cm}^{-2}$  as AQDS experienced two electrons with no catalyst required.

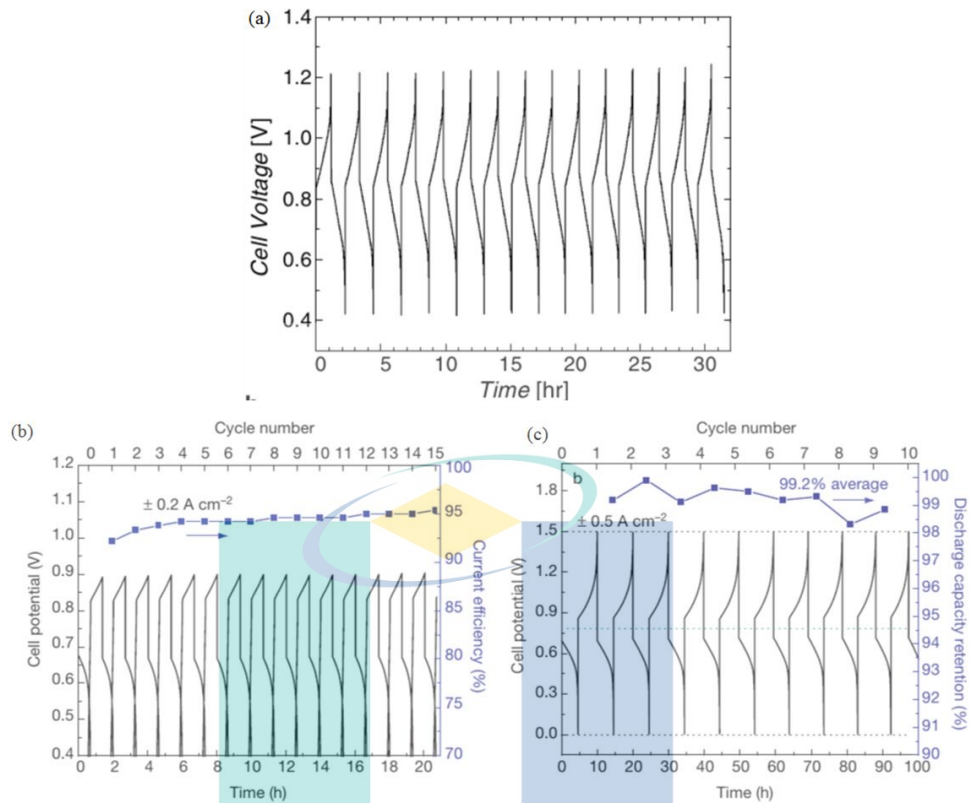


Figure 2.14 Charge-discharge profile (a) 1 M AQS + 2 M H<sub>2</sub>SO<sub>4</sub> / 3 M HBr + 0.5 M Br<sub>2</sub> + 2 M H<sub>2</sub>SO<sub>4</sub> under 0.25 A cm<sup>-2</sup> (b) 2 M HBr + 0.5 M Br<sub>2</sub>/0.1 M AQDS + 2 M H<sub>2</sub>SO<sub>4</sub> under 0.2 A cm<sup>-2</sup> (c) 3 M HBr + 0.5 M Br<sub>2</sub>/1 M AQDS + 1 M H<sub>2</sub>SO<sub>4</sub> under 0.5 A cm<sup>-2</sup>.

Source: (a) Gerhardt, Tong, Chen, Gordon, & Aziz, (2016) (b and c) Huskinson et al., (2014)

To avoid the utilization of bromine gas, another positive electrolyte investigation work by Nawar et al. introduced 1,4-benzoquinone (BQDS) pairing hydroquinone with exhibits the cell able to operate under the current density >500mA (Nawar, Huskinson, & Aziz, 2013). Another bromine-free quinone based studies demonstrated by Yang *et al.* replaced Br<sub>2</sub> with 0.2 mol dm<sup>-3</sup> 1,2-benzoquinone-3,5-disulfonic acid (BQDS) as the catholyte pairing with anthraquinone-2-sulfonic acid (AQS) or anthraquinones-2, 6-disulfonic acid (AQDS) at negative electrode reported a higher open circuit voltage of 1.23V (Yang et al., 2014). Permatasari *et al.* presented studies employed 4,5-dihydroxybenzene-1,3-disulfonic acid pairing with 2,7-AQDS, (Permatasari, Lee, & Kwon, 2020). Based on simulation and experimental investigation, 1,2 benzoquinone, 2,3 anthraquinone and 2,3 napthoquinone are among the electropositive materials that suitable as positive side for quinone based RFB (Er et al., 2015).

### 2.5.2 Negative Electrolyte

As a solution towards more environmentally friendly approach and cheaper energy cost with abundant resources and availability of modification space, quinone is considered a promising alternative to replace vanadium (Wedeg et al., 2016). Natural aromatic carbonyl such as naphthoquinone (NQ), benzoquinone (BQ) and anthraquinone (AQ). Anthraquinone is abundantly obtainable from the roots of plants (e.g., rubiaceae) by sulphonation and is water soluble. Anthraquinone is widely used in food producing industry as dyes, medical application as chemotherapeutic agents, laxatives, neurotherapeutic agent and manufacturing industry as a catalyst (K. Khan, Karodi, Siddiqui, Thube, & Rub, 2012; Son, Kim, Kim, & Park, 2016). Quinone with smaller molecular weight, the merit of low cost, excellent redox activity, scalability and biodegradable (P Leung et al., 2017; Winsberg, Hagemann, Janoschka, Hager, & Schubert, 2017).

The chemistry and biochemistry of quinone with advantageous of having infinite chemical space, allow broader design space available via molecular modification. With addition, the characteristics of the two electron transfer with a theoretical specific capacity of  $496 \text{ mAh g}^{-1}$  make quinone the promising organic active material for RFB (Ding, Zhang, Zhang, Zhou, & Yu, 2018; Huskinson et al., 2014; Son et al., 2016; Wedeg, Drazevic, Konya, & Bientien, 2016; B. Yang et al., 2016). For negative side, quinone candidates such as AQ, AQDS and AQS highly investigated in most of the literature (Likit-Anurak, Uthaichana, Punyawudho, & Khunatorn, 2017; Singh, Kim, Kang, & Byon, 2019). Compared with AQDS (0.222 V), AQS (0.187 V) and DHAQDS (0.120 V), ARS has the lowest electrode potential of 0.082 V making ARS a good candidate as negolyte for redox flow battery.

The least negative redox potential value among 9,10-anthraquinone (AQ) sequence arrangement were as follows: anthraquinone-2-sulfonic acid (AQS), 2,7-anthraquinone (AQDS), alizarin red S (ARS), 1,8-dihydroxyanthraquinone-2,7-disulfonic acid (DHAQDS) and 1,4-dihydroxyanthraquinone-2,3-dimethylsulfonic acid (DHAQDMS) are shown in Figure 2.15. 9, 10-anthraquinone (AQ) was derived from the oxidation of anthracene with two ketone group attach to ninth and tenth carbon in a three-ring structure. From Er *et al.* (2015) and Bachman *et al.* (2014) computation studies, 9,10 anthraquinone (AQ) was found suitable for the negative side, where the results displayed

2.05 eV in the first reduction and 1.61 eV in the second reduction. ARS is considered a potential molecule and shows good electrochemical behaviour at low concentration.

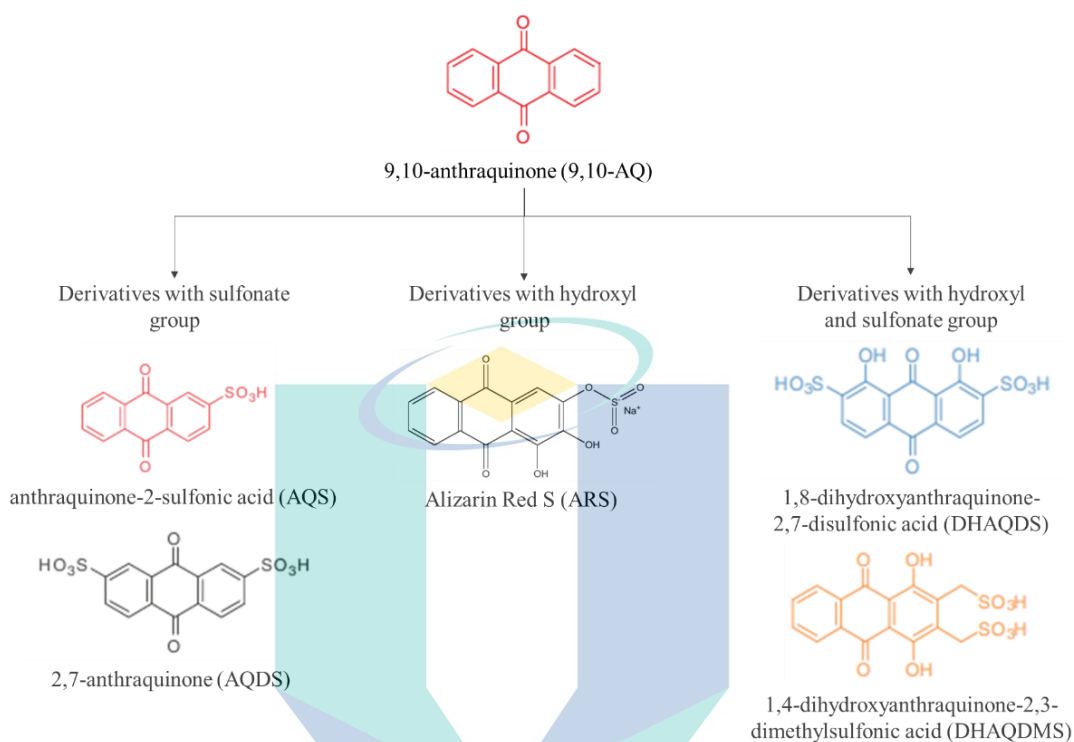


Figure 2.15 9,10-anthraquinone (AQ) with its derivatives with the functional group  
Source: Gerhardt et al., (2016)

The substituted AQ derivative DHAQDS is 90 mV lower than AQDS while DHAQDMS is the lowest with 0.02 V vs standard reduction potential compared to other derivatives. Nevertheless, DHAQDMS suffered from poor stability upon reduction (Gerhardt et al., 2016). As a result, the substitution of the functional group on the carbonyl materials can rational the chemical properties of the respective molecules. For example, additional of the hydroxyl group into AQDS can further optimize the reduction potential and solubility of AQDS leading to achieve higher cell potential and energy density (Huskinson et al., 2015). 1-, 4-, and 8-positions of 9,10-AQ are among the locations for hydroxyl substitution as it allows the AQ nucleus to form a hydrogen bond with semiquinone radical and quinone dianion to lower the reduction potential (Guin, Das, & Mandal, 2011).

The solubility and reduction potential of the AQDS derivative 1, 8-dihydroanthraquinone (1, 8-DHAQ) were compared, the reduction potential 0.08 V that

is lower than 2, 6-DHAQ (0.13 V) and theoretical solubility of 5 mol L<sup>-1</sup> (Chen et al., 2017). This exposed the possibility of modification for organic based electroactive material, one of the ways to lower the reduction potential of carbonyl compound is with the addition of the hydroxyl group potential. According to the reported literature, AQDS with higher solubility (>1 mol dm<sup>-3</sup>) and high volumetric (>50 W h I<sup>-1</sup>), gravimetric energy density (> 50 W h kg<sup>-1</sup>) and low electrode potential (0.222V vs the standard hydrogen electrode) make AQDS one of the prospective negolyte candidates for RFBs (Huskinson et al., 2014). AQDS expected to deliver a high potential, E<sup>0</sup> and increase of aqueous solubility (decrease in ΔG<sup>0</sup>) due to the existence of the electron-withdrawing group - two sulphonate groups (Er et al., 2015). From both numerical studies (Er et al., 2015; Wedege et al., 2016), these specified that the position of sulphonate group significantly influences the electrode potential of 9, 10-anthraquinone derivatives.

The difference between 2,7-anthraquinone (AQDS) and anthraquinone-2-sulfonic acid (AQS) is the number of the sulphonate groups attached to the 9,10-anthraquinone ring. As illustrated in Figure 2.15, AQDS with two sulphonate groups while AQS with the single sulphonate group. By grafting sulphonate group to 9,10-AQ produced mono-sulphated 9, 10-anthraquinone or anthraquinone-2-sulfonic acid (AQS), resulting the decrease in electrode potential of 0.163 V that is lower than AQDS (Q. Zhao, Zhu, & Chen, 2017). The position and existence of the sulphonate group in 9, 10-anthraquinone reduced the electrode potential of AQS. The electron potential for AQS is lower than 9,10-AQ indicating the sulphonate group acts as an electron donating group with a decrease in the electrode potential instead of the electron-withdrawing group. AQS is stable in bromine whereas ARS is unstable, higher OCV was obtained with an increase in peak galvanic compared to AQDS/Br RFB.

Despite choosing ADQS, Zhang et al. reported another quinone derivative as the negolyte. 3, 4-dihydroxy-9, 10-anthraquinone-2-sulfonic acid or in short named as alizarin red S (ARS) to be used as negative electrolyte (S. Zhang et al., 2016). On the other hand, alizarin red S is available as sodium salt of 1, 2-dihydroxyl-9, 10-anthraquinonesulfonic acid (refer to Figure 2.15) also referring as Mordant Red 3 is commonly used as a dye in textile industry (Adegun et al., 2016). Besides, the price for ARS is said to be low (USD \$6 per kilogram), which it can be extracted from cheap quinone and natural resources (e.g. plant) compared to vanadium (~USD \$40 per

kilogram). The standard electrode potential for ARS is 0.082 V (Gerhardt et al., 2016; S. Zhang et al., 2016) which is lower than (0.187 V) and 1,8-dihydroxyanthraquinone-2,7-disulfonic acid, DHAQDS (0.12 V) and AQDS (0.13 V). In which, lower electrode potential made ARS suitable to serve as the negative side of RFB.

The main difference between AQS and ARS is the existence of two-hydroxyl group in ARS, which is theoretically predicted to lower the electrode potential to 0.082 V (S. Zhang et al., 2016) that is the lowest among the AQS (0.163 V) and AQDS (0.222 V). Standard electrode potential for AQS is 0.082V which is also lower than AQDS (0.13V) and this made AQS suitable to serve as negative side of RFB, respectively, the cell reported a voltage of 0.826V with 99 % columbic efficiency was achieved with 0.05M concentration for both sides (B. Yang et al., 2014).

## 2.6 Electrode Material

Besides electrolyte, porous electrode is the critical component for redox reactions (i.e., mass and charge transfer) in flow battery. Carbonaceous material such as carbon felt has been chosen as the subject of investigation due to its capabilities of acid and alkaline resistance, good mechanical strength, good conductivity and low cost. Porous electrode felt with disadvantages relevant to the low wettability and electrochemical activity due to the hydrophobic surface and poor kinetic on redox reaction. Porosity, wettability, and permeability of electrode are three important to achieve high surface area of the electrode. Therefore, investigation of the properties of the electrode in the electrocatalytic activity, conductivity, hydrophilicity, and surface morphology play a critical role in improving the performance of ORFB (Smith, Davies, Baynes, & Nichols, 2015).

Ideally, a porous electrode that serves as the active site should be chemical inert against highly acidic solutions such as sulphuric acid. Besides, a porous electrode needs to be catalytic, less undesired by-product, low over potential, good electrical conductivity lower than  $1 \Omega \text{ cm}^{-2}$ , adequate lifetime, and moderate cost good mechanical strength to withstand the compression and pressure (D. Zhang, Liu, & Liu, 2014, M. Park, Ryu, Wang, & Cho, 2017). Commonly, polyacrylonitrile (PAN) carbon materials such as carbon felt and graphite felt are applied (T. Liu, Li, Zhang, & Chen, 2018). High  $\text{sp}^2$ -carbon content in PAN based felt greatly impact on the conductivity of carbon as the electrons are transferred along the delocalised  $\pi$ -orbitals (Melke et al., 2014).



The reaction involved in the electron transfer process happens comprised of three ways that are mitigation, diffusion and convection involving electrolyte-electrode interface, between electrolyte and bulk electrolyte as displayed in Figure 2.16. For the oxidation process, the electron movement known as mass transfer from the electrolyte to the surface of the electrode can be further defined in the equation of Fick's law and the Nernst equation.

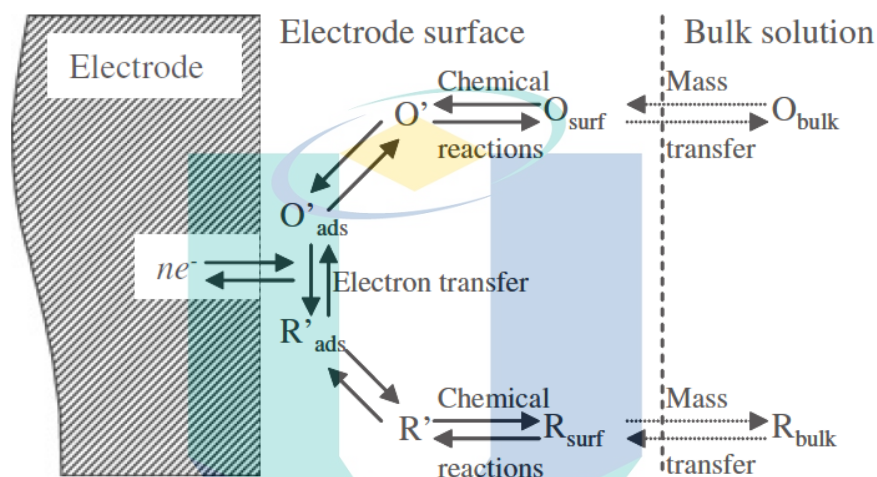


Figure 2.16 Process involved in the electrode reaction

Source: Zoski, (2006)

Nevertheless, based on most conducted literature, as far as authors are aware, research on organic related studies only focuses on the customisation of electrolyte but not on felt investigation. To improve the physicochemical properties of felt (i.e., increase active surface area and kinetic reversibility), the research on modifications with a single stage method has been proposed. In this section, various types of surface modification, electron transfer mechanisms such as mass and charge transfer in redox reaction are reviewed.

## 2.7 Modification/Electrode Activation

Three major factors govern the reaction rate and current at electrodes: (i) the increment of active surface area to enhance mass transfer on the electrode surface, (ii) kinetics of electron transfer and (iii) surface reactions (adsorption) (Zoski, 2006). Low specific surface properties on electrode with poor catalytic activity and low wettability from hydrophobic surface for redox reactions are critically affected the cell performance.

Prior studies have stated that the porous electrode should be permeable to redox molecules and allow the electrolyte to react between active reaction areas (Flox, Rubio-García, Skoumal, Andreu, & Morante, 2013; Le, Bechelany, & Cretin, 2017).

In addition, the available electrode surface area indirectly affected the activity between the catalyst and redox species. The enhancement of porous electrode characteristics has become one of the important studies in understanding the redox mechanism and polarisation reduction in RFBs. From the review, it is discovered that, pre-treatment on surface can significantly improve the electrode kinetically for better electron transfer and electrochemical properties.

Therefore, porous electrode design for optimum performance high electronic and ionic conductivity, interfacial electrochemical charge transfers rates, effective mass transfer of the reactant species, low fluid drag and corrosion resistant are discussed in most of the published papers (Minke et al., 2017, Le et al., 2017). A various type of electrode customization methods reported for improving the electrochemical activity in redox flow battery, energy efficiency of RFB is related with the conductivity of electrode that the electrochemical reaction of active materials occurs on the electrode surface.

The relationship between porous electrode characteristics and redox electrochemical reaction in RFBs active compartment has been widely investigated in recent. Different methods of surface pre-treatment attributed to the reaction kinetics of porous electrode by reduce charge transfer resistance, increase the surface oxide content, increase wettability, surface area and accelerate catalytic reaction with electrolyte. Pre-treatment methods on felt surface are categorised into (a) thermal, (b) chemical, (c) plasma, (d) carbon nanotube-based modification and (e) metal or metal oxide deposition as discussed. In this context, physical and chemical modifications of porous electrodes have become important techniques. Common strategies are to improve the reaction kinetics by reducing charging transfer resistance, increasing the surface oxide content, and facilitating catalytic reaction with the electrolytes. Recent efforts have also focused on more straightforward and lower-cost processes that are suitable for mass production (Le et al., 2017).

Single stage surface modification includes acid/alkaline treatment (Kabir, Gyan, & Cheng, 2017; Zhou, Zeng, Zhu, Wei, & Zhao, 2016) , nitrogen doping (K. J. Kim,

Kim, Kim, & Park, 2011; J. J. Park, Park, Park, & Yang, 2016; M. Park, Ryu, Kim, & Cho, 2014; Shi, Liu, He, & Shen, 2014), thermal treatment (O. Di Blasi et al., 2015; Z. González et al., 2017, 2011; Melke et al., 2014; X. Wu, Xu, Xu, et al., 2014), metal oxide (Fetyan et al., 2018; Flox, Skoumal, Rubio-Garcia, Andreu, & Morante, 2013; Ghimire et al., 2018; Yun, Park, Park, Lee, & Yang, 2018), water activation (Kabtamu, Chen, Chang, & Wang, 2017) and others (Abbas et al., 2018; Jiang, Shyy, Ren, Zhang, & Zhao, 2019).

### 2.7.1 Thermal Treatment

The simplest way for felt modification is thermal treatment which the samples are placed in nitrogen or oxygen flowing furnace or microwave under temperature range of 390°C - 900°C (Flox, Skoumal, et al., 2013; Melke et al., 2014; X. Wu, Xu, Xu, et al., 2014). Kazakos *et al.* (1985) and Wu *et al.* (2014) proposed and demonstrated thermal treatment under temperature of 400°C, work presented by Kazakos applied conventional heating method with period more than 10 hours. The electrode with different pre-treatment conditions were evaluated to reveal the relationship between electrochemical performance, temperature and heating period. The result found out that 400°C activated carbon exhibited the most significant increase in efficiency with low mass loss of 1.07%, the comparison studies demonstrated higher mass loss of 11.02% in 500°C. The improvement of felt wettability was attributed to the increased of oxygen containing functional group such as C-OH and C=O. The functional group catalyst the electrode reaction such as the formation of -C-O-V- with vanadium (Sun & Skyllas-Kazacos, 1992b).

Beside thermal treatment in furnace heating, thermal treatment in microwave have also been investigated. Thermal heating by conventional method is time and energy consuming. Wu *et al.* compared thermal treatment of graphite felt at 400°C in microwave thermal for 15 minutes and conventional thermal treatment for 9 hours. The finding shows that graphite felt treated by microwave for 15 minutes demonstrated the lowest charge resistance of 6.55Ω with 50 cycles of charge discharge cycles were achieved. With consideration of most parameters, optimal electrode pre-treatment temperature from 400 – 500°C for the best overall performance is achieved.

### 2.7.2 Chemical Treatment

Chemical treatment is one of the widely used method to introduce oxygen functional group via soaking or boiling in acid (nitric or sulphuric) or alkaline (KOH) solution for hours (L Wei, Zhao, Zhao, An, & Zeng, 2016). Micropores can be generated at the surface of felt by chemical etching process leading to insertion of oxygen containing functional group. High concentration of chemical solution enhanced the chemical activity of treated carbon felt. Sun *et al* introduced chemical modification by refluxing felt in mixture of sulphuric and/or nitric acid, this increased of electrocatalyst of felt attributed by the increased of C-O and C=O on the surface of felt (Sun & Skyllas-Kazacos, 1992b). By comparing two works presented by Sun *et al.*, chemical treated felt achieved better energy efficiency of 91% whereas thermal treated felt obtained 88%.

Blasi *et al.* studied the carbon felt modified by 68% nitric acid at 115°C for 2 hours, the results suggested that nitric acid help to increase the percentage of O1s from 4.16% to 8.82%. Previous studies have not tested the correlation between graphitic basal phase with % of oxygen functional group, the finding from Blasi *et al.* claimed higher oxygen group caused higher ohmic and charge transfer resistance leads to higher polarization resistance. and not favarouble for reaction electro-kinetics. Blasi suggested that optimum ratio between graphitic basal phases and oxygenated catalytic sites can be the solution to improve the electro-kinetics of vanadium redox reaction. The treated felt was further tested in stack assembly with total area of 75 cm<sup>2</sup> and flow field which performed a cell resistance of 0.71 ohm cm<sup>2</sup> and energy efficiency of 65% at current density of 60 mA cm<sup>-2</sup> (A. Di Blasi et al., 2013).

Chemical activation such as KOH also being used as etching agent to develop pores on the surface of carbon materials and insertion of oxygen containing group (Zhengyang Zhang, Xi, Zhou, & Qiu, 2016). Results from KOH etched felt demonstrated cycling ability up to 200<sup>th</sup> cycle in high current density of 150 mA cm<sup>-2</sup> with VE and EE only remain at 74% and 64%. The work reported with optimal mass ratio of 1.25, the result reported superior durability has been achieved at a density of 150 mA cm<sup>-2</sup>. This finding reveals the possibility of using alkaline based etching method to perform chemical oxidation towards felt, however, there is no discussion on the effect of KOH residues in acidic based electrolytes for further understanding.

### 2.7.3 Plasma Treatment

Similar as thermal and chemical treatment, plasma treatment is applied to improve the electrochemical and wettability of carbon based felt. In contrast with thermal treatment, plasma treatment was carried out in a radiofrequency (rf) plasma chamber filled with oxygen/nitrogen. The activation using plasma is time efficient with uniform physical and chemical changes across the felt surface. Enhancement on electrochemical activity was observed in the comparison studies between rayon and PAN based graphite felts by Dixon *et al.* It has found out that PAN felt works better than rayon with higher C-O and C=O group compared to rayon (D Dixon et al., 2016). Through plasma treatment process with oxygen gas, large amount of phenolic (C-O) and carbonyl (C=O) were formed on the surface due to the gamma ray irradiation (D Dixon et al., 2016; K. J. Kim et al., 2011). Oxygen plasma applied in Dixon studies whereas Estevez studies added hydrogen peroxide after oxygen plasma treatment. The addition of hydrogen peroxide after plasma treatment has positively influenced with large insertion of O-C=O onto the surface demonstrated an electrical efficiency of 74.4 % at 150 mA cm<sup>-2</sup> (Estevez et al., 2016).

Besides oxygen atmospheric plasma treatment, nitrogen plasma was performed as another method to create catalytic reaction area. It was found out by N plasma treatment, pyrrolic and pyridinic nitrogen were successfully crafted on the surface of PAN based felt. The presence of these group enhanced the wettability of felt, in the same time facilitated the adsorption of ion (Ouyang et al., 2016). The result shows significant morphology change for N<sub>2</sub> plasma treatment whereas the defect and edge sites on felt after long exposure (Ditty Dixon et al., 2019). Huang's work compared between nitrogen, oxygen, and mixed nitrogen-oxygen plasma. Among the samples, mixed nitrogen-oxygen treated felt showed the better electrochemical performance and excellent cycling stability compared to single doped felt (Y. Huang, Deng, Wu, & Wang, 2017).

### 2.7.4 Carbon Nanotube Based Modification

Carbon nanotube (CNT) known as 1-D carbon has been broadly used as a new kind of electrode in batteries application owing to their electrical conductivity, mechanical resistance and thermal conductivity (Roch et al., 2015). There are two types of carbon nanotube available which are (a) single-walled carbon nanotube (SWCNT) and (b) multi-walled carbon nanotube (MWCNT). The relationship between electrochemical

catalytic effect and physiochemical (i.e. surface area, electrical conductivity, porosity, and electrochemical activity) studies on oxidized MWCNT were discussed in literature (W. Li, Liu, & Yan, 2013).

Mixed acid ( $\text{H}_2\text{SO}_4 + \text{HNO}_3$ ) treated SWCNT demonstrated an increased in oxidation peak current from  $110.8 \mu\text{A}$  to  $172.1 \mu\text{A}$  was credited by the larger area of active site and increased of oxygen functional group (i.e., quinonyl and phenolic group) (W. Li, Liu, & Yan, 2012). Nevertheless, hydrogen evolution reaction facilitated in the modified SWCNT caused the battery efficiency to decrease but suggesting a better electrochemical reaction at anodic side. Another finding utilised carboxyl stability modification by using Nafion solution in MWCNTs, the adhesion of Nafion maintained the stability of carboxyl group on MWCNT surface evenly thus contributed to high coulombic (93.9%) and energy (82.0%) efficiencies (G. Wei, Jia, Liu, & Yan, 2012).

Heteroatom-doped carbons such as N-doped CNT with metal precursor such as Fe, Ni and Co showed the enhancement on the interaction between water molecules and doped carbon whereas nitrogen was the most active sites for oxygen reduction reaction (ORR) (D.-S. Yang et al., 2018). Better activity and lower charge transfer resistance ( $R_{ct}=13.8 \Omega$ ) than N-CNT (Ni)  $14.1 \Omega$  and (Co)  $14.5 \Omega$  in 30 charge-discharge cycles at current density of  $100 \text{ mA cm}^{-2}$ . Besides metal cursor modified CNT, graphite coated carbon nanotube composite electrode also reported with ability to improve the electrochemical performance for both electrolyte in vanadium system (Zhu et al., 2008).

### 2.7.5 Metal or Metal Oxide Deposition

In addition to surface treatment, several other techniques of modification have been studied to improve the electrochemical redox reaction for RFB application. Another alternative way to increase the active sites for felt is the introduction of metal or metal oxide as electrocatalyst onto the surface of felt. With electrodeposition of metal (Ir, Pt, Cu and Bi.) or metal oxide/nitride/carbide ( $\text{Cr}_2\text{O}_3$ ,  $\text{Bi}_2\text{O}_3$ ,  $\text{Nd}_2\text{O}_3$ ,  $\text{CuPt}_3$ ,  $\text{TiC}$ ) on the surface of electrode enable high electronics conductivities with larger specific surface area. Large activated surface area has help to promote the electroconductivity and enhance the electrochemical reaction between electrode and electrolyte (Tseng et al., 2014; Xiang & Daoud, 2018; C. Yang et al., 2015; Yun et al., 2018).

From Sun *et al.* work, Ir modified felt exhibited the best catalytic behaviour compared to other metal. This finding was also supported by the Wang *et al.* study which demonstrated that felt with Ir deposition has low resistivity ( $5.1 \times 10^{-6} \Omega \text{ cm}$ ) compared to pristine felt ( $8 \times 10^{-2} \Omega \text{ cm}$ ). The result indicated that high surface area of Ir deposition has reduced resistance by 25% compared to non-modified felt, which decreases the reaction over potential of vanadium ion redox couples (W. Wang & Wang, 2007). Another important finding was that bimetallic  $\text{CuPt}_3$  modified felt demonstrated energy efficiency of 84% at low current density of  $20 \text{ mA cm}^{-2}$  and can performed up to 30th charging cycle. The result strongly confirmed that  $\text{CuPt}_3$  accelerated the oxygen and electron transfer process between electrolyte and electrode surface with presence of OH functional group (Flox et al. 2013). Copper nanoparticle decorated felt presented by Wei *et al.* demonstrated energy efficiency of 80.1% at high current density of  $200 \text{ mA cm}^{-2}$ , the restriction for this application was the stability and suitability of copper for vanadium (Lei Wei, Zhao, Zeng, Zhou, & Zeng, 2016).

Next, the study related to TiN decomposition demonstrated stability up to 50 cycles on high current density application which up to  $300 \text{ mA cm}^{-2}$  (L Wei, Zhao, Zeng, Zeng, & Jiang, 2017), while for TiC stable for 65 cycles for low current density application ( $60 \text{ mA cm}^{-2}$ ) (Ghimire et al., 2018). Ti with nitrogen increased the absorption of  $\text{V}^{3+}$  and also facilitated the electron transfer process in vanadium solution (L Wei et al., 2017). Nevertheless, selected metal such as lead and titanium are easily passivated in the potential range of  $\text{VO}_2^+/\text{VO}^{2+}$ , which this resulting an increase in area resistance (Chakrabarti *et al.*, 2014). Fetyan's studies on neodymium oxide coated carbon felt indicated that  $\text{Nd}_2\text{O}_3$  has good catalytic effect towards vanadium redox couples. The result revealed less degradation occurred on the felt surface compared to thermal treated felt (Fetyan et al., 2018), higher energy efficiency achieved whereas the oxygen-donating function group was well preserved on the surface of the felt.

Several reported studies used metal oxide particles to decorate the carbon felt electrodes, which improve kinetics and suppress the side reactions of gaseous evolution. Nonetheless, many of these metal oxides (i.e. oxides of nickel and neodymium (Fetyan et al., 2018)) were neither low-cost nor abundant, which are not attractive for developing RFBs based on less metallic components (i.e. organic flow batteries). The aforementioned studies reported improvements on overall RFB performance and

attributed to the increase of electron transfer or diffusion coefficient, however, the intrinsic catalysis was unable to convoluted from the increase of activated electrochemical surface area (Forner-Cuenca & Brushetta, 2019). From most of the research studies, metal oxide has triggered undesired side reaction such as hydrogen evolution reaction that causes a decrease in coulombic efficiency and capacity retention rate during charging discharging process in RFBs. Additionally, the high cost and poor mechanical stability of metal catalyst remain as challenge for the implementation of metal coating for felt.

## 2.8 Surface Morphologies of treated felt

Scanning electron microscopy (SEM), field emission scanning electron microscopy (FESEM) or high-resolution transmission electron microscopy (HRTEM) with high electron emission has been utilised to provide insights and high-resolution image for surface morphology and appearance studies. Generally, the findings enable researcher to further evaluate the coating effect or treatment effect on the surface of electrode. Furthermore, the construction of structure on the surface of felt is one of the key parameters for felt for higher electronics conductivity or increase the surface area with 3D structure.

The comparison between surface morphologies and surface treatment methods such as nitric acid, modified hummer, thermal and sulphuric acid. As shown in Figure 2.17 (a), surface of carbon felt are coated with HNO<sub>3</sub> treated carbon nanoparticles. With the cotton like carbon nanoparticles provides more active sites for reaction, one interesting finding from this work is 2 mg cm<sup>-2</sup> loading in current density of 100 mA cm<sup>-2</sup> is better in terms of cycle stability, coulombic and voltage efficiency maintained around 90%. The displayed morphology result contributes to the understanding of carbon nanoparticles coating reduced ohmic loss with the increased surface area and improved electrocatalytic activity.

For modified hummer treated felt as illustrated in Figure 2.17(b) show no significant changes on the surface of felt. Wu *et al.* highlighted the degree of roughness increased after the treatment resulting increase in specific area and surface energy (X. Wu, Xu, Shen, et al., 2014) where the coulombic, voltage and energy efficiencies of the cell at 50 mA cm<sup>-2</sup> were 95%, 81.3% and 77.2% with 50 cycles. However, the carried



investigation only limited to  $80 \text{ mA cm}^{-2}$ . Interestingly, pores are observed in the investigation of mixed  $\text{NH}_3/\text{O}_2$  thermo-chemical felt as presented in Figure 2.17 (c). The presence of pores is caused by the pressure of mixed  $\text{NH}_3/\text{O}_2$  after long duration of treatment. The result indicated that felt treated under  $500 \text{ }^\circ\text{C}$  presented 73% increase in electroactive surface and the graphite like C-N bond is responsible for the enhancement of electrochemical activity.

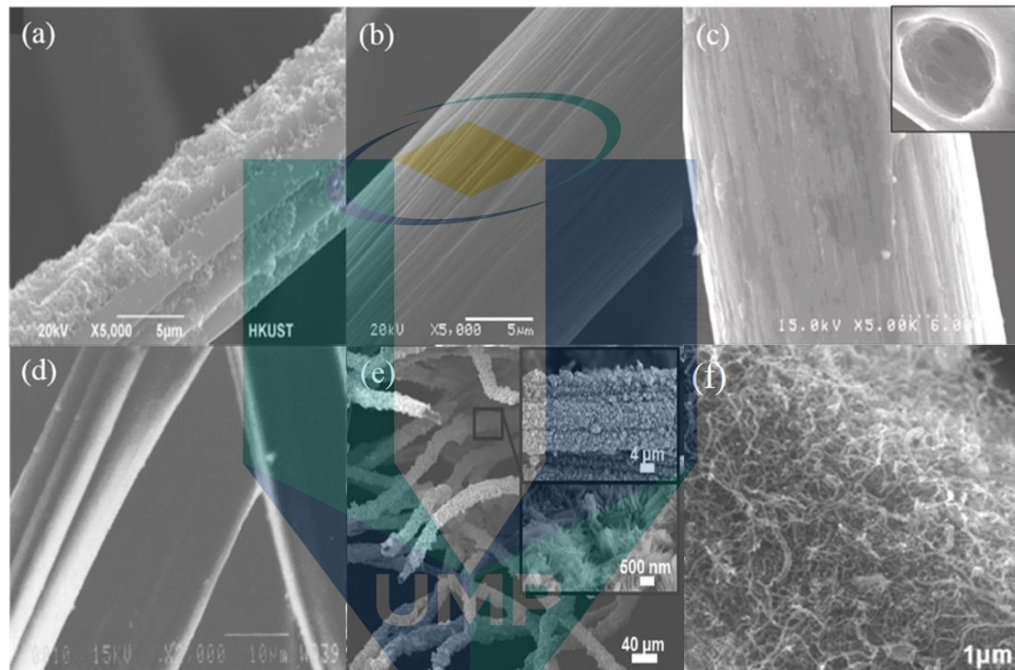


Figure 2.17 SEM image (a)  $\text{HNO}_3$  treated carbon nanoparticles coated felt (b) modified Hummer felt (c) thermal treated felt ( $\text{NH}_3/\text{O}_2$ ) (d) 98%  $\text{H}_2\text{SO}_4$  treated felt (e) N- and  $\text{WO}_3$  decorated felt (f) CNF/CNT grown surface

Source: (a) L Wei et al., (2016) (b) X. Wu, Xu, Shen, et al., (2014) (c) Flox, Rubio-García, et al., (2013) (d) Sun & Skyllas-Kazacos, 1992a) (e) Hosseini et al., (2018) (f) M. Park, Jung, Kim, Lee, & Cho, (2013)

No changes applied on felt surface after the treatment of sulphuric acid is reported by Sun *et al.* (2013) as demonstrated in Figure 2.17(d). Regardless of the presented surface morphology, there is no additional evident obtained from SEM captured photo for further understanding. Thus, the investigation is continued with XPS investigation whereas C-O and C=O groups are crafted to the felt after the treatment. Concerning no obvious changes on felt surface, the work concluded that the existing of C-O and C=O groups facilitates the electron and oxygen exchange for vanadium redox reaction.

To creating more active sites on felt for vanadium redox reaction, Hosseini *et al.* suggested N- and WO<sub>3</sub>- decorated positive electrode as shown in Figure 2.17 (e), a thickness layer of 1 μm of WO<sub>3</sub>- layer has formed on the surface of felt. From higher magnification image shown, the agglomerated structure is the formation of carbon nanorods. The thickness of felt has been increased roughly 2 μm after hydrothermal treatment with urea (Hosseini *et al.*, 2018). Concentric cylinder shape carbon nanotubes (CNT) and carbon nanofiber (CNF) with edge planes are deposited on the surface of carbon felt, As shown in Figure 2.17, the unique shape of CNT and CNF with range from 10 to 80 nm are formed.

The morphologies of plasma treated felt are as illustrated at Figure 2.18, there was not many changes as displayed in (a) while (b) show hole formed after treatment at the felt surface. The method used in (a) and (c) was oxygen plasma, conversely, the formation of hole appears in felt illustrated in (c) due to the higher power used in related plasma treatment. From reported result, that hole formation has reduce the contact resistance between electrode and electrolyte that bring to a higher anodic peak current.

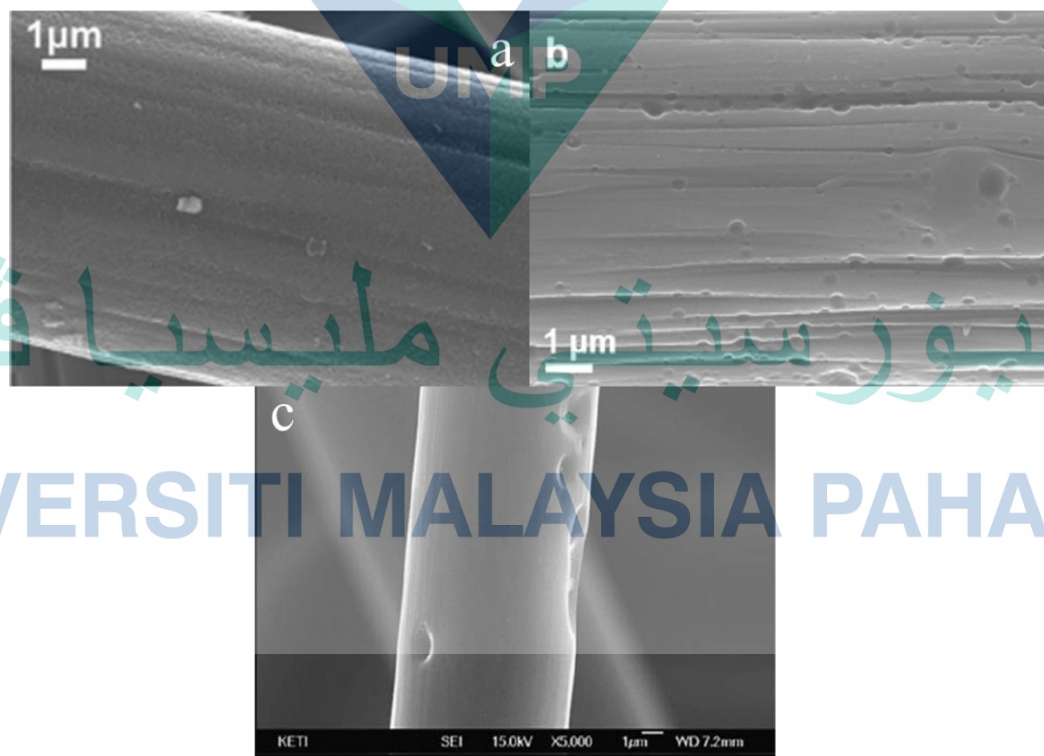


Figure 2.18 The morphology of treated felt illustrated by SEM image (a) oxygen plasma (b) nitrogen plasma (c) oxygen plasma

Source: (a) D Dixon *et al.*, (2016) (b) Ditty Dixon *et al.*, (2019) (c) K. J. Kim *et al.*, (2011)

For metal based, most of the results demonstrated nanostructure has been formed on the surface of felt after metal deposition proses as illustrated in Figure 2.19(a)-(f). Mosaic tiles look alike nanostructures  $\text{CuPt}_3$  has been uniformly deposited on the surface of graphite oxide are captured by HRTEM as shown in Figure 2.19(a). The deposition of metal such as  $\text{CuPt}_3$  evenly leading to higher current value compared to bare felt, due to the electroconductivity of felt increase accelerates the electron transfer between electrode and electrolyte interface has significantly enhance the electrocatalytic activity in vanadium redox reaction.

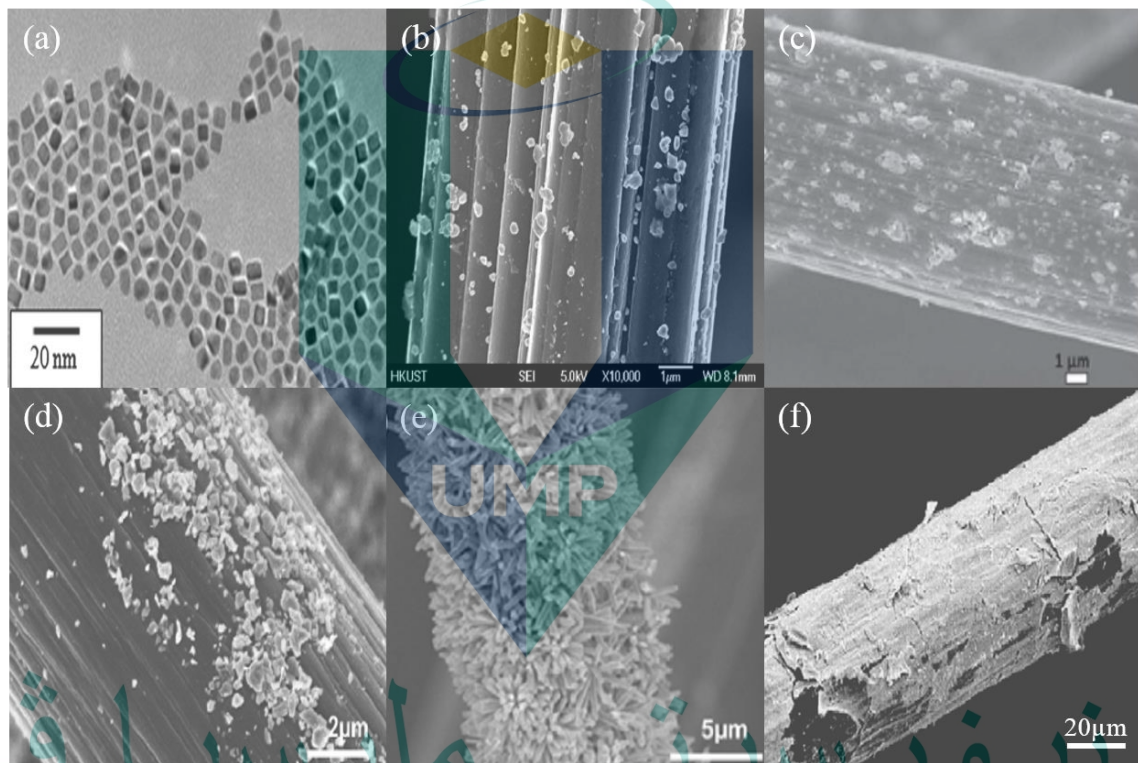


Figure 2.19 HRTEM and SEM of metal or metal oxide deposition (a)  $\text{CuPt}_3$  (b)  $\text{Cu}^{2+}$  (c) TiC (d) NiO (e) TiN (f) Ir deposition on surface of felt.

Source: (a) Flox, Skoumal, et al., (2013) (b) Lei Wei et al., (2016) (c) Ghimire et al., (2018) (d) Yun et al., (2018) (e) L Wei et al., (2017) (f) W. Wang & Wang, (2007)

For metal nanoparticles deposited such as  $\text{Cu}^{2+}$ , TiC and NiO on the surface of felt as revealed in Figure 2.19(b - d). Wei *et al.* added conductive copper salt into the electrolytes and performed charging process without pre-treatment procedures (Lei Wei et al., 2016). The deposition of Cu on the electrode happens in high density of  $300 \text{ mA cm}^{-2}$  suggesting new method to catalyst the process of the redox reaction. Nevertheless, the additive need to be further investigate as it must withstand the corrosive environment

and not participant in the reaction. Similar to metal deposition method, uneven particles size likely caused by the agglomeration of TiC particles are reported on the surface of negative electrode in Ghimire's work (Ghimire et al., 2018). Surface morphologies for different metal and metal oxide decorated felt surface has been illustrated in, as compared (f) illustrated large coverage of Ir successfully deposited on the surface of felt followed by TiN (e) and TiC (c) deposition.

## 2.9 Electrochemical measurement

Electrochemical measurement is used to study the charge exchange between the electrode and electrolyte solution. A typical three-electrode setup is needed to perform electrochemical measurement. Indeed, there are several electrode setups based on the requirement of studies. As presented in Table 2.3, most of the work employs Pt wire as the counter electrode. Saturated calomel, silver/silver chloride electrode and standard hydrogen electrode are commonly used as a reference electrode. The working electrode varies depending on the target of investigation, glassy carbon electrode is normally used for analyte investigation. For the modified electrode investigation, treated carbon is hooked on Pt wire. This electrode has larger surface area than the glassy carbon electrode that required Potentiostat with high current setting.

Table 2.3 Three electrode setup

Studies	Electrolyte	Working electrode	Counter electrode	Reference electrode	Ref
CO <sub>2</sub> activated graphite	0.05 M V <sub>2</sub> SO <sub>4</sub> + 2 M H <sub>2</sub> SO <sub>4</sub>	Felt with PTFE holder	Pt wire	Saturated calomel	(Chang et al., 2017)
CNT grafted CF	0.1 M VOSO <sub>4</sub> + 2 M H <sub>2</sub> SO <sub>4</sub>	Carbon felt with Pt wire	Pt wire	Saturated calomel	(G. Wei et al., 2012)
Copper nanoparticle deposited GF	0.1 M electrolyte (50% V <sup>3+</sup> + 50% VO <sup>2+</sup> ) + 3 M H <sub>2</sub> SO <sub>4</sub>	Graphite electrode (0.785 cm <sup>2</sup> )	Pt wire	Saturated calomel	(Lei Wei et al., 2016)
N, Co-doped CF	0.1 M VOSO <sub>4</sub> + 2 M H <sub>2</sub> SO <sub>4</sub>	Plasma treated GF	Pt foil	Saturated calomel	(Y. Huang et al., 2017)

### 2.9.1 Cyclic Voltammetry

Cyclic voltammetry (CV) is an electrochemical technique that measures the current develops in molecular species that voltage can be predicted by Nernst equation. It is useful in investigation of reduction and oxidation related to electron transfer process for molecular species (Elgrishi et al., 2018). The potential control can be applied by potential between the working electrode and potential electrode while the electrochemical event occurred on the surface of electrode measure of working and counter electrode.

Cyclic voltammetry can effectively investigate these reactions with reverse scan depending on the scanning rate and concentration of solution composition. The concentration of active material is defined in Randle-Sevcik equation 3.1 that affects the peak current of the electrolyte. The voltage applied on the reference electrode and measured current by working electrode increased when the scan rate increased from negative to positive potential where the chemical is oxidised. Then, the measured current decreased when the chemical is reduced.

### 2.9.2 Electrochemical Impedance Spectroscopy

Electrochemical impedance spectroscopy (EIS) is an experimental technique that has been widely used for the investigation for the determination of limitation at electrode surface for fuel cells, capacitor and RFB applications. This method applies small amplitude of AC signal to an electrochemical system. The AC signal provides a quantitative analysis of the ratio of voltage to the current or the phase angle of the impedance varies with the sine frequency. Changes in EIS can be used to predict the impedance evolution of redox active reaction in electrode. Current that resulting in reduction or oxidation of an electroactive material across the electrode interface are known as faradaic current,  $I_F$ . Faradaic current,  $I_F$  described by Faraday's law is directly proportional to the charge transferred in faradaic process against time taken. From EIS data, it can be described with a physical model by fitting the data into electrical circuit that is represented by resistor, inductor and capacitor under ideal case.

The second type of current present in the redox reaction can be non-faradaic current that there is a change in solution-electrode interface due to the changes in the applied charging or discharging potential. The electrode-solution interface is described of having capacitance,  $C_d$  where capacitance is directly proportional to charge in the

process over electron. For non-uniform kinetics, constant phase element (CPE) is implemented to describe the distributed capacitive behaviour, while Warburg element describes the mass transport limited frequency and complex diffusion on electrode material.

## 2.10 Chapter Conclusion

The research on RFB is mainly focused on electrolyte and electrode. The desirable properties for active species used as electrolytes in RFB are multi-electron transfers and fast kinetics to get high redox potential. The energy density of RFB highly depends on the electrolyte redox potential. Selection on electrolyte for flow battery application is crucial in which the cell voltage is highly dependent on the difference between negolyte and posolyte. In the context of electrolyte, dissolution of active species into supporting electrolyte sulphuric acid can enhance the energy density for RFB.

In addition, using inexpensive quinone redox organic molecules can significantly reduce the cost of RFB. The incorporation of these organic materials enables a practical approach to achieve low-cost redox flow batteries with performance characteristics comparable with metal based RFB systems. Recent studies on the electrocatalytic activity on porous electrode and bipolar electrode only focused on  $\text{VO}_2^+/\text{VO}^{2+}$  and  $\text{V}^{3+}/\text{V}^{2+}$  redox pair. Lack of studies on the felt modification are reported for other types of RFB, especially on organic-based. Furthermore, the maturity of RFB technologies in terms of electrode and electrolyte are still questionable as it must undergo revolution towards denser, more reliable, and cost-effective system. Based on the literature review for the recent years, several challenges have faced in RFB system:

1. Extend investigation on potential quinone derivative – alizarin red s

For alizarin red s, it is still a hurdle to achieve highly soluble active material with high cell voltage. In the case of aqueous RFB, only few literatures reported on the application of alizarin red s. The work is limited to a low concentration of ARS.

2. Extend the stability of alizarin red s with supporting acid

To date, ARS still suffers from low energy attributed to low solubility of active material. Hence, the effect of supporting salt in improving the solubility of active material

such as alizarin s need to be considered. The concentration of ARS can be a key element for further improvement as negative electrolyte for RFB.

3. Two-stage modification for electrode modification and investigation of treated electrode in negative/positive quinone media

The electrode modification is one of the major research areas in RFB. As reported in section 2.7, studies have reported different modification using alkaline, acid or hydrogen peroxide for electrode activation in felt. Most of the modification is focused on single-stage treatment as part of an attempt to improve RFB performance that is limited to vanadium based. The effect of two-stage treated felt in quinone-based electrolyte has not been studied. To have comprehensive understanding towards the effect of two-stage treated felts in quinone media such as alizarin red s and benzoquinone is required.

4. Investigation of acid treated felt in different supporting acid for positive quinone media.

Supporting electrolytes such as sulphuric acid is widely used not only for redox flow battery but also to other secondary batteries to improve conductivity and solubility, thereby minimise the ohmic loss. For zinc-based redox flow cells, methanesulfonic acid is used as a supporting electrolyte. In this study, the investigation for methanesulfonic and sulphuric acid with the effect of acid treated felt in positive electrolytes.

اونيورسيتي ملايسيا قهغ

UNIVERSITI MALAYSIA PAHANG

## CHAPTER 3

### METHODOLOGY

#### 3.1 Introduction

This chapter presents the electrolyte investigation, electrode modification, material characterisation, spectroscopy characterisation, electrochemical measurement and measurement procedure employed for this study. Material preparation methods for electrode and electrolyte are explained in the first section. Followed by the physical characterisation of pristine and treated electrodes using scanning electron microscope, contact angle and spectroscopic measurement. Spectroscopy characterisation applied such as XPS to identify the functional group for pristine and treated electrode is also described in detail. Finally, the measurement procedure for electrochemical measurement is explained.

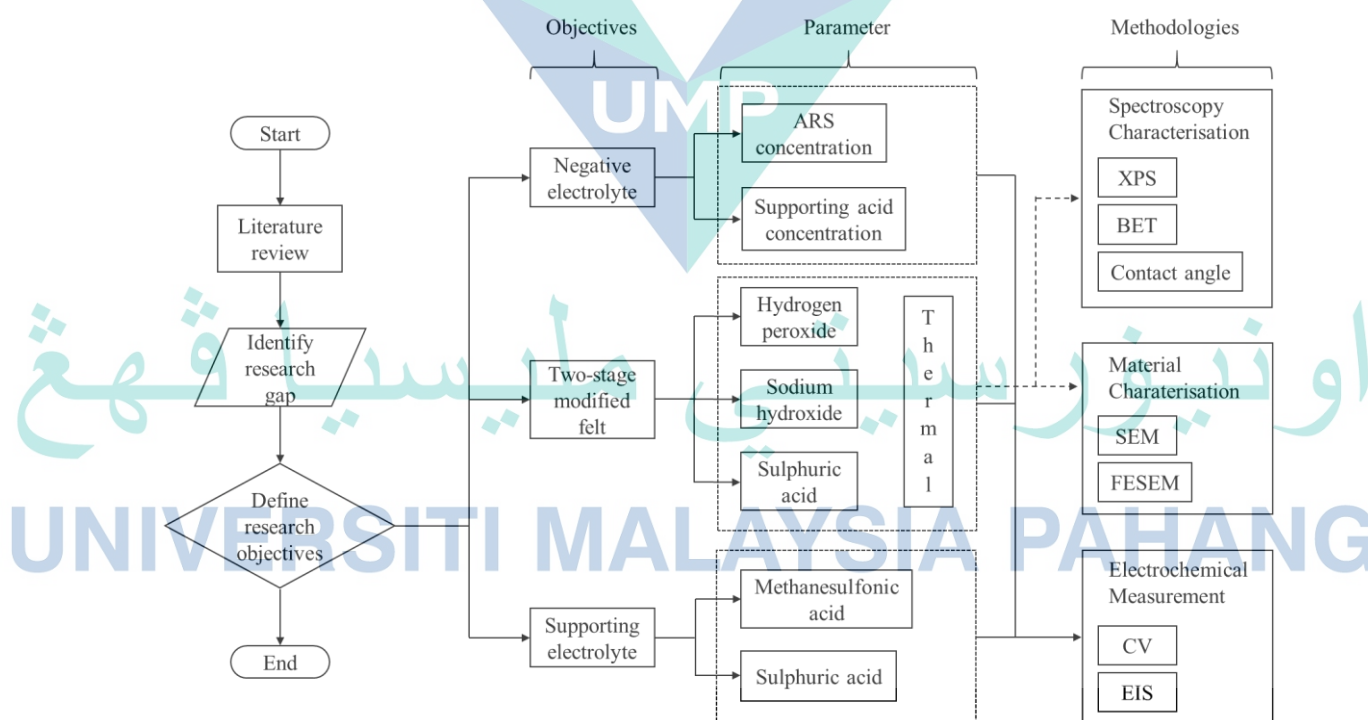


Figure 3.1 Research flow with highlighted objectives and proposed methodologies.

As illustrated in Figure 3.1, this thesis started with literature review to identify research gap. For this work, three research objectives related to negative electrolyte,



modified electrode and supporting electrolyte were identified from the literature review. To identify the best composition for quinone-based derivative–ARS in three selected concentrations. Electrochemical measurement is conducted to investigate the redox activity of ARS in 1 mol dm<sup>-3</sup> sulphuric acid. The work continued with extended investigation of ARS in higher concentration of supporting electrolyte 2.5 mol dm<sup>-3</sup>.

The second objective for this work covered a novel two-stage modified electrode, three modified electrodes are fabricated and obtained. Material characterisation has been employed to illustrate the topology of the treated felt, whereas spectroscopy investigation XPS is also conducted to reveal the functional group etched on the surface of treated felt. To further investigate the effect of modified felts in quinone-based reaction, this work presented electrochemical measurements such as EIS and CV in selected positive electrolyte – benzoquinone (BQDS). The last objective focused on the investigation of acid with thermally treated felt. The last objective focused on the investigation of acid with thermally treated felt. The effect of supporting acid (i.e., sulphuric acid and methanesulfonic acid) for acid treated felt in selected posolyte BQDS is investigated.

### 3.2 Materials Preparation

#### 3.2.1 Electrode Selection

The carbon felt manufactured by CFC CARBON is used throughout the research. Pristine felt without treatment is used as one of the samples for investigation. Three types of two-stage treatments is fabricated to investigate the effect of different treated felt in selected positive electrolyte. The preparation steps are explained in section 3.2.3. These electrodes are evaluated through electrochemical and spectroscopic investigation.

#### 3.2.2 Treatment Reagent Preparation

For cleaning treatment purpose, purchased hydrogen peroxide 30% (w/v) is used without any modification. For acid treatment purpose, lab-scale 98% sulphuric acid has been diluted into 30% (w/v). For alkaline treatment purposes, 30% (w/v) sodium hydroxide solution is prepared by mixing 30g into 1 litre deionized water.

### 3.2.3 Felt Preparation

In this work, a novel two-stage treatment is proposed. Three types of surface characterisation which are acid, hydrogen peroxide and alkaline are fabricated. These treatment reagents are normally used as oxidising agent (Milner, Scott, Head, Curtis, & Yu, 2017). At first, the PAN-based carbon felt was cut into the desired size 4 cm x 4 cm x 0.6 cm. Then, PAN type felts are undergoing oxidising process then thermally treated under 450°C. As suggested in most of the literature, the optimal electrode pre-treatment temperature from 400 – 500°C in >2h for the best overall performance is achieved (X. Wu, Xu, Xu, et al., 2014). Preheat process is to reduce the time taken by the furnace to achieve temperature of 450°C. The undertaken stage for surface treatment is described in Figure 3.2.

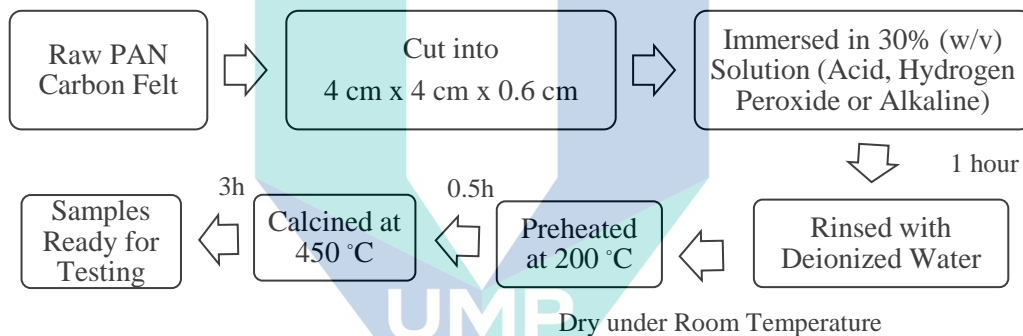


Figure 3.2 Flow for the fabrication of treated felt samples.

#### 3.2.3.1 Sodium hydroxide with Thermally Treated Carbon Felt

For  $CF_{NaOH}$ , the carbon felt sample is treated by immersing in 30% (w/v) sodium hydroxide solution for 1h. After that, the treated felt samples are rinsed using deionised water to remove excessive solution. The samples are left for drying at room temperature for 24h. Following these, all treated felt samples are preheated at 200°C for 0.5h, and subsequently calcined at 450°C for 3h under  $N_2$  atmosphere in a horizontal furnace. Sodium hydroxide with thermal treated felt is named as  $CF_{NaOH}$ .

#### 3.2.3.2 Hydrogen Peroxide with Thermally Treated Felt

For the second type, the carbon felt sample is treated in a hydrogen peroxide solution (Aldrich, 30 wt. % in water) for 1 h in a sonication bath. After that, the treated felt samples were rinsed using deionised water to remove excessive solution. The samples were left for drying at room temperature for 24h. Following these, all treated felt samples were preheated at 200°C for 0.5h, and subsequently calcined at 450°C for 3h under  $N_2$

atmosphere in a horizontal furnace. Hydrogen peroxide with thermal treated is named as  $CF_{H_2O_2}$ .

### 3.2.3.3 Acid with Thermally Treated Felt

Acid treated carbon felt sample is treated by immersion in 30% (w/v) of sulphuric acid solution for 1h. After that, the treated felt samples are rinsed using deionised water to remove excessive solution. The samples are left for drying at room temperature for 24h. Following these, all treated felt samples were preheated at 200°C for 0.5h, and subsequently calcined at 450°C for 3h under  $N_2$  atmosphere in a horizontal furnace. Sulphuric acid with thermal treated felt is named as  $CF_{H_2SO_4}$ .

## 3.2.4 Electrolyte Preparation

### 3.2.4.1 Negative Electrolyte

Alizarin red s (CAS no. 130-22-3, Sigma Aldrich) powder form. For ARS investigation, prepared solution consists of (a)  $0.05 \text{ mol dm}^{-3}$  (b)  $0.10 \text{ mol dm}^{-3}$  (c)  $0.15 \text{ mol dm}^{-3}$  ARS in  $1 \text{ mol dm}^{-3}$  or  $2.5 \text{ mol dm}^{-3}$   $H_2SO_4$  as the supporting electrolyte. The supporting electrolyte is prepared by dilute 96% concentrated sulphuric acid into  $1 \text{ mol dm}^{-3}$  and  $2.5 \text{ mol dm}^{-3}$  supporting sulphuric acid using suitable amount of deionised water. Please refer to appendix A for the solubility and electrochemical data of alizarin red s. Organic dye – alizarin red s with three benzene rings as illustrated in Figure 3.3 is used as negative electrolyte in this study:

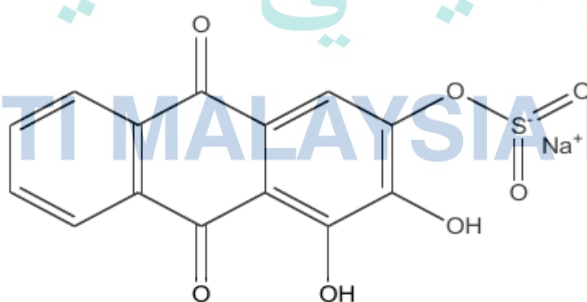


Figure 3.3 Chemical structure for Alizarin red s.

### 3.2.4.2 Positive Electrolyte

1,4-benzoquinone was used as received without further purification. For felt investigation, electrolytes with active species were prepared by dissolving  $0.1 \text{ mol dm}^{-3}$

1,4-benzoquinone (also known as hydroquinone) in  $1 \text{ mol dm}^{-3} \text{ H}_2\text{SO}_4$ . Please refer to appendix A for the solubility and electrochemical data of 1,4-benzoquinone or known as 1-4 BQ. Organic quinone derivative BQ with single benzene ring illustrated in Figure 3.4 is used as positive electrolyte in this study.

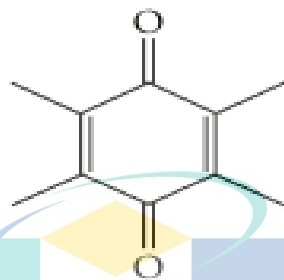


Figure 3.4 Chemical structure for 1,4-benzoquinone.

### 3.3 Material Characterisation

In this study, two-stage treatment methods such as hydrogen peroxide or sodium hydroxide with thermal treatment were proposed as the oxidising method for felt characterisation. For felt characterization incorporated with surface modification with selected treatment and have been analysed using scanning electron microscopy (SEM) and field emission scanning electron microscopy (FESEM) imaging.

#### 3.3.1 Scanning Electron Microscope

Scanning electron microscopy (SEM) was used to provide visual images of treated felt with magnification up to 300,000 times. The focused accelerated electrons beam in SEM is used to visualise surface material in high resolution image data. High energy electron is focused and shot on the surface of the sample and the reflected electron was analysed to explain the morphology (shape and size) and topology (surface feature) of material. In this study, scanning electron microscope investigation is performed using Carl Zeiss EVO 50. Image with magnification of 5,000 times is used to identify the surface morphology of untreated felt.

#### 3.3.2 Field Emission Scanning Electron Microscope

Field emission scanning electron microscopy (FESEM) was used to investigate the topography of treated carbon. High magnification FESEM image was used to differentiate. In the second part of the work, field emission scanning electron microscopy

(FESEM, JEOL JSM-7800F) with magnification up to x300k is employed to better observation of treated surface. The difference between SEM and FESEM is the emitter type and the acceleration voltage. FESEM with cold source of emitter possesses a higher acceleration voltage compared to SEM is more suitable to observe smaller samples with clear and well-focused images.

### 3.4 Spectroscopy Characterisation

FESEM and SEM only reveal the changes on the surface with respect to the degradation caused by treatment. Therefore, spectroscopic measurements such as XPS is performed to identify the functional group that inserted on the raw and treated felt. Wettability properties of felt also investigated in this work. As reported in literature, wettability properties will significantly affect the absorption of felt towards electrolytes. With the purpose of further elucidating the wettability properties of treated felt, this study continued with contact angle measurement. For contact angle measurement, water droplet was used to inspect the absorption of felt.

#### 3.4.1 X-ray Photoelectron Spectroscopy

With the aim of examining the composition of the surface functional group, X-ray photoelectron spectroscopy (XPS) with Al monochromatic X-ray source is used to determine the carbon and oxygen ratio for raw and treated felt samples. All curves are fitted using Gaussian Lorentzian function. XPS determined the element by referring to the kinetic energy spectrum by X-ray radiation with a constant energy, high voltage radiation is ejected in vacuum and reflected by the surface of specimen. The results provided valuable quantitative information on the chemical state from the desired material. Deconvolution of the C1s and O1s level spectra are performed by fitting of the following peaks: 284.2 eV, 285 eV, 286 eV, 531 eV, 532 eV, 532.9 eV and 534 eV that arose from graphitic  $sp^2$  C-C,  $sp^3$  C=C, aliphatic C-OH, C=O, C-O and C-C=O (detail explained in 4.3.2).

#### 3.4.2 Contact Angle Measurement

To further investigate the hydrophilicity of carbon felt before and after treatment, contact angle measurements are performed. All felt samples were analysed using Dataphysics OCA 15 plus Contact Angle measuring device with SCA 20 software. The

time dependent method is chosen for this study, whereas droplet shape is investigated over time. The horizontal drop test is performed with the camera pointed parallel to the substrate to view the absorption of liquid. Water droplet is the selection liquid to check the wettability of felt. Felt samples are placed on the sliding magnetic based, water droplet is dropped by the syringe and absorption on the sample is observed. For hydrophobic sample, the contact angle,  $\theta$ , is measured referring to the capture photo, the result determination is illustrated in Figure 3.5. The hydrophilic characteristic of material can be measured from the contact angle form between water and solid surfaces. If the contact angle between water and solid surfaces is  $< 90^\circ$ , the water is adsorbed by the surface in a short time. If the contact angle is  $\geq 90^\circ$ , the water normally remains as droplet on the surface.

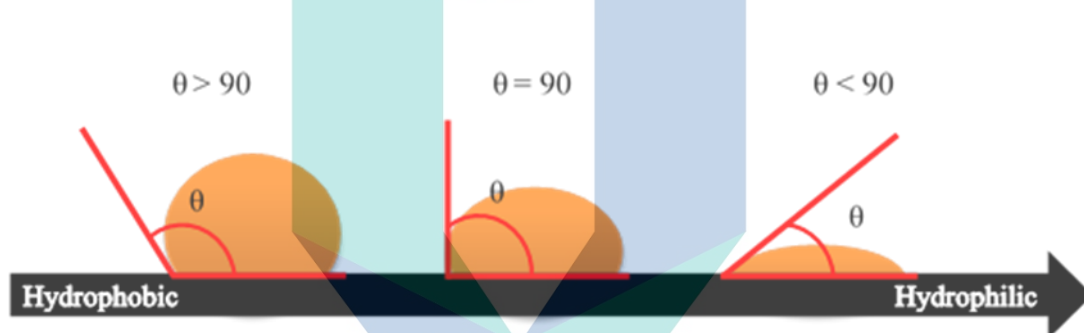


Figure 3.5 Contact angle between water droplet and surface.

### 3.4.3 BET Surface Area Measurement

Brunauer-Emmet-Teller (BET) is used to gather information on surface area by using gas such as argon and nitrogen. The result explained the physical adsorption of gas molecules by the sample and reveals physical properties of the investigated samples. In this experiment, nitrogen gas is used in BET measurement using Micromeritics' ASAP  
 © 2020.

UNIVERSITI MALAYSIA PAHANG

### 3.5 Electrochemical Measurement

Quantitative analysis of redox active reaction, for chemistry-related investigation, electrochemical techniques, such as cyclic voltammetry and EIS is conducted to evaluate the effect of treated carbon felt in selected positive electrolyte. The EIS technique can further define the electron transfer reaction in electrolyte and charge transfer resistance. The impedance technique allows the prediction on the electron reaction happens

internally with fitting to the relevant electrical circuit, which are unable to reveal through CV studies. Each characterisation technique is described as follows:

### 3.5.1 Cyclic Voltammetry

Cyclic voltammetry (CV) is used to monitor the reaction rates of redox couples and to evaluate the electrochemical properties related to the electrode surface. Mostly, three electrode method has been chosen for the electrochemical investigation as illustrated in Figure 3.6. Electrochemical cell investigation normally consists of three electrodes, namely working electrode, counter electrode, and reference electrode. In CV, the potential measurement between working and reference electrode is measured. In the CV method, potential sweep rate or scan rate determined the mass transfer rate. The kinetic analysis of the electrochemical process is relying on the resulting peak voltage and current.

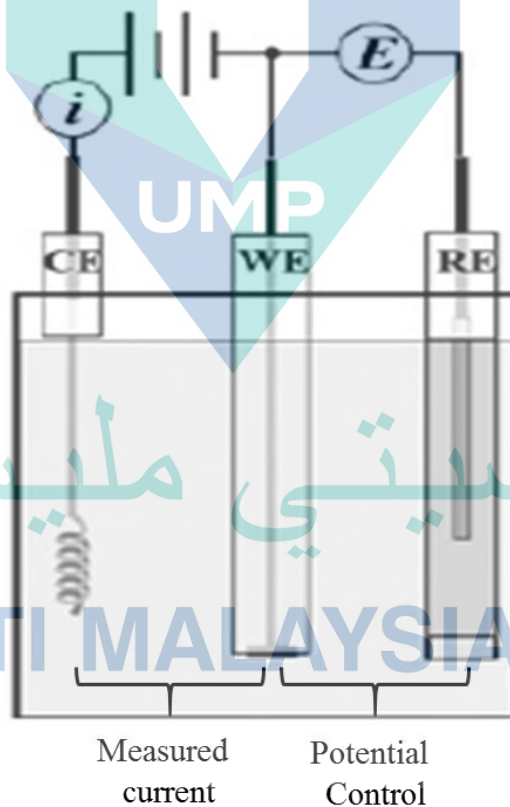


Figure 3.6 Three electrode system equivalent circuit diagram.  
Source: Zoski, (2006)

The electrochemical cycling measurement is performed from lower potential to higher potential. As displayed in Figure 3.7, species Ox is consumed at electrode and

reduction current is observed from point 1 – 7. The generation of Ox by oxidation of Re with peak oxidation current has been observed from point 8 – 10. The analysis of CV depends on the cathodic ( $I_{pc}$ ), anodic peak ( $I_{pa}$ ) and peak separation ( $\Delta E_p$ ). The peak of the anodic and cathodic current in CV test defined the mass transport, diffusion, and reversibility of the system, while the electrode potential of the half-cell can be determined by the average of the anodic and cathodic potential.

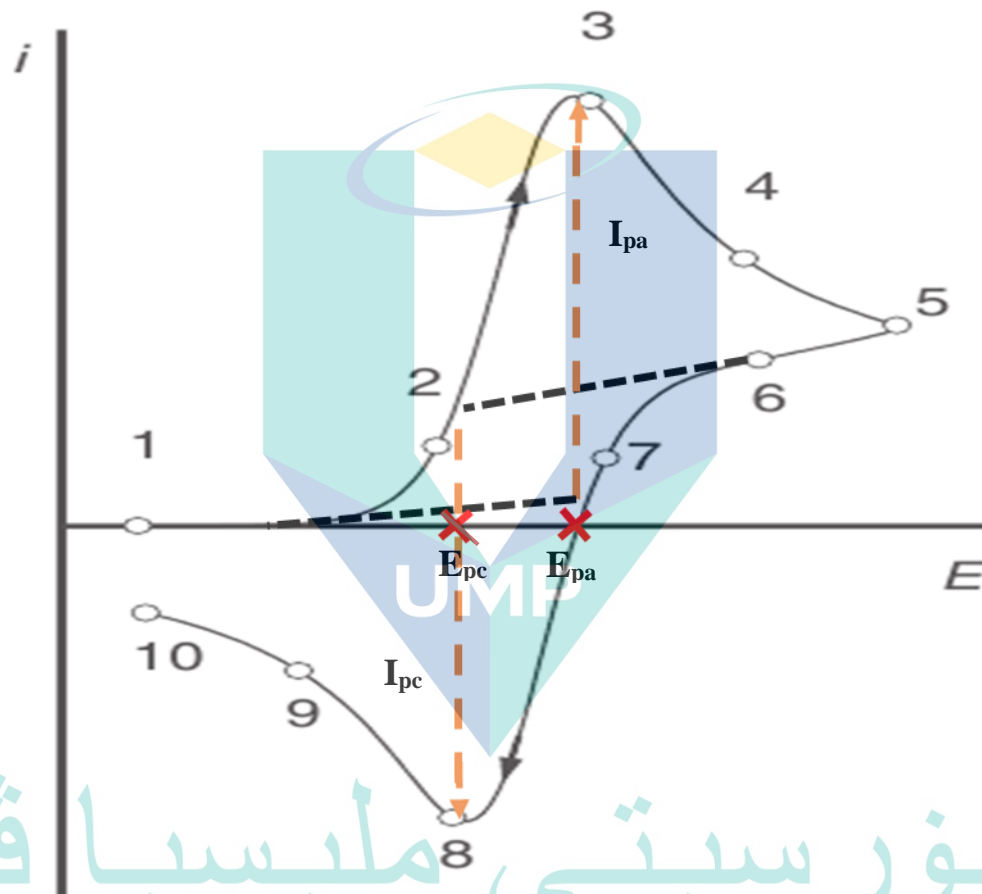


Figure 3.7 Cyclic voltammetry example with labels

Source: Zoski, (2006)

The analysis of the CV curve depends on the maximum anodic current, cathodic current and potential peak separation ( $\Delta E$ ). From Figure 3.7,  $I_{pa}$  is calculated from the difference between the intercept line from point 1 and point 3, while  $I_{pc}$  is calculated between the intercept line from point 6 and 8. The difference electrode potential,  $\Delta E_p$  is calculated from the difference between cathodic,  $E_{pc}$  and anodic potential,  $E_{pa}$  from the yield CVs. The peak separation of potential ( $\Delta E_p = E_{pa} - E_{pc}$ ), anodic (point 3) and



cathodic peak current (point 8) are used to estimate the reversibility of alizarin red S reaction in sulphuric acid. The lower the  $\Delta E_p$  indicates the faster electron transfer value. The ratio of the anodic and cathodic current provides information for the reversibility of the reaction. The diffusion rate, D is calculated using Randles-Sevcik equation, the steps are as follows:

$$i_p = 2.69 \times 10^5 n^3 S_A D^{\frac{1}{2}} C v^{\frac{1}{2}} \quad 3.1$$

For equation 3.1,  $i_p$  is known as the anodic peak of reduction peak of electroactive material and  $S_A$  is the electroactive surface area ( $0.2475 \text{ cm}^2$ ).  $V$  presented the scan rate performed for the investigation ( $\text{V s}^{-1}$ ),  $n$  is the number of electrons in the redox reaction and  $C$  is the selected concentration ( $\text{mol dm}^{-3}$ ) of the electroactive species at the electrode. According to Yang *et al.*, 2014 for quinone derivative such as ARS and BQ,  $n$  is 2 due to the two electrons. By substitute  $n = 2$ ,

$$i_p = 7.61 \times 10^5 S_A D^{\frac{1}{2}} C v^{\frac{1}{2}} \quad 3.2$$

After rearranging equation 3.2,

$$D = \left[ \frac{i_p}{7.61 \times 10^5 S_A C v^{\frac{1}{2}}} \right]^2 \quad 3.3$$

### 3.5.2 Electrochemical Impedance Spectroscopy

EIS is used to study the electrochemical properties of the modified surfaces and the internal chemical transformation. In this study, an electrical model has been fitted from EIS result. Parameters in fitted circuit represent the chemical reaction that occurred internally. This fitted parameter enables the researcher to understand or predict the factors that affect the redox reaction. Three important R-value represented three resistance are denoted as R1, R2 and R3 in these regions that are electrolyte, electrode-electrolyte interface and the electrode surface, as presented in Figure 3.8.

R1 represented the ohmic resistance in bulk electrolyte, R2 denotes as charge transfer resistance that occurred at the interface of the electrode material and the electrolyte, whereas R3 demonstrated the resistance that occurred on the electrode, such as the formed pores as illustrated in Figure 3.8. The high frequency range (MHz-kHz) involved ohmic resistance, polarization process and diffusion-related process, medium frequency range (>Hz) on faradaic reaction and low frequency range (<Hz) is referring to the diffusion and mass transport limitations.

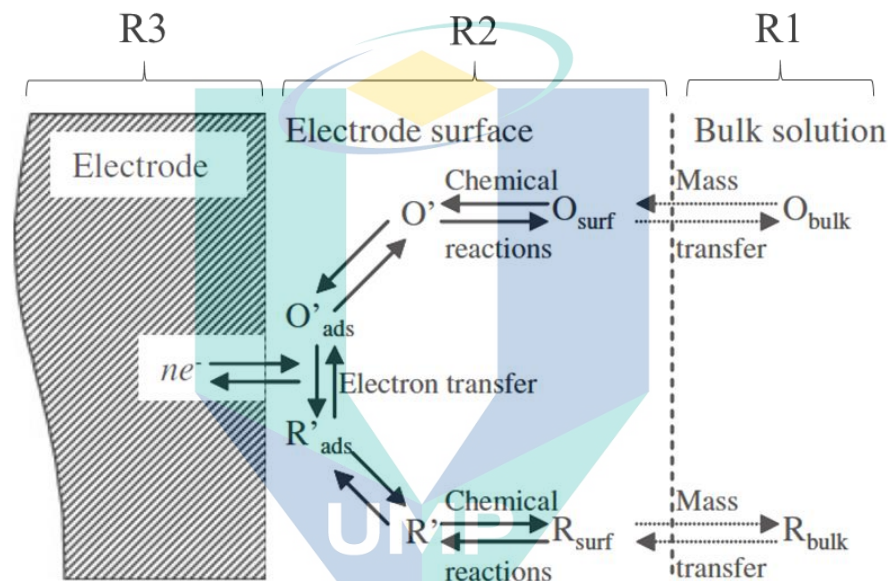


Figure 3.8 Process involved in electrode reaction in three states: bulk solution, electrode surface and electrode.

Source: Zoski, (2006)

### 3.6 Measurement Procedure

Two types of potentiostat used in this work, which are AUTOLAB (101N) and AUTOLAB (M101) with higher current setting ranging from 10 nA to 10 mA. The scan rate is conducted ranging from 10 mV s<sup>-1</sup> till 25 mV s<sup>-1</sup>. For CV measurements, the electrode potential was swept initially from 0 to 1.0 V vs. Ag|AgCl, and back to 0 V vs. Ag|AgCl in the reversed scan. For the negolyte studies, a three-electrode system is employed which glassy carbon electrode as working electrode (CHI 104) with an area of 0.2475 cm<sup>2</sup>, whereas platinum (CHI 115) and Ag/AgCl (CHI 111) were used as the counter and reference electrodes.

Glassy carbon electrode has been chosen as the working electrode for negolyte experiment to investigate the conductivity ion with respect to the concentration of ARS

in supporting electrolyte. Before the measurement, glass carbon electrode was polished with alumina and rinsed with de-ionized water to avoid contamination on the surface of electrode. The electrolyte volume of 25ml is used for the investigation, which three electrodes are dipped in the solution during the investigation.

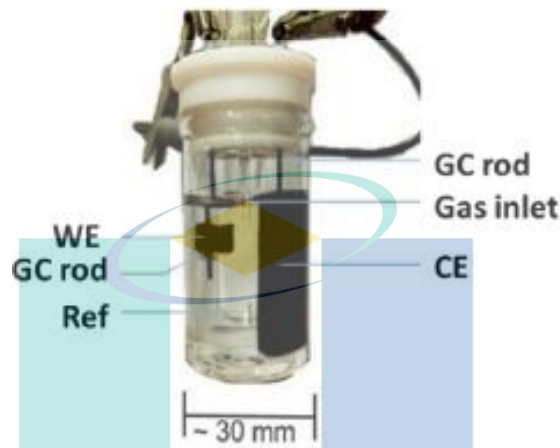


Figure 3.9 Three electrode system.  
Source: Derr *et al.* (2017)

For the treated felt investigation, the carbon felt sample is replaced the glassy carbon electrode as demonstrated in Figure 3.6. A piece of 0.25 cm × 0.25 cm x 0.6 cm (total area of 0.0375 cm<sup>3</sup>) is cut from 4 cm x 4 cm x 0.6 cm sample using a cutter tool with a platinum wire is used to hook up the felt as demonstrated in Figure 3.9. This setup was repeated with a different type of treated felt. A platinum wire and silver-silver chloride (Ag|AgCl) are employed as counter and reference electrodes, respectively. M101 with larger current range (10 nA to 10 mA) was used for felt investigation due to the higher surface area of felt.

For EIS, measurement using alternating current (AC) is used to induce the electrochemical reactions on the working electrode. The experimental setup consists of the potentiostat with AC impedance analyser, a solution, three electrode setup and computer to acquire data over a period. A small amplitude of AC signal will be used to predict the impedance evolution of electrode. An amplitude of 100mV at open circuit with frequencies ranging between 1 MHz and 0.1 Hz is selected for electrode-related investigation in this work. All measurements are completed at room temperature.

## CHAPTER 4

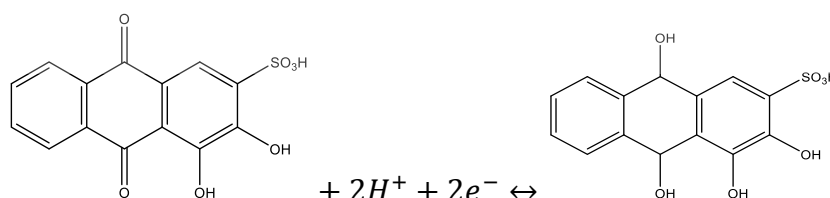
### RESULTS AND DISCUSSIONS

#### 4.1 Introduction

This chapter focuses on the discussion of experimental results conducted for achieving the pre-determined objectives. The first part is focusing on the electrochemical analysis of potential negolyte candidate i.e., ARS. A set of metrics such as diffusion coefficient, anodic current, cathodic current and reversibility of ARS in sulphuric acid are reported. The second part of this work presented the second objective that is to evaluate a novel two-stage surface treatment for porous electrode felt. The proposed surface-treated felts are evaluated using spectroscopy methods (i.e., FESEM, XPS and contact angle) and electrochemical measurement results are reported in this section. This chapter continued with the investigation of 2D electrode - glassy carbon electrode as reference for 3D porous electrode investigation. The selected acid with thermal treated electrode is used to investigate the effect of supporting acid on the redox reaction. The findings and discussion are concluded in the last section of this chapter.

#### 4.2 Electrochemical Measurement of Potential Negolyte Candidate - Alizarin Red S

In this study, a low-cost quinone-based electrolyte alizarin red s (ARS) organic dye is proposed to serve as the negative electrolyte reaction for organic redox flow batteries. ARS with two-electron transfer capability is one of the candidates as negative electrolyte for organic-based RFB. The redox peaks are attributed by the following reversible reaction as illustrated in 4.1.



4.1

Studies conducted by most of the literature are limited to  $0.1 \text{ mol dm}^{-3}$  -  $0.1 \text{ mol dm}^{-3}$  (Dadpou & Nematollahi, 2016; Tabor et al., 2019). With the oxidation and reduction characteristics of organic compounds such as ARS has been recently discussed, a preliminary study of its electrode reaction in acidic aqueous is investigated. The objective is to investigate the best composition of negative electrolyte that incorporates with ARS in higher concentrations of active material, three selected concentrations of 0.05, 0.10 and  $0.15 \text{ mol dm}^{-3}$  in  $1 \text{ mol dm}^{-3}$  sulphuric acid. Before the extension study on the effect of supporting acid, it is critical to identify ARS concentration with the highest redox reaction. The electrochemical properties for three selected concentrations were obtained for comparison. The comparison and discussion on the effect of ARS concentration were reported in 4.2.1.

Noted that several aspects have been considered ARS cathodic and anodic charge transfer processes such as (i) concentration of ARS (ii) concentration of supporting electrolyte. The work continued with the investigation on the effect of the concentration of supporting acid. The studies are conducted for two selected ARS concentrations, which are 0.05 and  $0.15 \text{ mol dm}^{-3}$  in higher sulphuric acid concentration of  $2.5 \text{ mol dm}^{-3}$ . The results and discussion for this purpose are reported in section 4.2.2.

#### 4.2.1 The effect of ARS Concentration

The electrochemical behaviour of the different active material concentration can be related to the concentration of active material. The important factor affecting conductivity of electrolyte in electrochemical process is the concentration of active material (charge carrier), where in this case of investigation ARS is the active material in supporting electrolyte combination. The first investigation was conducted to investigate the effect of ARS concentrations. First, the electrochemical properties of the ARS with respect to concentrations ranging from  $0.05 \text{ mol dm}^{-3}$  and  $0.15 \text{ mol dm}^{-3}$  in  $1 \text{ mol dm}^{-3}$  sulphuric acid are evaluated using glassy carbon electrode. As observed from CV results in Figure 4.1, the oxidation and reduction peaks for three selected samples lies in the increased potential trend, in which the electropositive potential,  $E_p$  of ARS is increase with the increased of active material concentration.

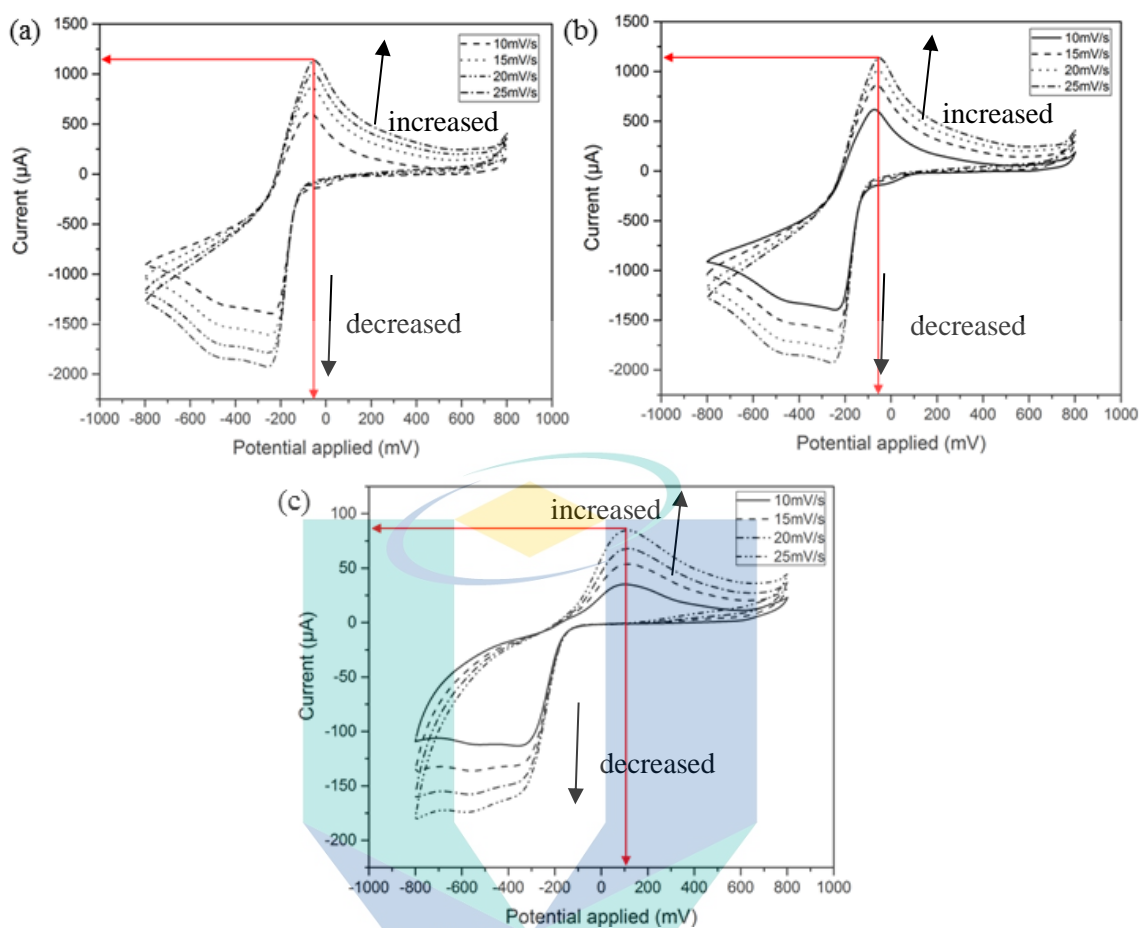


Figure 4.1 Cyclic voltammetry of (a)  $0.05 \text{ mol dm}^{-3}$  ARS (b)  $0.10 \text{ mol dm}^{-3}$  ARS (c)  $0.15 \text{ mol dm}^{-3}$  ARS in  $1 \text{ mol dm}^{-3}$  of  $\text{H}_2\text{SO}_4$  with scan rate ranging from  $10 \text{ mV s}^{-1}$  till  $25 \text{ mV s}^{-1}$ .

As can be seen in the displayed CVs in Figure 4.1, asymmetric shape with cathodic and anodic peak currents is obtained for all tested concentrations. The diffusion and transfer rate from the reversibility reaction of ARS are the reasons for the presented asymmetric shape CV. From the observation, the anodic peak currents,  $I_{pa}$  for  $0.05 \text{ mol dm}^{-3}$  ARS reached the highest of  $749.86 \mu\text{A}$ .  $0.10 \text{ mol dm}^{-3}$  ARS demonstrated a close value of  $731.96 \mu\text{A}$ , whereas the lowest anodic current is  $0.15 \text{ mol dm}^{-3}$  ARS with  $38.77 \mu\text{A}$ .

The study included the investigation for different scan rates that the cyclic voltammetry (CV) is performed for scan rates from  $10 \text{ mV s}^{-1}$  to  $25 \text{ mV s}^{-1}$ . Comparing the CV associated with increased scan rates, the presented results indicated that anodic current,  $I_{pa}$  linearly increases with the increase of scan rate, as shown in Figure 4.1. The results are supported by Randles-Sevcik equation (Equation 3.1), whereas the anodic

current,  $I_{pa}$  is directly proportional to the square root of scan rate. The shape of the CVs changes significantly when the mass transport overcomes the rate of electron transfer.

Regarding the active material concentration, a higher ARS concentration up to  $0.15 \text{ mol dm}^{-3}$  leads to decrease in cathodic and anodic peaks. This decrease is caused by the solubility limitation of ARS as mentioned in literature (S. Zhang et al., 2016). This suggests that the concentration of ARS concentration in  $0.05 \text{ mol dm}^{-3}$  demonstrated the highest peak in compared of higher concentration. The position of the anodic peak of ARS in higher concentration of  $0.15 \text{ mol dm}^{-3}$  slightly shifts towards the positive direction (111.41 mV) as per illustrate in cyclic voltammetry for  $25 \text{ mV s}^{-1}$  whereas the lowest concentration of ARS achieved  $-50.353 \text{ mV}$ . The results indicate that a higher concentration of ARS shows good reversibility, but low anodic and cathodic peak currents.

#### 4.2.2 The effect of Sulphuric Acid Concentration

Sulphuric acid normally chosen as the supporting electrolyte due to its strong oxidizing potential and acidity that contributed to the higher oxidation rate. To well understand the impact of supporting electrolyte concentration, two concentrations ( $1 \text{ mol dm}^{-3}$  and  $2.5 \text{ mol dm}^{-3}$ ) of sulphuric acid have been chosen in this study. By comparing Figure 4.1 and Figure 4.2, noted that the electrode potential,  $E^0$  of ARS slightly shifted to more positive value that this indicated the higher concentration of electron withdrawing group such as sulphonate group leading to an increase value of  $E^0$ . The difference manifest as CVs asymmetric about ARS redox potential, likely caused by different diffusion coefficients and rate constants for forward and reverse reactions.

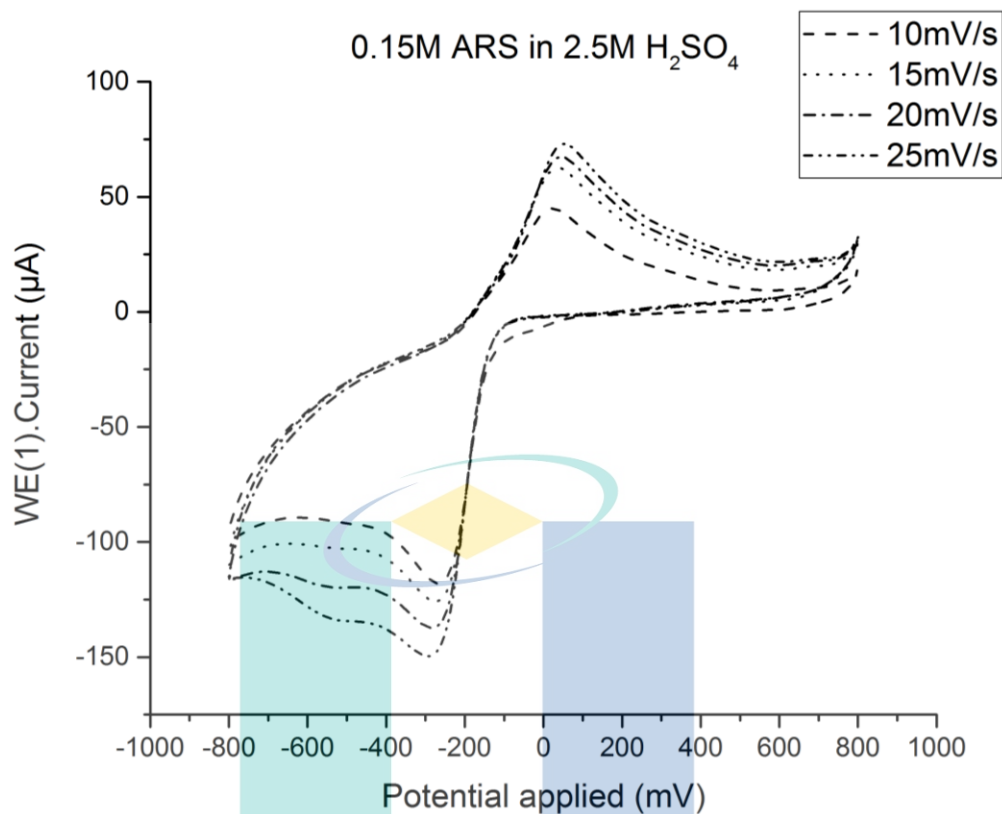


Figure 4.2 Cyclic voltammery of 0.15 mol dm<sup>-3</sup> ARS in 2.5 mol dm<sup>-3</sup> of H<sub>2</sub>SO<sub>4</sub> with scan rate ranging from 10 mV s<sup>-1</sup> till 25mV s<sup>-1</sup>

Figure 4.3 compared the electrolyte characteristic performed by varying with the concentration of H<sup>+</sup> and ARS concentration. Among three chosen solution concentrations, the highest concentration of 0.15 mol dm<sup>-3</sup> and lowest 0.05 mol dm<sup>-3</sup> were selected for investigating the effect of supporting acid concentration. By comparing the voltammery of the four solutions shown in Figure 4.3, the curve of 0.05 mol dm<sup>-3</sup> ARS in 1 mol dm<sup>-3</sup> H<sub>2</sub>SO<sub>4</sub> clearly illustrates the highest cathodic of 764.22 mA, whereas 0.15 mol dm<sup>-3</sup> ARS in 1 mol dm<sup>-3</sup> H<sub>2</sub>SO<sub>4</sub> achieves the highest value for anodic of -96.61 mA was presented of a scan rate of 10 mV s<sup>-1</sup>. The ionic conductivity of 1 mol cm<sup>-3</sup> H<sub>2</sub>SO<sub>4</sub> is 390 mS cm<sup>-1</sup> while 2.5 mol cm<sup>-3</sup> H<sub>2</sub>SO<sub>4</sub> >630 mS cm<sup>-1</sup> is reported by Ding et al., 2018. This indicated that higher concentration of sulphuric acid leads to a higher ionic conductivity.

Nevertheless, low diffusion rate is reported in this work due to the limited solubility of ARS. This statement is supported by the result reported in S. Zhang et al., 2016, which ARS has poor experimental stability. Therefore, the finding suggests that suitable modification on the chemical compound is necessary. The CV peak potential



separation ( $\Delta E_p$ ) for 0.05 mol dm<sup>-3</sup> ARS in 1 mol dm<sup>-3</sup> H<sub>2</sub>SO<sub>4</sub> of -173.35 mV as calculated diffusion rate is  $6.424 \times 10^{-4}$  cm<sup>2</sup> s<sup>-1</sup> with cathodic peak current of 749.86 mA at 10 mV s<sup>-1</sup> scan rate. This indicates that in the reaction of ARS, there is no significant improvement in higher sulphonate groups. The voltage potential of redox couples in high sulphonate concentration increases slightly compared to low concentration, but there is no significant difference in the oxidation peak for the solution.

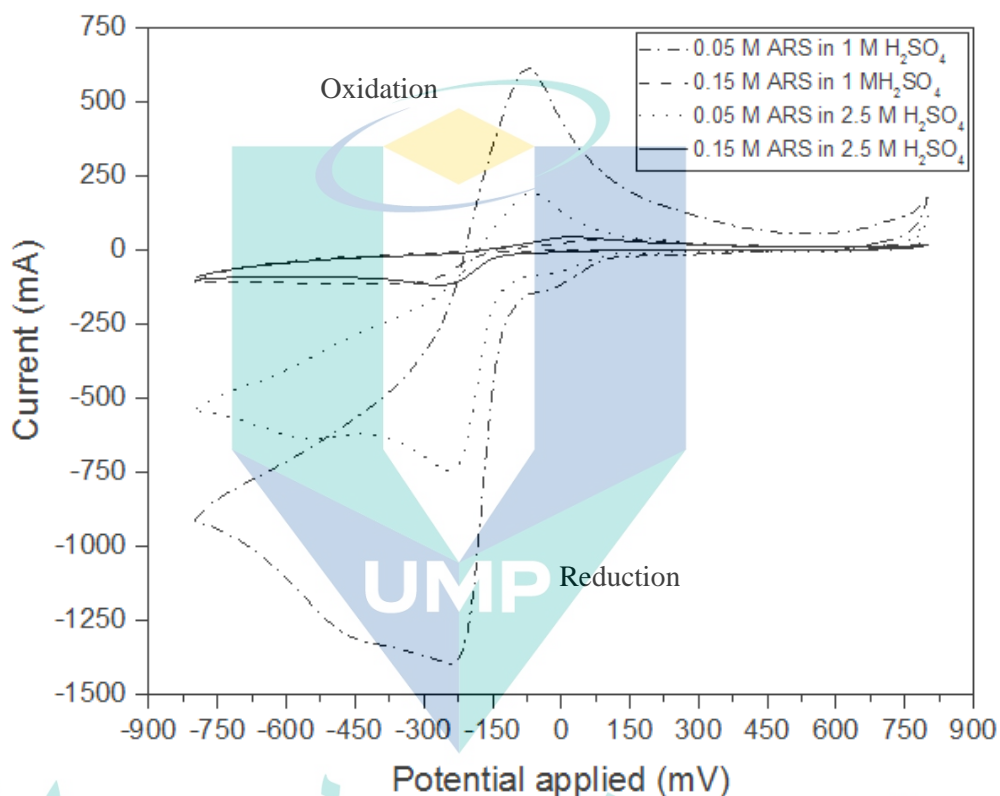


Figure 4.3 Cyclic voltammetry of 0.05 mol dm<sup>-3</sup> and 0.15 mol dm<sup>-3</sup> ARS in different concentrations (i.e. 1 mol dm<sup>-3</sup> and 2.5 mol dm<sup>-3</sup>) of H<sub>2</sub>SO<sub>4</sub> with scan rate of 10 mV s<sup>-1</sup>

For similar scan rate of 10 mV s<sup>-1</sup>, CV peak potential separation ( $\Delta E_p$ ) for ARS at a higher concentration of 2.5 mol dm<sup>-3</sup> H<sub>2</sub>SO<sub>4</sub> of -191.06 mV and the diffusion rate of  $4.677 \times 10^{-7}$  cm<sup>2</sup> s<sup>-1</sup>. Both diffusion rates are faster compared to Zhang et al., which has calculated diffusion values of  $2.14 \times 10^{-6}$  cm<sup>2</sup> s<sup>-1</sup> for 1m mol dm<sup>-3</sup> (S. Zhang et al., 2016). The result indicated that the diffusion of ARS depends on the supporting acid concentration and solubility in base electrolyte. The average peak separation in cyclic voltammetry of ARS is -273.9 mV, which is lower than 59 mV/n (where n is 2) showing ARS undergoes multi-electron quasi-reversible process (S. Zhang et al., 2016). This

indicated a higher concentration of ARS allow faster ion diffusion and higher electrochemical kinetics activity in the redox reaction.

By referring to Table 4.1, 0.05 mol dm<sup>-3</sup> ARS achieved higher anodic current and higher diffusion coefficient as compared to 0.15 mol dm<sup>-3</sup> ARS. The diffusion coefficient ratio (D) of the electron was calculated and tabulated in Table 4.1 by using Randles-Sevcik equation. Nevertheless, the limitation of ARS solubility causing low anodic and diffusion rate for 0.15 mol dm<sup>-3</sup>. The comparison for two concentrations of ARS is reported in Table 4.1. Table 4.1 indicate the measure and calculate value for investigated solution. Therefore, the electrochemical activity of ARS is best demonstrated in 0.05 mol dm<sup>-3</sup>. Moreover, it was observed that the higher anodic current, I<sub>pa</sub> can be achieved at a higher concentration of supporting acid. This is due to the ionic conductivity is linearly increased with the concentration of sulphuric acid. The result indicated that the diffusion rate for a higher concentration of ARS is lower compared to low concentration of ARS, which resulted in the limitation of ARS solubility. This happens due to the decrease in mass transport, which contributed to the increase in the viscosity of the electrolyte.

Table 4.1 Measured data for 0.05 mol dm<sup>-3</sup> and 0.15 mol dm<sup>-3</sup> ARS in 1.0 mol dm<sup>-3</sup> and 2.5 mol dm<sup>-3</sup> of H<sub>2</sub>SO<sub>4</sub> in terms of anodic current (I<sub>pa</sub>), cathodic current (I<sub>pc</sub>), calculated potential (E<sub>p</sub>) and diffusion value.

ARS, mol dm <sup>-3</sup>	H <sub>2</sub> SO <sub>4</sub> , mol dm <sup>-3</sup>	I <sub>pc</sub> , mA	I <sub>pa</sub> , mA	I <sub>pa</sub> /I <sub>pc</sub>	E <sub>pc</sub> , mV	E <sub>pa</sub> , mV	*ΔE <sub>p</sub>	*Diffusion Value, cm <sup>2</sup> s <sup>-1</sup>
0.05	1.0	-1193.4	749.86	0.63	-245.83	-72.48	-173.35	6.424 x 10 <sup>-4</sup>
0.15	1.0	-96.61	38.77	0.40	-350.21	93.48	-443.69	2.045 x 10 <sup>-4</sup>
0.05	2.5	-675.34	260.57	0.38	-248.97	-57.91	-191.06	4.677 x 10 <sup>-7</sup>
0.15	2.5	-109.28	49.80	0.46	-267.21	20.52	-287.73	5.985 x 10 <sup>-7</sup>

\*calculated value

### 4.3 Evaluation of Carbon Felt with Two-Stage Treatment

The essential power density for RFB is the active site for redox reaction, the electrode felt holds the ideal characteristics of providing active sites for redox reaction without interfere in the electrolyte interaction between both sides. With the intention to reduce charge transfer and increase the mass transfer between the electrode and electrolyte interface, the ideal electrode must have high surface area, chemically stable

in acidic environment and must process good charge transfer towards the positive electrolyte reaction for ORFB.

Furthermore, surface modification on felt with respect to achieve low charge transfer resistance on high surface area of carbons is presented. The characterisation and electrochemical investigation on (a) hydrogen peroxide with thermal treated carbon felt and (b) sodium hydroxide with thermal treated carbon felt are presented in Figure 4.4.

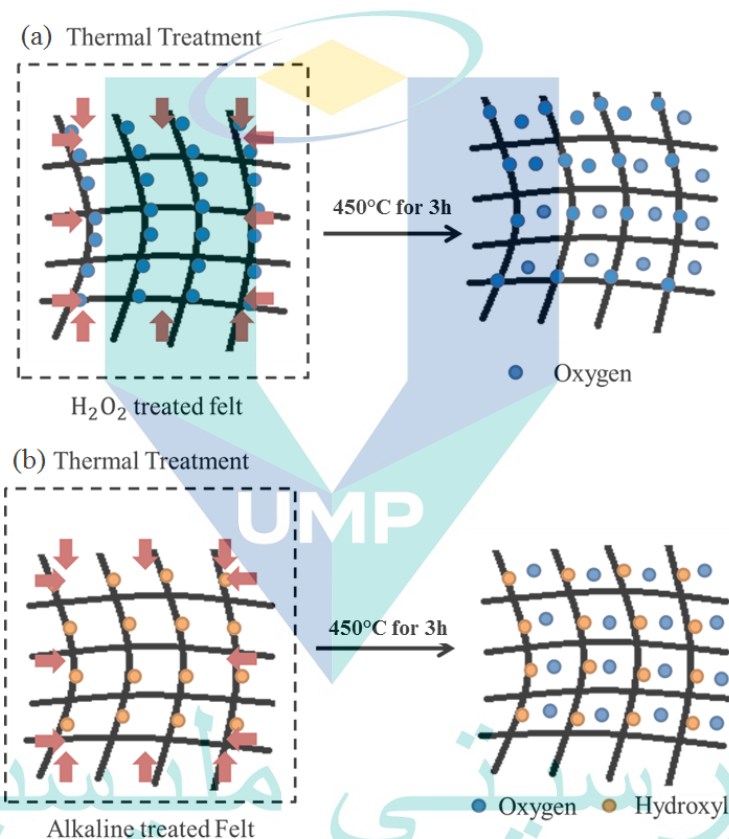


Figure 4.4 Two-stage treated felt (a) hydrogen peroxide with thermal (b) sodium hydroxide with thermal.

#### 4.3.1 FESEM Surface Topology Analysis

An investigation of the surface properties of the untreated electrode has been performed in Figure 4.5. The results show the surface morphology observed by SEM and FESEM for untreated felt. From observation in Figure 4.5, the surface of the raw felt with evident debris (in red circle) before applying to any surface treatment, which caused untreated felt suffered from hydrophobic characteristics.

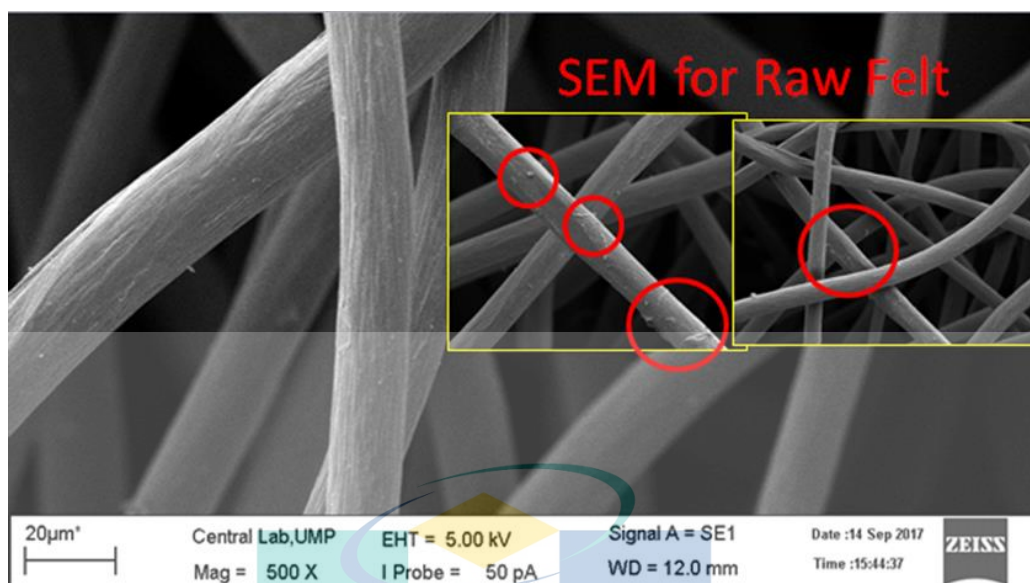


Figure 4.5 Morphology characterization for SEM image for raw felt with magnification of x500

To further investigate the debris on the surface of untreated felt, this study continues to capture a higher resolution image using FESEM. High resolution image is captured using FESEM machine with x5k and x15k magnification. The surface topology of untreated carbon felt obtained from FESEM is shown in Figure 4.6. As shown in Figure 4.6a to d, there is few surface contaminations on the surface of felt. The contaminated surfaces shown are the reason that surface treatment is required. The contaminated particle such as oil grease on the surface is mainly because of the manufacturing process of carbon felt. Felt suffered from low electrochemical activity (i.e., hydrophobic characteristics) and poor reversibility towards quinone redox reaction is one of the challenges faced in research.

Unfavourable hydrophobic surface decreased the mass/ion transport by surface diffusion and viscous flow on porous electrode. Poor kinetic reversibility in electrochemical activity is owing to low surface area resulting in high ohmic and charge transfer losses, whereas felt acts as the redox reaction sites in charge–discharge. To remove debris (in red circle), the felt is subjected to undergo pre-treatment or surface modification. To investigate the effect of two-stage treatment on the surface of the electrode, FESEM studies are conducted for sodium hydroxide with thermal, hydrogen peroxide with thermal and sulphuric acid with thermal treated felt.

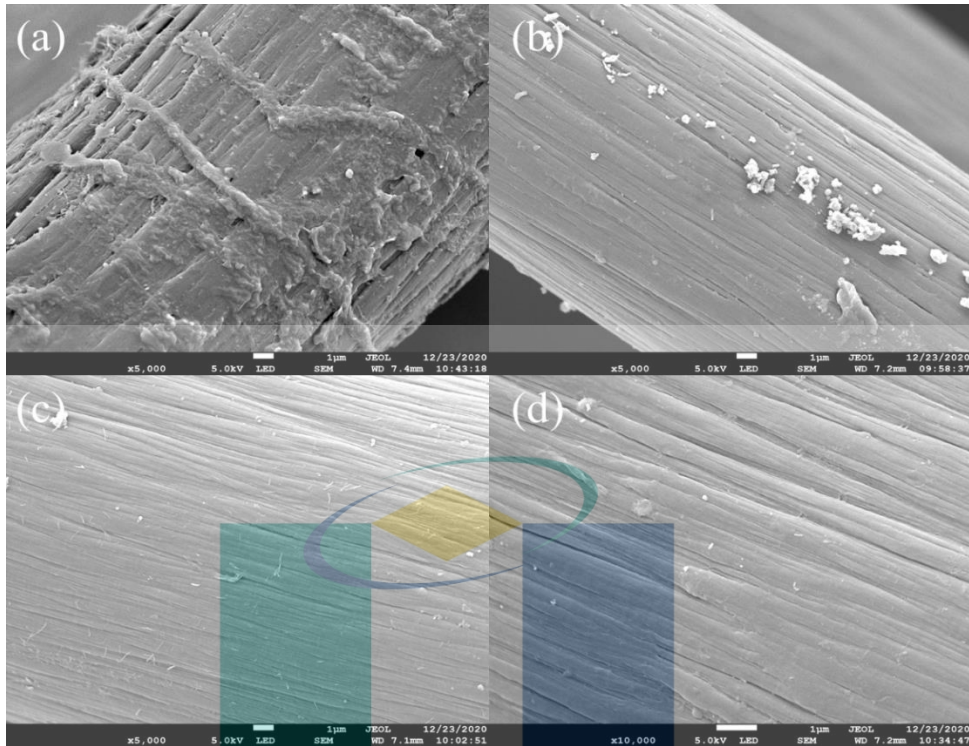


Figure 4.6 FESEM images with magnification x5k for untreated carbon felt.

Figure 4.7a-b presented surface morphology observed by FESEM for sodium hydroxide with thermal treated felt, as well as hydrogen peroxide with thermal treated felt in Figure 4.7c-d. By comparing Figure 4.7a and b, the surface structure of sodium hydroxide with thermal treated felt changes, while hydrogen peroxide with thermal treated felt maintains the felt. For the felt involving sodium hydroxide treatment (Figure 4.7a and Figure 4.7b), a rougher surface containing holes in the 50 – 100 nm is observed on the surface of the fibres (Figure 4.7b). These surface holes are expected to increase the effective surface for the electrode/electrolyte interaction as reported in numerical studies that pore size distribution with the porosity effect will significantly affect the current distribution (Ma et al., 2018). In contrast, Figure 4.7c and Figure 4.7d shows that the carbon felt sample treated by hydrogen peroxide had a similar morphology before modification (as pristine sample) and exhibit a smoother surface than the carbon felt treated by sodium hydroxide.

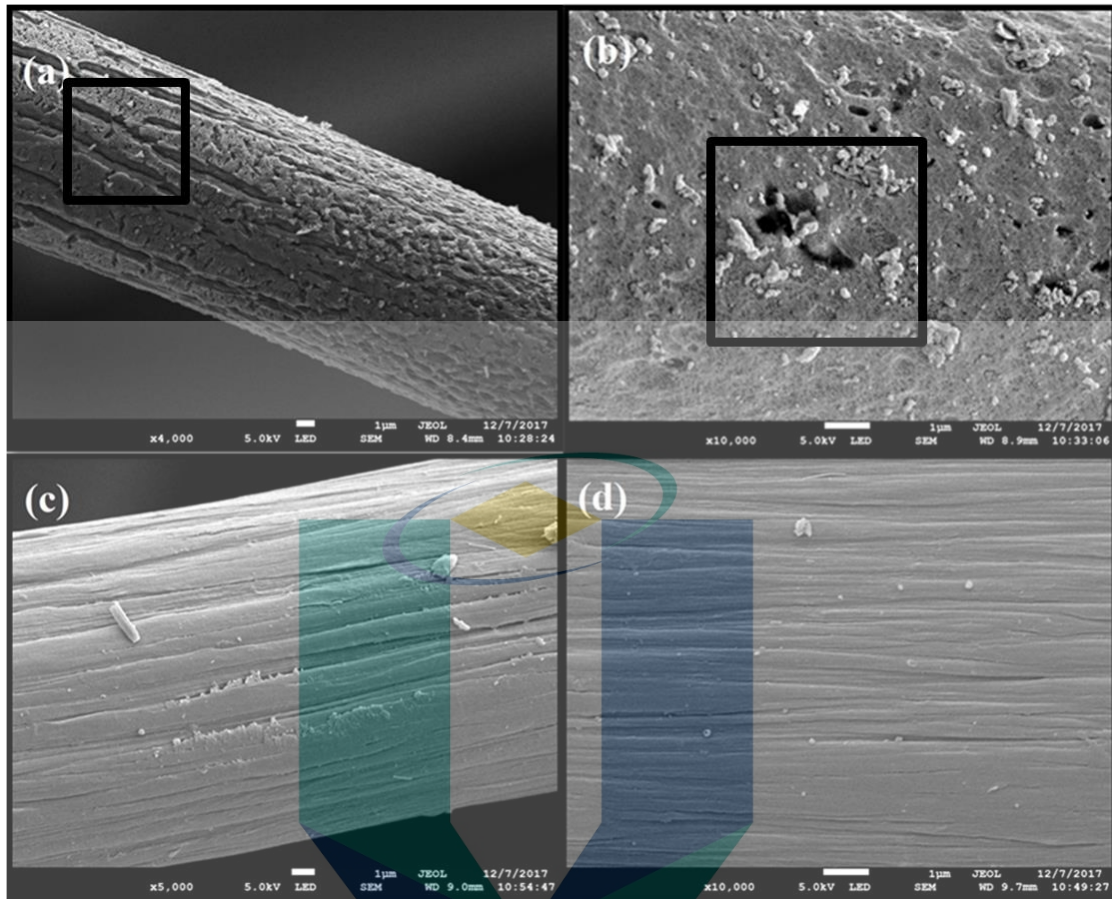


Figure 4.7 FESEM images with magnification x5k and x10k for surface modification (a, b) NaOH with thermal treated felt, (c, d) hydrogen peroxide with thermal treated felt

After undergoing the proposed two-stage surface treatment, the micropores are formed (as illustrated in Figure 4.8a and b) on the surface of acid with thermal treated felt. Compared to untreated felt with debris as display in Figure 4.6 and Figure 4.5, acid with thermal treated felt,  $\text{CF}_{\text{H}_2\text{SO}_4}$  displayed a cleaner surface. The micropores formed on the surface of felt are smoother than sodium hydroxide with thermal treated felt (please refer to Figure 4.7). Pristine carbon felt with total surface area is  $21.1059 \text{ m}^2 \text{ g}^{-1}$ ,  $61.8433 \text{ m}^2 \text{ g}^{-1}$  for sodium hydroxide with thermal treated felt and hydrogen peroxide with thermal treated carbon felt is  $49.3928 \text{ m}^2 \text{ g}^{-1}$ .

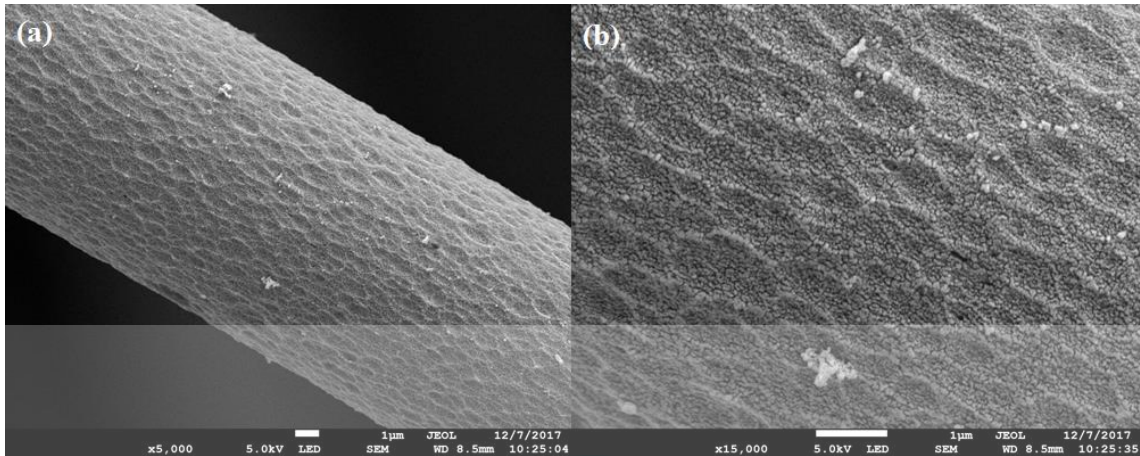


Figure 4.8 FESEM images with magnificant of (a) x5k (b) x15k for surface modification of sulphuric acid with thermal treated felt.

#### 4.3.2 X-ray Photoelectron Spectroscopy (XPS) Spectrum Studies

The FESEM technique is limited the topology of the felt surface, it is important to investigate the surface composition and functional groups present. To identify the existence of the functional group on the felt surface, XPS analysis is conducted for the treated carbon felts with sodium hydroxide and hydrogen peroxide treatments ( $CF_{NaOH}$  and  $CF_{H_2O_2}$ ). In addition to larger surface area (rougher morphologies as seen in Figure 4.7a and Figure 4.7b), this can be affected by the catalytic properties of functional groups created in the treatment processes as well as the wettability of the resulting electrodes.

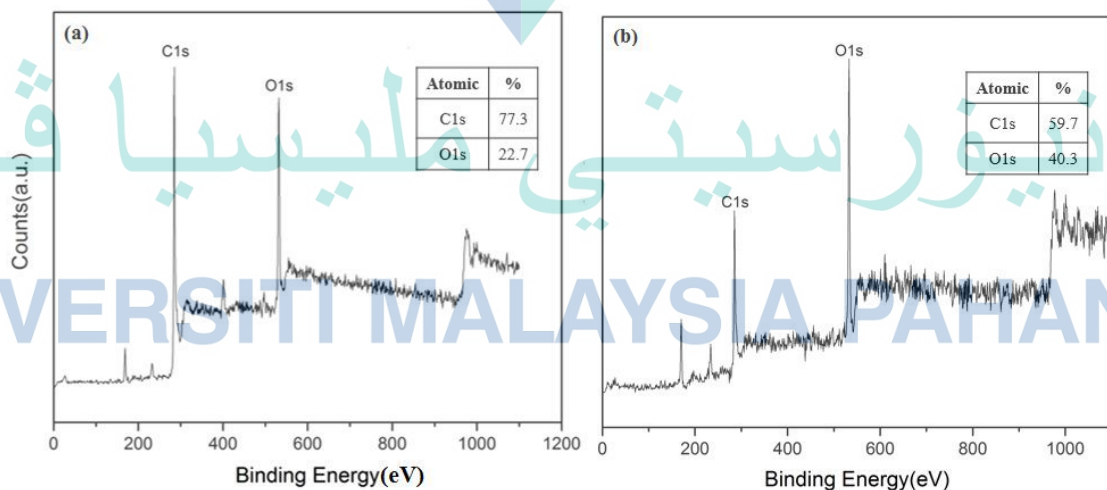


Figure 4.9 The XPS wide scan of (a)  $H_2O_2$  with thermal treatment and (b)  $NaOH$  with thermal treatment treated felt.

As seen in XPS wide scan spectrum (in Figure 4.9), there are two obvious peaks which are C1s and O1s after both treatments. The corresponding elemental content of the samples listed in Table 4.2. The results show that the obvious difference in the oxygen content among the samples, which CF<sub>NaOH</sub> has higher oxygen content compared to CF<sub>H2O2</sub>.

Table 4.2 Surface composition CF<sub>H2O2</sub> and CF<sub>NaOH</sub> for from XPS (atomic %).

Sample	Carbon %	Oxygen %
CF <sub>H2O2</sub>	77.3	22.7.
CF <sub>NaOH</sub>	59.7	40.3

The XPS peaks are fitted using Gaussian-Lorentzian curves. As shown in Figure 4.10(a), for the case of CF<sub>H2O2</sub> carbon felt, C1s spectra can be deconvoluted into 3 fitted peaks that the binding energies are in the range of 284 – 286 eV, corresponding to graphitic sp<sup>2</sup> C–C (285 eV) (O. Di Blasi et al., 2015), sp<sup>3</sup> C=C (284.2 eV) (O. Di Blasi et al., 2015) and C–O (286 eV) (M. Park et al., 2013). Oxygen functional groups are found in these treated samples, as presented in the O1s spectra for CF<sub>H2O2</sub> (Figure 4.10c) and CF<sub>NaOH</sub> (Figure 4.10d).

The spectrum of CF<sub>NaOH</sub> sample in O1s peaks can be deconvoluted into four peaks, which refer to aliphatic C–OH (531 eV), C=O (532 eV), C–O (534 eV) (K. J. Kim et al., 2011) and C–C=O (532.9 eV). The abundance of oxygen containing group, e.g., hydroxyl in CF<sub>NaOH</sub> serves as redox reaction sites as it exhibits high reversibility, which serves as liquid carriers of hydrogen in liquid electrolyte (P Leung et al., 2017; M. Park, Ryu, Wang, & Cho, 2017) compared to CF<sub>H2O2</sub>. Similarly, the spectrum of CF<sub>H2O2</sub> exhibits three peaks revealing the presences of C=O (532 eV), C–O (534 eV) and C–C=O (532.9 eV) functional groups.



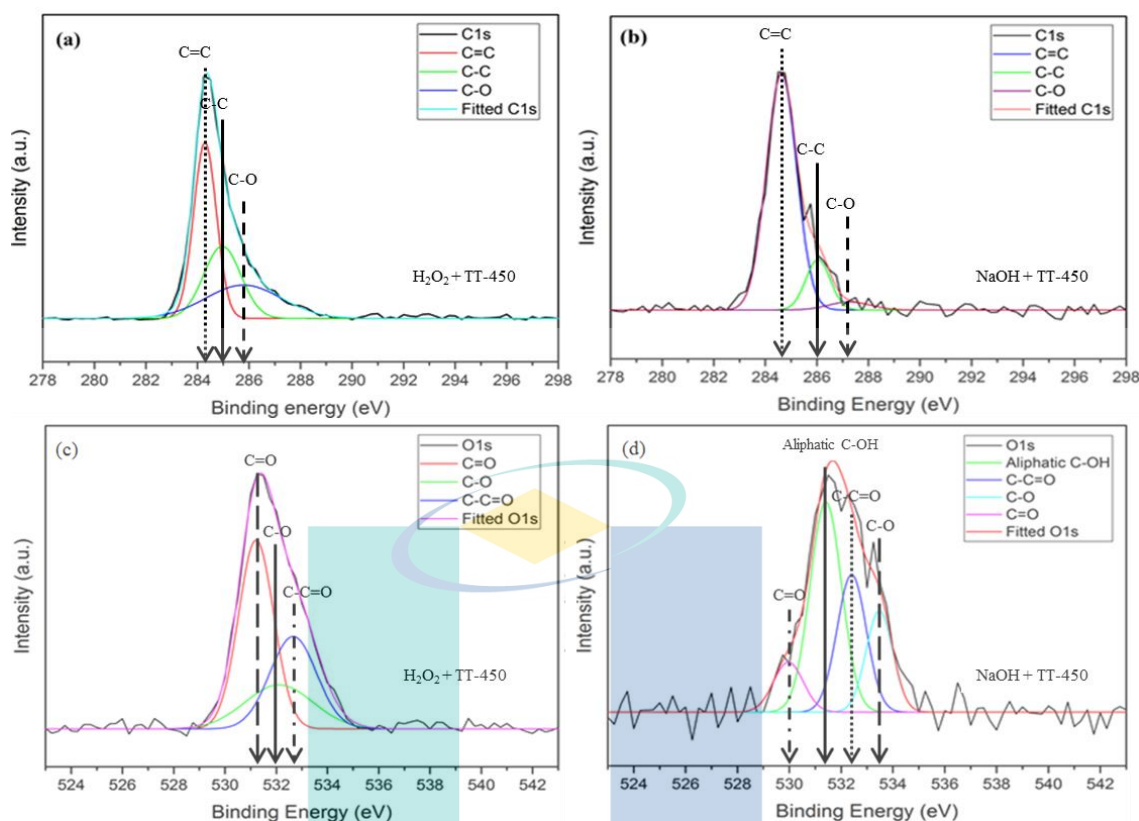


Figure 4.10 XPS curve fitting of (a) C1s spectra and (c) O1s spectra of  $H_2O_2$  with thermal treatment and (b) C1s spectra and (d) O1s spectra of NaOH with thermal treatment.

The ratios for these peaks in C1s are reported in Table 4.3. The result shows that the composition of C-O in the hydrogen peroxide treated sample (27.40%) is higher than that 3.82% of sodium hydroxide. It can be seen that  $CF_{NaOH}$  shows graphitic carbon peak (C=C) of 82.06% at 284.3 eV and  $sp^3$  C-C appeared at 286 eV (ZH Zhang, Zhao, Bai, Zeng, & Wei, 2017).

Table 4.3 Element composition ratio of carbon and oxygen functional groups of  $CF_{NaOH}$  and  $CF_{H_2O_2}$  on C1s and O1s XPS curve fitted spectra.

	C1s peak				O1s peak		
	C=C	C-C	C-O	C=O	C-O	C-C=O	Aliphatic C-OH
$CF_{H_2O_2}$	43.60	29.05	27.40	47.65	21.44	30.91	N. A.
$CF_{NaOH}$	82.06	14.12	3.82	10.02	18.23	27.08	44.67

### 4.3.3 Contact Angle Measurement

The formation of these functional groups is expected to improve the hydrophilic properties of carbon felt electrode, which enables more effective access of the electrolytes into the porous structures and results in larger active surface areas for battery reactions. The insertion of the functional group has been presented and discussed in section 4.3.2, however, the result shown only the percentages of the functional group. Therefore, the influences of these functional groups on wettability characteristics are further studied with the combination of the contact angle measurement and water droplet method as shown in Figure 4.11. Before surface modification, pristine carbon felt is highly hydrophobic, with a contact angle of up to  $128^\circ$  (Figure 4.11a). The water contact angle,  $\theta$  on the pristine carbon felt surface showed  $>120^\circ$ , which indicated hydrophobic characteristics.

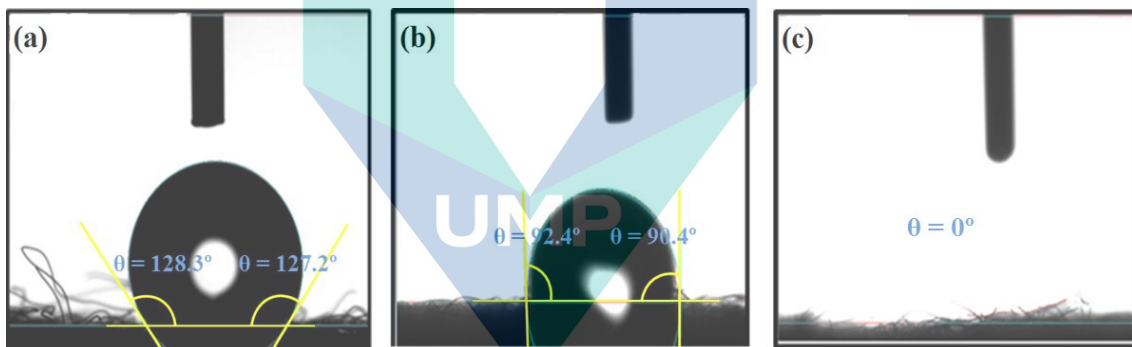


Figure 4.11 The contact angle measurement using water droplets on (a) pristine carbon felt (b)  $\text{H}_2\text{O}_2$  with thermal treatment and (c)  $\text{NaOH}$  with thermal treatment.

Alternatively, this property has been improved after the surface treatments used in this work. For instance, hydrogen peroxide and thermally treated carbon felt ( $\text{CF}_{\text{H}_2\text{O}_2}$ ) with initial droplet contact angle of  $92.4^\circ$  and  $90.4^\circ$  are shown in Figure 4.11. The water is then absorbed completely into the felt structure after 0.5 min (Figure 4.11b). The results indicated a better hydrophilic characteristic displayed by  $\text{CF}_{\text{NaOH}}$  as from the contact angle measurement by using water,  $\text{CF}_{\text{NaOH}}$  absorbed the water directly after the water drop touch on the surface.

This phenomenon is attributed to the high content of highly hydrophilic C–OH and C=O group as determined in the XPS study (Figure 4.10c and d). The immediate absorption of water in treated felt observed in contact angle measurements, signifying the improved hydrophilicity of electrodes with the proposed treatment. According to Pasala *et al.*(2018), improved hydrophilicity properties reduce electrical resistance, improve the mass transport of the active species, consequently, increase the electron kinetics between electrode-electrolyte (Pasala, Ramavath, He, Ramani, & Ramanujam, 2018).

#### 4.4 Electrochemical Investigation for 2D Electrode in Positive Electrolyte

In this section, the analysis for comparing the effect of different supporting acid is presented. The electrolyte composition is one of the parameters that determined the capacity of RFB. The ionic conductivity of the electrolyte affected the electrode reaction kinetics and the resistance of the battery. This work present cyclic voltammetry investigation involving glassy carbon electrode in BQDS as reference. The cyclic voltammograms of 1,4-benzoquinone solution are measured using a glassy carbon electrode with scanning rates ranging from 2 to 10 mVs<sup>-1</sup>. The CVs illustrated in Figure 4.12 have shown two proton-electron peaks as one at the positive and another lies at a negative potential. These peaks correspond to the electrochemical formation of 1,4-benzoquinone. As the potential is scanned cathodically, peak cathodic current ( $I_{pc}$ ) is observed in which the current is distributed by the delivery of BQ ion via diffusion from the bulk solution. As the time passed the diffusion layer becomes thicken and this slow down the diffusion of BQ ion to the surface of the electrode, as this has decreased cathodic current as the scan continued. The peak cathodic current ( $I_{pc}$  for pristine felt is decreasing from -0.052 A to -0.171 A with an increase in scan rates.

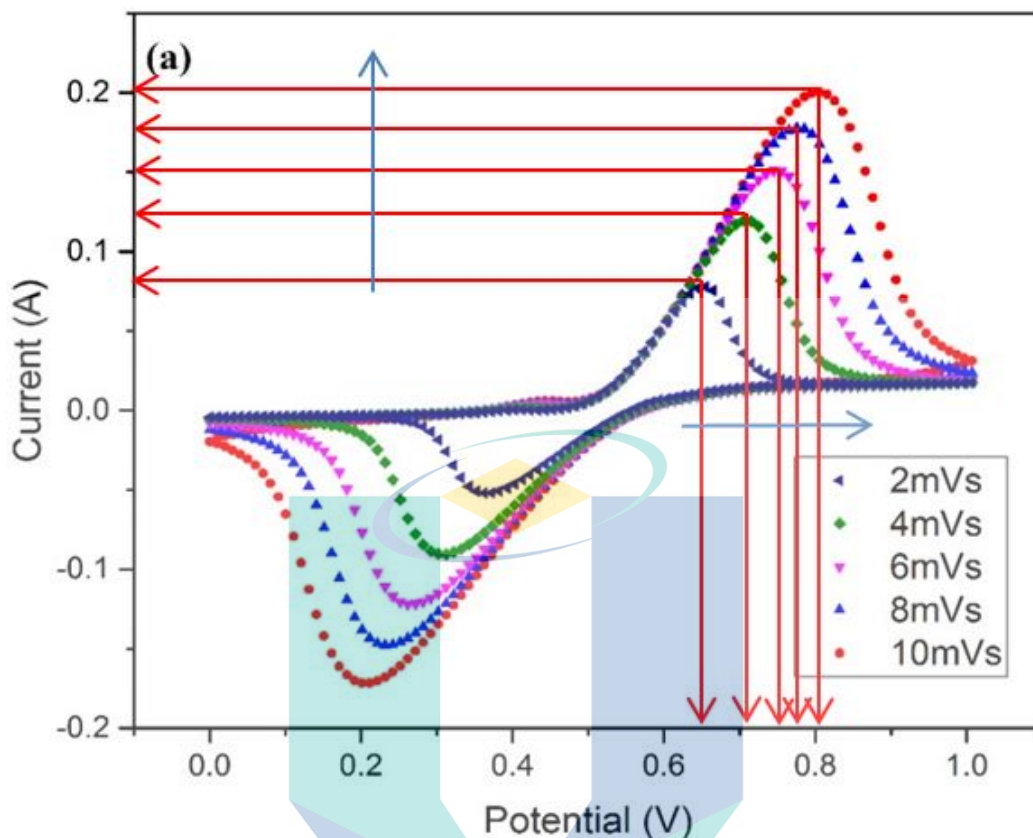


Figure 4.12 The experimental CV of glassy carbon electrode in  $0.1 \text{ mol dm}^{-3}$  1,4-benzoquinone in  $1 \text{ mol dm}^{-3}$  of  $\text{H}_2\text{SO}_4$  with range of scan rate from  $2 \text{ mV s}^{-1}$  till  $10 \text{ mV s}^{-1}$

In this part of work, 2D electrode glassy electrode carbon is used. Cyclic voltammetry was performed in of  $2 \text{ mV s}^{-1}$  to  $10 \text{ mV s}^{-1}$  displayed an increase in anodic current ( $I_{pa}$ ) from  $0.078 \text{ A}$  to  $0.200 \text{ A}$ . The calculated results are tabulated in Table 4.4 that the potential separation sequence is  $10 \text{ mV s}^{-1} > 8 \text{ mV s}^{-1} > 6 \text{ mV s}^{-1} > 4 \text{ mV s}^{-1} > 2 \text{ mV s}^{-1}$ . Electrode potential,  $\Delta E_a$  is the difference between anodic and cathodic potential, the reversibility of treated felt at the scan rate of  $10 \text{ mV s}^{-1}$  is considered poor when  $\Delta E_a$  is approximately  $0.605 \text{ V}$ , whereas  $|I_{pa}/I_{pc}|$  is larger than 1. Overall, the cyclic voltammetry projected in Figure 4.12 presented  $C_rE_r$  mechanism. The definition of C is a homogeneous chemical reaction, and E indicated electron transfer step and subscript r represent reversibility. In the  $C_rE_r$  mechanism, the selected redox couple undergoes reversible chemical reaction.

Table 4.4 Electrochemical parameters with respect to cathodic and anodic (current, voltage, ratio) of glassy carbon electrode in 0.1 mol dm<sup>-3</sup> 1,4-benzoquinone + 1.0 mol dm<sup>-3</sup> of H<sub>2</sub>SO<sub>4</sub> in terms of anodic current (I<sub>pa</sub>), cathodic current (I<sub>pc</sub>) and potential (E<sub>p</sub>)

Scan rate, mV/s	I <sub>pa</sub> , A	I <sub>pc</sub> , A	E <sub>pa</sub> , mV	E <sub>pc</sub> , mV	ΔE <sub>a</sub> , mV	I <sub>pa</sub> /I <sub>pc</sub>
2	0.078	-0.052	0.655	363	0.292	1.50
4	0.119	-0.090	0.705	312	0.393	1.32
6	0.151	-0.121	0.745	262	0.483	1.24
8	0.178	-0.147	0.775	232	0.543	1.27
10	0.200	-0.171	0.806	201	0.605	1.17

#### 4.5 Electrochemical Studies for Modified 3D Electrode

This section presented electrochemical studies of the proposed two-stage treated felt by using cyclic voltammetry and electrochemical impedance spectroscopy. The result for pristine felt, hydrogen peroxide with thermal and sodium hydroxide with thermal treated felts is compared in this section. The CV result discussed the on the highest achieved anodic, cathodic current and the achieved potential. The work extended to electrochemical impedance spectroscopy investigation to further elucidate the effect of the proposed treatment for the electrode.

In this study, a 3D porous electrode is used in which diffusion happens to the exchange of electrolyte inside the electrode. The modified felts are further evaluated in 0.1 mol dm<sup>-3</sup> 1,4-benzoquinone with 1 mol dm<sup>-3</sup> sulphuric acid, H<sub>2</sub>SO<sub>4</sub>. In this study, one of the quinone derivatives which consist of one benzene ring - 1, 4-benzoquinone is selected with the working environment presented in concentration of 0.1 mol dm<sup>-3</sup> and 1 mol dm<sup>-3</sup> of sulphuric acid, H<sub>2</sub>SO<sub>4</sub>.

##### 4.5.1 Cyclic Voltammetry (CV)

To investigate the kinetics of the redox reactions of these treated carbon felts, together with the pristine were presented in terms of redox potential, peak separation and peak current (anodic and cathodic current) are illustrated in Figure 4.13. Two pairs of distinct reversible peaks were observed in both electrodes, demonstrating the two proton and two electron-transfers for the typical quinone/1,4-benzoquinone reaction. As observed from the CV result, the oxidation peaks for three samples are in this order pristine felt < CF<sub>H2O2</sub> < CF<sub>NaOH</sub>.

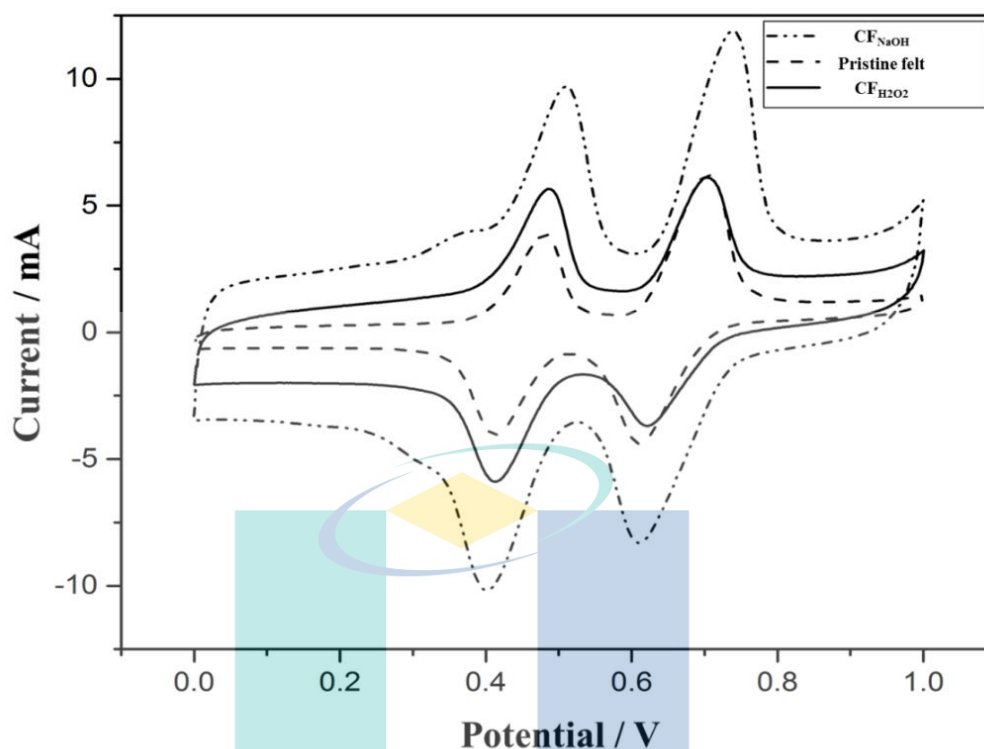


Figure 4.13 Cyclic voltammograms of pristine felt,  $\text{H}_2\text{O}_2$  with thermal and NaOH with thermal treated felt in  $0.1 \text{ mol dm}^{-3}$  1,4-benzoquinone +  $1 \text{ mol dm}^{-3}$   $\text{H}_2\text{SO}_4$  at scan rate of  $20 \text{ mV s}^{-1}$ .

Noted that  $\text{sp}^3$  bonding for  $\text{CF}_{\text{NaOH}}$  (in Table 4.3) is higher compared to  $\text{CF}_{\text{H}_2\text{O}_2}$  and pristine felt, the reversibility of  $\text{CF}_{\text{NaOH}}$  is lower owed to the stable and non-conductive  $\text{sp}^3$  bonding slower the electron transfer of the redox reaction process. In compare with pristine felt and  $\text{CF}_{\text{NaOH}}$ ,  $\text{CF}_{\text{H}_2\text{O}_2}$  exhibited the highest electrocatalytic activity towards anodic and cathodic redox reaction at second peak of CV. This is proven by showing the highest redox potential at second peak ( $0.622 \text{ V}$ ) and good kinetic reversibility as the result shows a lower peak to peak separation ( $\sim 82 \text{ mV}$ ) at the second peak indicating reduction in mass transport and charge transfer resistance resulted from the improved hydrophilic characteristics of hydrogen peroxide treated felt. Among these samples, the carbon felt with sodium hydroxide ( $\text{CF}_{\text{NaOH}}$ ) is observed to have the highest current output.

Table 4.5 indicated that pristine felt demonstrated the best reversibility in redox reaction. Pristine carbon felt material is found to be the most promising positive electrode material due to its low material cost and high reversibility towards both electrolytes (ARS and 1,4-benzoquinone), nevertheless, the hydrophobic characteristics of felt may cause excessive resistance and required more time to achieve the equilibrium of electrolyte circulation in flow battery compartment.

Table 4.5 Electrochemical parameters with respect to cathodic and anodic (current, voltage, ratio) of CF<sub>NaOH</sub> and CF<sub>H<sub>2</sub>O<sub>2</sub></sub> carbon felt.

Type	I <sub>pc</sub> , mA		I <sub>pa</sub> , mA		E <sub>pc</sub> , mV		E <sub>pa</sub> , mV		ΔE		I <sub>pa</sub> /I <sub>pc</sub>	
	1 <sup>st</sup>	2 <sup>nd</sup>	1 <sup>st</sup>	2 <sup>nd</sup>	1 <sup>st</sup>	2 <sup>nd</sup>	1 <sup>st</sup>	2 <sup>nd</sup>	1 <sup>st</sup>	2 <sup>nd</sup>	1 <sup>st</sup>	2 <sup>nd</sup>
CF <sub>NaOH</sub>	-7.3	-6.58	6.762	8.715	401	611	510	739	109	128	0.93	1.32
CF <sub>H<sub>2</sub>O<sub>2</sub></sub>	-4.809	-3.26	4.288	4.669	410	622	486	704	76	82.2	0.89	1.43
Pristine Felt	-3.625	-4.37	3.354	5.383	413	611	481	707	68	96	0.93	1.23

#### 4.5.2 Electrochemical Impedance Spectroscopy (EIS)

The EIS study is performed to further understand the electrochemical activity of the pre-treated electrode. The recorded Nyquist plots for CF<sub>H<sub>2</sub>O<sub>2</sub></sub> and CF<sub>NaOH</sub> treated carbon felt are recorded with the following assumptions (a) transport properties of electrolyte and felt are constant, (b) current collector and contact resistances are negligible and (c) self-discharge is ignored. From the recorded Nyquist plot displayed in Figure 4.14., the equivalent circuit can be fitted to elucidate internal reaction that happens in three regions, which are electrolyte, electrolyte electrode and electrode surface.

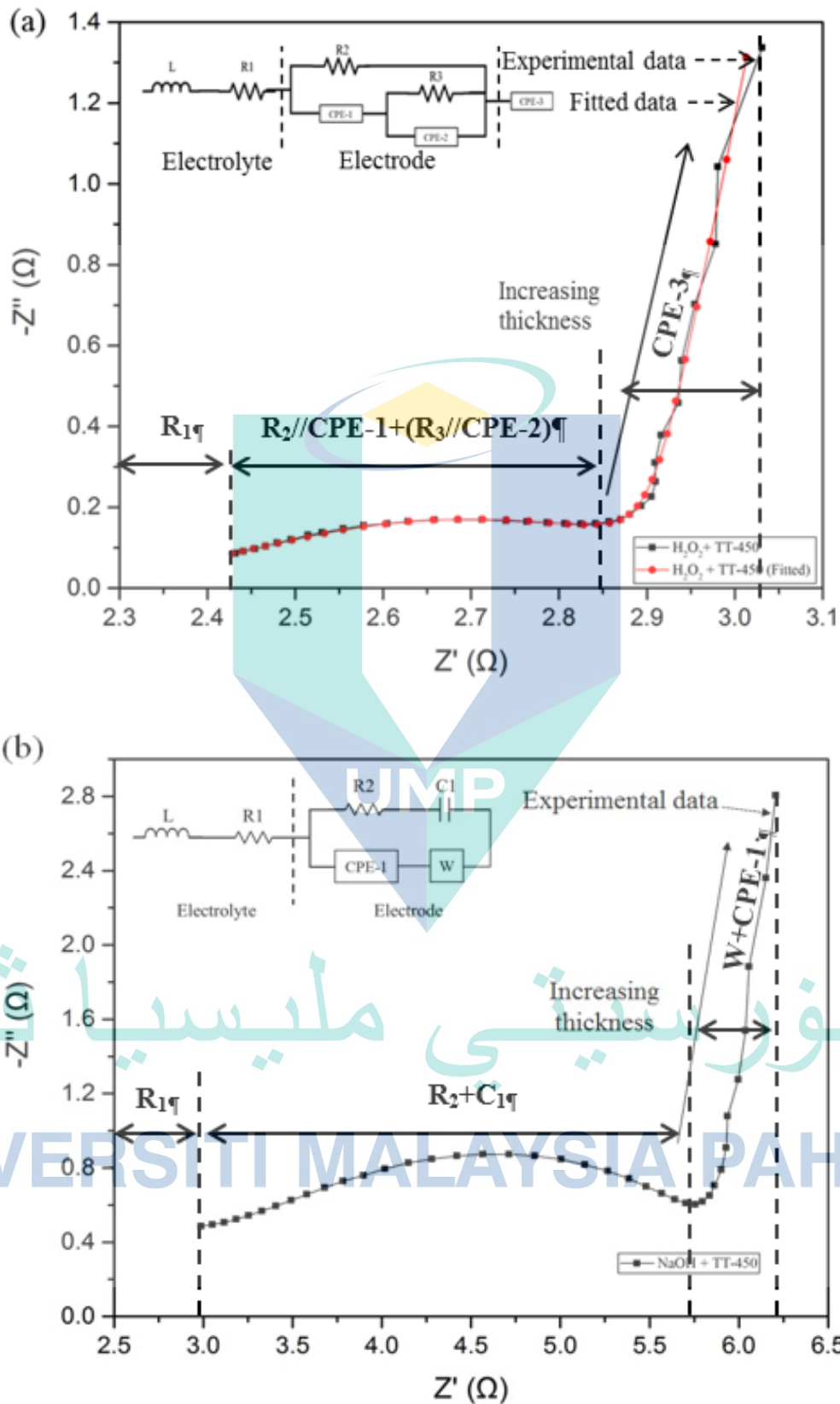


Figure 4.14 Nyquist plots (a)  $\text{H}_2\text{O}_2$  with thermal treatment (b)  $\text{NaOH}$  with thermal treatment carbon felt in  $0.1 \text{ mol dm}^{-3}$  1,4-benzoquinone +  $1 \text{ mol dm}^{-3}$   $\text{H}_2\text{SO}_4$  vs.  $\text{Ag}/\text{AgCl}$  fitted to equivalent circuit.



The Nyquist plots for electrochemical impedance studies can be fitted with a simplified equivalent circuit illustrated in Figure 4.14 whereas  $R_1$  represented the ohmic resistance in the electrolyte,  $R_2$  in  $CF_{NaOH}$  denotes the charge transfer resistance that occurred at the interface of the electrode material and the electrolyte.  $R_3$  in EIS fitting for  $CF_{H_2O_2}$  demonstrated the charge transfer resistance that occurred in pores of the electrode.

In both cases, the current flows through the solution, which represents by ohmic resistance,  $R_1$ . The  $R_1$  value for sodium hydroxide is  $2.56 \Omega$ , whereas hydrogen peroxide is  $16.9 \Omega$ . Alkaline with thermal with the higher oxygen functional group has significantly reduced the ohmic resistance, consequently improving electrochemically active sites and enhance the electron transfer. The fitted  $R_2$  is representing the charge transfer resistance ( $R_{ct}$ ) value for sodium hydroxide is  $3.66 \Omega$ . The interpretation of resistances  $R_A$  in electrochemical impedance spectra indicated the sum of that the charge transfer resistance occurred at electrode pores and material. The charge transfer resistance for each treated electrode varies depending on the treated effect on the carbon felt.

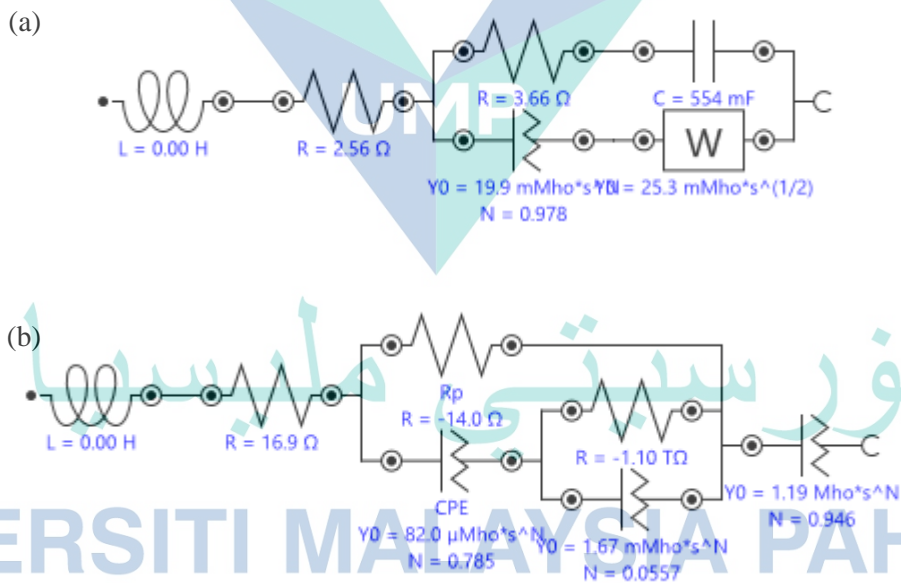


Figure 4.15 Fitted data (a) NaOH with thermal treatment (b)  $H_2O_2$  with thermal treatment carbon felt.

As reported in literature (Pivac & Barbir, 2016), side reactions during reduction and oxidation process with intermediate species and electrode thickness contributed to the inductive loops that recorded in low frequencies. Noted that the impedance of  $CF_{NaOH}$  carbon felt is lower in low frequencies compared to hydrogen peroxide treatments, this

suggests that alkaline treatment improved the fibre structure in compared to pristine carbon felt and hydrogen peroxide treated felt.

Figure 4.15 defined that electrons can be transferred across the electrode/electrolyte interface via two parallel pathways which represented by Warburg impedance and constant phase element (CPE-1) in series and charge transfer resistance ( $R_2$ ) with electrical double layer ( $C_1$ ). Both low frequencies represented by CPE-1 is described as to constant phase element that related to the double-layer capacitance of the interface between electrode and electrolyte whereas only  $CF_{H_2O_2}$  with CPE-2 which related to interfacial of the microporous layer (Orazem & Tribollet, 2011). Warburg impedance in Figure 4.15(b) describes the mass transport diffusion for low frequency region whereas capacitance represents the contact resistance for porous electrode. The parameter obtained after the fitting data were listed for less than 10% error. Good agreements between experimental and theoretical data were obtained for both graphs.

#### 4.6 The Effect of Different Supporting Acid

The proposed study is targeted to investigate the effect of electrolyte composition with respect to supporting acid. To investigate the effect of different supporting acid, the investigation continued with acid treated felt,  $CF_{H_2SO_4}$  conducted in two different supporting acid which are sulphuric and methanesulfonic acid. In this part of work, a 3D electrode is used to elucidate the effect of different supporting acid. According to Fick's first law of diffusion, the current is proportional to the gradient of concentration on the electrode surface. Herein, two electrolytes composition with acid are firstly characterized and analysed.

##### 4.6.1 Sulphuric Acid

Figure 4.16 shows the CV curves of  $0.1 \text{ mol dm}^{-3}$  1,4-benzoquinone couple in  $1 \text{ mol dm}^{-3}$  at different scanning rates are measured on the acid with thermal treated carbon felt,  $CF_{H_2SO_4}$ . As shown in the scheme in Figure 4.16, acid treated felt,  $CF_{H_2SO_4}$  in acid sulphuric demonstrated  $C_rE_r$  mechanism, in which oxidation peak and reduction peak represent electron transfer happen within the reaction. The redox potentials for different scanning rate in sulphuric acid as supporting acid are slightly different.

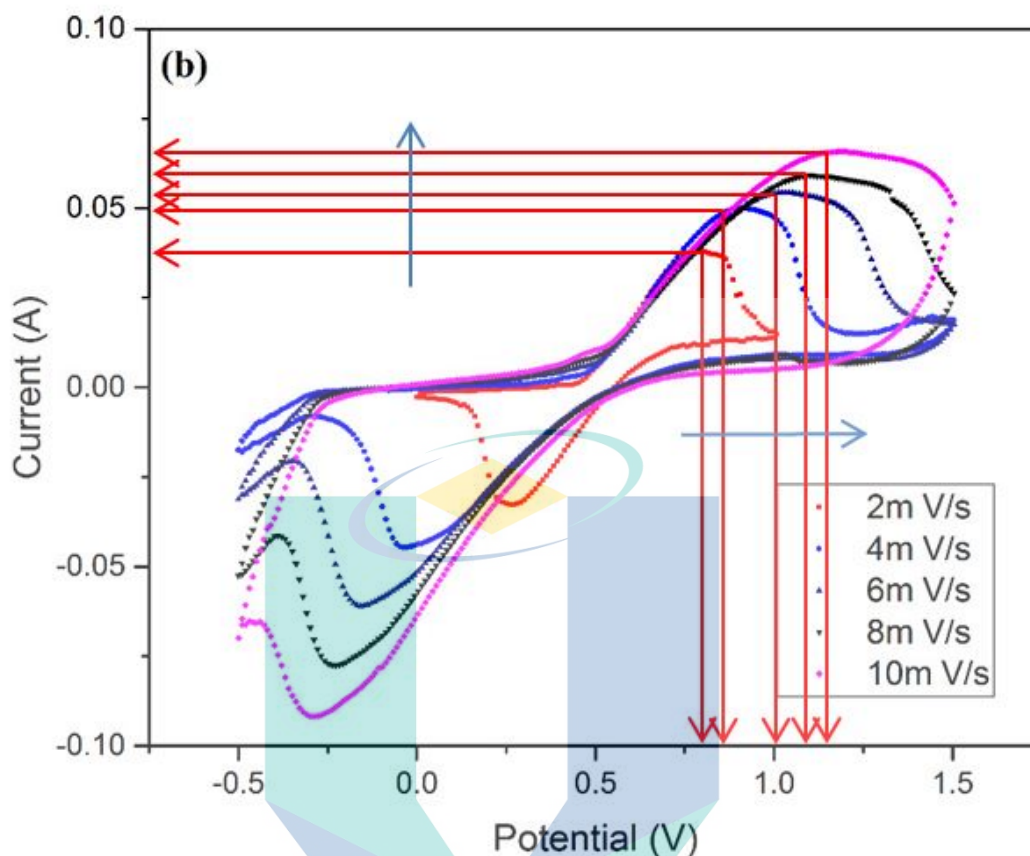


Figure 4.16 Cyclic voltammetry curves of acid with thermal treated felt,  $\text{CF}_{\text{H}_2\text{SO}_4}$  in  $0.1 \text{ mol dm}^{-3}$  1,4-benzoquinone +  $1 \text{ mol dm}^{-3}$   $\text{H}_2\text{SO}_4$  ranging from 2 to  $10 \text{ mV s}^{-1}$

Table 4.6 summarized the cyclic voltammetry measurement and calculated data. The calculated  $|I_{pa}/I_{pc}|$  sequence is  $4 \text{ mV s}^{-1} > 2 \text{ mV s}^{-1} > 6 \text{ mV s}^{-1} > 8 \text{ mV s}^{-1} > 10 \text{ mV s}^{-1}$ . As for peak separation,  $\Delta E_a$ , smaller peak separation is observed at the scan rate of  $2 \text{ mV s}^{-1}$  indicated a better kinetic reversibility is achieved. From the Table 4.6, the anodic peaks of  $\text{CF}_{\text{H}_2\text{SO}_4}$  are 0.790 V, 0.905 V, 1.031 V, 1.100 V and 1.117. It is worth to mention that larger peak separation was observed in higher scanning rate of  $10 \text{ mV s}^{-1}$ . Such a phenomenon indicated a slow redox kinetics or poor reversibility of  $\text{CF}_{\text{H}_2\text{SO}_4}$ .

Table 4.6 Electrochemical parameters with respect to cathodic and anodic (current, voltage, ratio) of  $\text{CF}_{\text{H}_2\text{SO}_4}$  carbon felt in sulphuric acid.

Scan Rate, mV/s	$I_{pa}$ , A	$I_{pc}$ , A	$E_{pa}$	$E_{pc}$	$\Delta E_a$	$ I_{pa}/I_{pc} $
2	0.0265	-0.033	0.790	0.266	0.524	0.80
4	0.0419	-0.044	0.905	-0.040	0.945	0.95
6	0.0464	-0.060	1.031	-0.158	1.189	0.77.
8	0.052	-0.075	1.100	-0.223	1.323	0.72
10	0.0581	-0.085	1.117	-0.278	1.395	0.68

#### 4.6.2 Methanesulfonic Acid

In this work, methanesulfonic acid was also used as the subject of investigation to evaluate the effect of acid-treated carbon felt with different supporting acid. The redox behaviour of acid-treated carbon felt in methanesulfonic acid is described in Figure 4.17. As shown in scheme (Figure 4.17), the anodic current shows a sharp rise at the positive potential except for the scan rate of  $10 \text{ mV s}^{-1}$ .

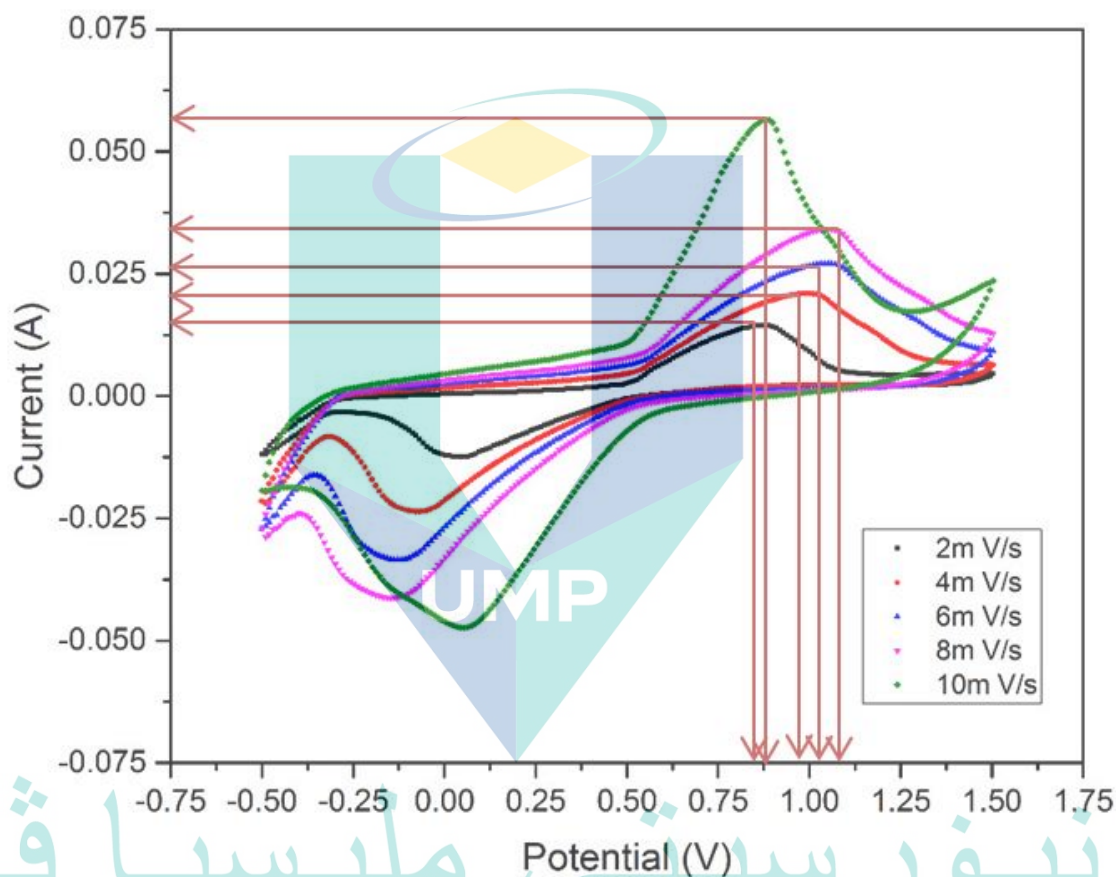


Figure 4.17 Cyclic voltammety curves of acid with thermal treated felt,  $\text{CF}_{\text{H}_2\text{SO}_4}$  in  $0.1 \text{ mol dm}^{-3}$  1,4-benzoquinone +  $1 \text{ mol dm}^{-3}$   $\text{CH}_3\text{SO}_3\text{H}$  ranging from 2 to  $10 \text{ mV s}^{-1}$

In methanesulfonic supporting electrolyte, the anodic peaks of different scan rates starting from  $2 \text{ mV s}^{-1}$  to  $10 \text{ mV s}^{-1}$  are 0.0125 A, 0.0187 A, 0.027 A, 0.034 A and 0.057 A. The peak current intensity is at large electrode potential separation,  $\Delta E_a$  is observed in scan rate of  $8 \text{ mV s}^{-1}$  indicated sluggish electron transfer. The electrode potential of different scan rates starting from  $10 \text{ mV s}^{-1} > 2 \text{ mV s}^{-1} > 4 \text{ mV s}^{-1} > 6 \text{ mV s}^{-1} > 8 \text{ mV s}^{-1}$ . It is worth to mention that best reversibility happens at the scan rate of  $10 \text{ mV s}^{-1}$ .

Table 4.7 Electrochemical parameters with respect to cathodic and anodic (current, voltage, ratio) of CF<sub>H2SO4</sub> carbon felt in methanesulfonic acid.

Scan Rate, mV/s	I <sub>pa</sub> , A	I <sub>pc</sub> , A	E <sub>pa</sub>	E <sub>pc</sub>	ΔE <sub>a</sub>	I <sub>pa</sub> /I <sub>pc</sub>
2	0.0125	-0.012	0.877	0.042	0.835	1.042
4	0.0187	-0.025	1.000	-0.074	1.074	0.748
6	0.027	-0.033	1.051	-0.127	1.178	0.818
8	0.034	-0.041	1.061	-0.137	1.198	0.829
10	0.057	-0.047	0.880	0.0538	0.826	1.213

#### 4.7 Chapter Conclusion

This thesis presented fundamental analysis of potential negolyte candidate-Alizarin red S for ORFB application. ARS is highly reversible at low electrode potential (c.a. 0.082 V vs. standard hydrogen electrode), indicating that ARS is a promising negative electrode material for organic redox flow batteries. With aim to investigate the best composition of negative electrolyte, three different concentrations of ARS and two concentrations of sulphuric acid were proposed as the first contribution for this work. To evaluate the electrochemical studies such as current, kinetics and diffusion of ARS, chemical assessment on ARS is completed by performing the cyclic voltammetry on different selected composition. The results reported that higher concentrations of ARS in base electrolyte have the lowest diffusion coefficient due to solubility issue of ARS. The diffusion coefficient of ARS in 0.05 mol dm<sup>-3</sup> is calculated in the range of 6.424 x 10<sup>-4</sup> cm<sup>2</sup> s<sup>-1</sup>, this has indicated fast diffusion rate and electrochemical kinetics for oxidation and reduction in lower concentrations of ARS. This study suggested that 0.05 mol dm<sup>-3</sup> ARS in 1 mol dm<sup>-3</sup> sulphuric acid gives good diffusion coefficient of 6.424 x 10<sup>-4</sup> cm<sup>2</sup> s<sup>-1</sup> in compared to the Zhang et al. 2.14 x 10<sup>-6</sup> cm<sup>2</sup> s<sup>-1</sup> and Dadpou et al. (2016) 1.58 x 10<sup>-6</sup> cm<sup>2</sup> s<sup>-1</sup> (Dadpou & Nematollahi, 2016; S. Zhang et al., 2016).

Second part for this work involved the improvement of electrode surface for positive redox reaction in organic quinone flow battery. This work targeted to investigate proposed characterisation on porous carbon electrode with the insertion of functional group. Three types of treatments (a) sodium hydroxide, (b) hydrogen peroxide or (c) sulphuric acid paired with thermal treatment are conducted on pristine carbon felt. The modification on the surface has been evaluated through electrochemical studies, such as

CV and EIS. The results show that  $CF_{H_2O_2}$  treated felt shows better catalytic activity at cathodic peak mainly attributes to hydroxyl (C–OH) and carboxyl (C–O and C=O) functional groups that contribute to the catalyst hence facilitates the redox reaction.

These inserted functional groups are responsible for electron transfer and resistance reduction favouring the reaction kinetics as active sites for benzene-1, 4-diol redox reaction. In the reported result,  $CF_{NaOH}$  presented better anodic and cathodic current owing to the highest surface area, however poor in reversibility. High charge transfer resistance was also found in  $CF_{NaOH}$ . The thermal oxidation process significantly improves the wettability of the carbon felt, which enables more effective of the electrolytes access into the porous structures and results in larger active surface areas for more efficient battery reactions. Improved electrochemical performance of quinone-based reaction is observed with the proportion of increase in surface areas (formation of microscopic holes) can improve catalytic and wettability properties.

The cyclic voltammetry curve of acid treated felt with different supporting acids such as methanesulfonic and sulphuric acid as illustrated in Figure 4.16 and Figure 4.17. It was observed that the etched sulphonic group promoted the electropositive potential of benzoquinone eventually widening the cell voltage for ORFB. This observation can be explained by analysing the effect of supporting acids (i.e., methanesulfonic and sulphuric acid). The result in Table 4.6 and Table 4.7, the electron transfer for acid treated felt work best in sulphuric acid, which the ratio of  $|I_{pa}/I_{pc}|$  is closer to 1 and the best reversibility of the lowest electrode separation of  $\Delta E_a$  occurred. Furthermore, the electrode potential and current intensity increase linearly along the scanning rate indicated the stability of redox reaction happen due to the similar acid used in treatment and supporting acid. This work reveals that sulphuric acid with acid treated carbon felt is one of the best acidic condition for BQDS redox reaction.

## CHAPTER 5

### CONCLUSION AND RECOMMENDATION

This thesis presented three contributions that included (a) the electrochemical evaluation of potential Alizarin red S as a candidate for negative electrolyte in organic based redox flow battery. The characterisation and electrochemical investigation of the proposed two-step treatment (b) sodium hydroxide with thermally treated carbon felt and (c) hydrogen peroxide with thermal treated carbon felt for organic based redox flow battery. Lastly, the comparison studies of sulphuric acid with thermally treated carbon felt in supporting acid – sulphuric and methanesulfonic are also included. This chapter presents the implication of the results of this study and future research direction in felt characterisation and organic electrolytes specifically for ORFB application.

As mentioned, one of the criteria to be applied as redox electrolyte is to use a higher number of electron valence materials. In this study, quinone-based electrolyte - ARS is chosen because of their abundance, multiple electrons with good electrical properties, fast electrochemical kinetics, and low cost. The advantages of two-electron quinone are the kinetic properties and stability of redox species. Meanwhile, as the energy density of the electrochemical energy storage system is depending on the large window differences between the electrode potential of the two electrolytes. An investigation on the potential of quinone derivative as negolyte alizarin red s (ARS) is reported. As stated, one of the criteria to be applied as redox electrolyte is to use a higher number of electron valence materials. The first objective of this work is to characterise ARS as potential negative electrolyte with concentration in terms of electron diffusion, electrolyte potential and reversibility for organic redox flow battery application. To achieve a larger window for potential redox couple for redox flow battery application, potential negative electrolyte ARS with theoretical 0.082V that is lower than 9,10-AQ (approximately 0.1V) is chosen for this investigation.

This work explored the characterisation of active material and supporting acid concentration. Consistent with the finding of Zhang et al., the experimental data show that the diffusion of ARS in lower concentration ( $0.05 \text{ mol dm}^{-3}$ ) is higher compared to a

higher concentration ( $0.15 \text{ mol dm}^{-3}$ ). The importance of this study is to further elucidate and understand the diffusion rate of ARS in sulphuric medium in varying concentrations. The optimum electrolyte composition for investigated negative electrolyte is  $0.1 \text{ mol dm}^{-3}$  ARS in  $1 \text{ mol dm}^{-3}$   $\text{H}_2\text{SO}_4$ . Functional groups, such as hydroxyl, sulphonate or phosphate are needed to enhance the solubility and electrochemical kinetics of ARS to extend its application. More benzene rings in quinone derivatives indicated more electronegative characteristics. For example, ARS = 3 benzene ring (electronegative) and 1,4-benzoquinone = 1 benzene ring (electropositive).

Instead of a single treatment, two-stage surface treatment on the electrode has been proposed and investigated in this study. This work is targeted to increase the active surface of electrode felt and remove the contaminated surface. Oxidising agents such as hydrogen peroxide and sodium hydroxide continued with oxidation steps using thermal are chosen to investigate the effect of neutral and alkaline composition of the inserted functional group on the surface of felt. This surface functionality is targeted to catalyse the redox reaction with selected electropositive materials such as BQ. By insertion of oxygen and hydroxyl groups, especially C-O, C-C=O, C=O and aliphatic C-OH, the functional group can improve the hydrophilic characteristics of carbon felt. In conclusion,  $\text{CF}_{\text{H}_2\text{SO}_4}$  presented well in reversibility compared to pristine,  $\text{CF}_{\text{H}_2\text{O}_2}$  and  $\text{CF}_{\text{NaOH}}$ . The work continued to compare the effect of supporting acid in the cathode reaction where  $\text{CF}_{\text{H}_2\text{SO}_4}$  demonstrated better reversibility and higher potential in sulphuric acid compared to methanesulfonic acid.

### 5.1 Future Work

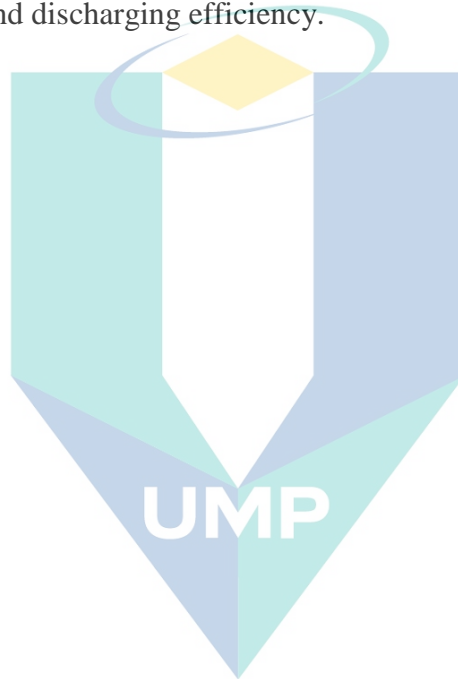
Organic material with a diversity of molecule customisation offers higher flexibility compared to inorganic redox material. By using organic synthesis techniques and the substitution of functional groups, the solubility, chemical stability, and kinetics reaction of organic redox species can significantly increase. In this work, the electrochemistry of ARS in sulphuric acid has been investigated and reported. Energy density can be increased by adopting a higher concentration of electroactive material such as ARS with 2 electrons properties. Nevertheless, the concentration of active material in supporting electrolyte is limited by the solubility of the active material. The result reported limitation of solubility issue faced by ARS causing the characterisation is limited to  $0.15 \text{ mol dm}^{-3}$ . With advantages such as potentially low cost and high flexibility in



chemical customisation, organic molecules serve as a better alternative substitution for RFB application. Therefore, future work in this area will be needed as follows:

1. Develop numerical studies for quinone-based electrolyte with respect to the number of benzene rings and functional groups towards aromatic type quinone. The current investigation only involved ARS with concentration limitation, the work can be extended to more quinone-based material with the more available functional groups in numerical and experimental studies.
2. Good electrochemical reversibility of ARS was demonstrated in cyclic voltammetry with two redox peaks. Still, the improvement for ARS solubility and stability by additives and synthetic modification is necessary. The electrochemical properties (i.e. solubility and redox potential) of organic redox molecules can be tailored through the insertion of the functional group. For instance, the solubility of quinone can be improved by the substitution of the hydrophilic functional group (i.e. -OH, -NH<sub>2</sub>, -COOH, -SO<sub>3</sub>H, and -PO<sub>3</sub>H<sub>2</sub>) (Er et al., 2015). With proper functional molecule modification and additives, this will lead to develop ARS as one of the potential negolyte candidates for RFB applications.
3. Computational studies such as density functional theory (DFT) offer low cost for fundamental research, prediction, and accuracy towards material studies, especially in felt. Computation studies involving a non-isothermal model by Chu et al. reveal the effect of current density, flow structure, temperature and electrolyte flow rate on quinone-bromide RFB (Chu, Li, & Zhang, 2016). The numerical studies reported flow structure and the optimum flow rate is required, temperature brings less influence on the AQDS/Br RFB performance. The development of computational chemistry has allowed the research on chemical properties among most chemical treatments, which the attraction of carbon felt towards the redox, is the main concern.
4. The exploration of material or suitable catalyst for the felt treatment experimentally or numerically allows identifying the potential of chemical treatment for the system related to the electrode/electrolyte interface and charge resistance. The diffusion of 1,4-benzoquinone on carbon is interesting for potentially treated carbon in performing redox reaction in flow battery.

5. In addition, the employment of flow field has been developed to facilitate electrolyte flow targeting on increasing redox active area. However, suitable flow structure is difficult to define with lacking in shared information from the researcher. Technical instruments for interior investigation are limited. This has limited the investigation for further understanding for the internal reaction for redox reaction in the compartment of RFB. Furthermore, the investigation of untreated and treated felt with flow distribution is also one of the future prospects, in which the flow distribution affects the electron distribution over area against the charging and discharging efficiency.



اونيورسيتي ملايسيا قهغ

UNIVERSITI MALAYSIA PAHANG

## REFERENCES

- Adam, G. B. (1979). U.S. Patent No. 4180623. Electrically rechargeable battery. Washington, DC: U.S. Patent and Trademark Office.
- Abbas, S., Lee, H., Hwang, J., Mehmood, A., Shin, H.-J., Mehboob, S., ... Ha, H. Y. (2018). A novel approach for forming carbon nanorods on the surface of carbon felt electrode by catalytic etching for high-performance vanadium redox flow battery. *Carbon*, 128, 31–37. doi:10.1016/j.carbon.2017.11.066.
- International Renewable Energy Agency (2016). *Remap: Roadmap for a Renewable Energy Future*. International Renewable Energy Agency. Retrieved from <https://www.irena.org/publications/2016/Mar/REmap-Roadmap-for-A-Renewable-Energy-Future-2016-Edition>.
- Al-Yasiri, M. & Park, J. (2018). A novel cell design of vanadium redox flow batteries for enhancing energy and power performance. *Applied Energy*, 222, 530–539. doi:10.1016/j.apenergy.2018.04.025.
- Albadi, M. H., Al-Busaidi, A. & El-Saadany, E. (2017). Seawater PHES to facilitate wind power integration in dry coastal areas-Duqm case study. *International Journal of Renewable Energy Research*, 7(3), 1363–1375.
- Alias, M., Kamarudin, S., Zainoodin, A. & Masdar, M. (2020). Active direct methanol fuel cell: An overview. *International Journal of Hydrogen Energy*, 45(38), 19620–19641. doi:10.1016/j.ijhydene.2020.04.202.
- Alva, G., Lin, Y. & Fang, G. (2018) M., An overview of thermal energy storage systems. *Energy*, 144, 341–378. doi: 10.1016/j.energy.2017.12.037.
- Amiryar, M. E. & Pullen, K. R. (2020). Analysis of Standby Losses and Charging Cycles in Flywheel Energy Storage Systems. *Energies*, 13(17), 4441. doi:10.3390/en13174441.
- Ardizzon, G., Cavazzini, G. & Pavesi, G. (2014). A new generation of small hydro and pumped-hydro power plants: Advances and future challenges. *Renewable and Sustainable Energy Reviews*, 31, 746–761. doi:10.1016/j.rser.2013.12.043.
- Assink, R. (1984). Fouling mechanism of separator membranes for the iron/chromium redox battery. *Journal of Membrane Science*, 17(2), 205–217. doi:10.1016/S0376-7388(00)82295-4.
- Bachman, J. E., Curtiss, L. A. & Assary, R. S. (2014). Investigation of the redox chemistry of anthraquinone derivatives using density functional theory. *The Journal of Physical Chemistry A*, 118(38), 8852–8860. doi:10.1021/jp5060777.

- Barbour, E., Wilson, I. G., Radcliffe, J., Ding, Y. & Li, Y. (2016). A review of pumped hydro energy storage development in significant international electricity markets. *Renewable and Sustainable Energy Reviews*, 61, 421–432. doi:10.1016/j.rser.2016.04.019.
- Barote, L. (2009). VRB modeling for storage in stand-alone wind energy systems. *PowerTech, 2009 IEEE*, 1–6.
- Bender, D. A., Byrne, R. H. & Borneo, D. R. (2015). *ARRA energy storage demonstration projects: Lessons learned and recommendations*. Sandia National Laboratories, Albuquerque, NM, Tech. Rep. SAND2015-5242.
- Burheim, O. S. (2017). *Engineering energy storage*. Academic press.
- Chan, K.-Y., Jia, B., Lin, H., Hameed, N., Lee, J.-H. & Lau, K.-T. (2018). A critical review on multifunctional composites as structural capacitors for energy storage. *Composite Structures*, 188, 126–142. doi:10.1016/j.compstruct.2017.12.072.
- Chang, Y.-C., Chen, J.-Y., Kabtamu, D. M., Lin, G.-Y., Hsu, N.-Y., Chou, Y.-S., ... Wang, C.-H. (2017). High efficiency of CO<sub>2</sub>-activated graphite felt as electrode for vanadium redox flow battery application. *Journal of Power Sources*, 364, 1–8. doi:10.1016/j.jpowsour.2017.07.103.
- Chen, L., Ma, C., Li, X., Lin, L., Yang, S. & Li, G. (2017). First Principles Design of Anthraquinone Derivatives in Redox Flow Batteries. *International Journal of Electrochemical Science*, 12(11), 10433–10446. doi:10.20964/2017.11.35.
- Cheng, J., Zhang, L., Yang, Y.-S., Wen, Y.-H., Cao, G.-P. & Wang, X.-D. (2007). Preliminary study of single flow zinc-nickel battery. *Electrochemistry Communications*, 9(11), 2639–2642. doi:10.1016/j.elecom.2007.08.016.
- Cho, J., Jeong, S. & Kim, Y. (2015). Commercial and research battery technologies for electrical energy storage applications. *Progress in Energy and Combustion Science*, 48, 84–101. doi:10.1016/j.peccs.2015.01.002.
- Chu, D., Li, X. & Zhang, S. (2016). A non-isothermal transient model for a metal-free quinone-bromide flow battery. *Electrochimica Acta*, 190, 434–445. doi:10.1016/j.electacta.2015.12.128.
- Cooper, A., Furakawa, J., Lam, L. & Kellaway, M. (2009). The UltraBattery—A new battery design for a new beginning in hybrid electric vehicle energy storage. *Journal of Power Sources*, 188(2), 642–649. doi:10.1016/j.jpowsour.2008.11.119.
- Craig, H., Ron, M., Taylor, S. & Bret, A. (2014). *Demonstration of EnerVault Iron-Chromium Redox Flow Battery*.

- Dadpou, B. & Nematollahi, D. (2016). Electrochemical Oxidation of Alizarin Red-S on Glassy Carbon Electrode: Mechanistic Study, Surface Adsorption and Preferential Surface Orientation. *Journal of The Electrochemical Society*, 163(7), H559–H565. doi:10.1149/2.0781607jes.
- Dekka, A., Ghaffari, R., Venkatesh, B. & Wu, B. (2015). A survey on energy storage technologies in power systems. *2015 IEEE Electrical Power and Energy Conference (EPEC)*, 105–111. doi:10.1109/EPEC.2015.7379935.
- Derr, I. (2017). *Electrochemical degradation and chemical aging of carbon felt electrodes in all-vanadium redox flow batteries*. (Doctoral thesis, Freie Universität Berlin, Berlin, Germany). Retrieved from <https://dnb.info/1135184836/34>.
- Di Blasi, A., Di Blasi, O., Briguglio, N., Aricò, A. S., Sebastián, D., Lázaro, M., ... Antonucci, V. (2013). Investigation of several graphite-based electrodes for vanadium redox flow cell. *Journal of Power Sources*, 227, 15–23. doi:10.1016/j.jpowsour.2012.10.098.
- Di Blasi, O., Briguglio, N., Busacca, C., Ferraro, M., Antonucci, V. & Di Blasi, A. (2015). Electrochemical investigation of thermally treated graphene oxides as electrode materials for vanadium redox flow battery. *Applied Energy*, 147, 74–81. doi:10.1016/j.apenergy.2015.02.073.
- Ding, Y., Zhang, C., Zhang, L., Zhou, Y. & Yu, G. (2018). Molecular engineering of organic electroactive materials for redox flow batteries. *Chemical Society Reviews*, 47(1), 69–103. doi:10.1039/C7CS00569E.
- Dixon, D., Babu, D. J., Bhaskar, A., Bruns, H.-M., Schneider, J. J., Scheiba, F. & Ehrenberg, H. (2019). Tuning the performance of vanadium redox flow batteries by modifying the structural defects of the carbon felt electrode. *Beilstein Journal of Nanotechnology*, 10(1), 1698–1706. doi:10.3762/bjnano.10.165.
- Dixon, D., Babu, D., Langner, J., Bruns, M., Pfaffmann, L., Bhaskar, A., ... Ehrenberg, H. (2016). Effect of oxygen plasma treatment on the electrochemical performance of the rayon and polyacrylonitrile based carbon felt for the vanadium redox flow battery application. *Journal of Power Sources*, 332, 240–248. doi:10.1016/j.jpowsour.2016.09.070.
- Er, S., Suh, C., Marshak, M. P. & Aspuru-Guzik, A. (2015). Computational design of molecules for an all-quinone redox flow battery. *Chemical Science*, 6(2), 885–893. doi:10.1039/C4SC03030C.
- Estevez, L., Reed, D., Nie, Z., Schwarz, A. M., Nandasiri, M. I., Kizewski, J. P., ... others. (2016). Tunable Oxygen Functional Groups as Electrocatalysts on Graphite Felt Surfaces for All-Vanadium Flow Batteries. *ChemSusChem*, 9(12), 1455–1461. doi:10.1002/cssc.201600198.

- Faraji, F., Majazi, A., Al-Haddad, K. & others. (2017). A comprehensive review of flywheel energy storage system technology. *Renewable and Sustainable Energy Reviews*, 67, 477–490. doi:10.1016/j.rser.2016.09.060
- Fetyan, A., El-Nagar, G. A., Derr, I., Kubella, P., Dau, H. & Roth, C. (2018). A neodymium oxide nanoparticle-doped carbon felt as promising electrode for vanadium redox flow batteries. *Electrochimica Acta*, 268, 59–65. doi:10.1016/j.electacta.2018.02.104.
- Flox, C., Rubio-García, J., Skoumal, M., Andreu, T. & Morante, J. R. (2013). Thermochemical treatments based on NH<sub>3</sub>/O<sub>2</sub> for improved graphite-based fiber electrodes in vanadium redox flow batteries. *Carbon*, 60, 280–288. doi:10.1016/j.carbon.2013.04.038.
- Flox, C., Skoumal, M., Rubio-García, J., Andreu, T. & Morante, J. R. (2013). Strategies for enhancing electrochemical activity of carbon-based electrodes for all-vanadium redox flow batteries. *Applied Energy*, 109, 344–351. doi:10.1016/j.apenergy.2013.02.001.
- Gahn, R. F. & Hagedorn, N. H. (1985). U. S. Patent No.4543302. *Negative electrode catalyst for the iron chromium REDOX energy storage system*. Washington, DC: U.S. Patent and Trademark Office.
- Gerhardt, M. R., Tong, L., Chen, Q., Gordon, R. G. & Aziz, M. J. (2016). Anthraquinone Derivatives in Aqueous Flow Batteries. *Advanced Energy Material*, 382–390. doi: 10.1002/aenm.201601488.
- Ghimire, P. C., Schweiss, R., Scherer, G. G., Wai, N., Lim, T. M., Bhattarai, A., ... Yan, Q. (2018). Titanium carbide-decorated graphite felt as high performance negative electrode in vanadium redox flow batteries. *Journal of Materials Chemistry A*, 6(15), 6625–6632. doi: 10.1039/C8TA00464A.
- Giner, J. & Cahill, K. (1980). *Advanced screening of electrode couples*. NASA CR-159738. Retrieved from <https://www.amazon.in/Advanced-screening-electrode-Aeronautics-Administration-ebook/dp/B07S9JQH1T>.
- Giner, J. D., Cahill, K. J. & others. (1980). U. S. Patent No. 4192910 *Catalyst surfaces for the chromous/chromic redox couple*. Washington, DC: U.S. Patent and Trademark Office.
- Gong, K., Ma, X., Conforti, K. M., Kuttler, K. J., Grunewald, J. B., Yeager, K. L., ... Yan, Y. (2015). A zinc-iron redox-flow battery under \$100 per kW h of system capital cost. *Energy & Environmental Science*, 8(10), 2941–2945. doi:10.1039/C5EE02315G.
- González, A., Goikolea, E., Barrena, J. A. & Mysyk, R. (2016). Review on supercapacitors: technologies and materials. *Renewable and Sustainable Energy Reviews*, 58, 1189–1206. doi: 10.1016/j.rser.2015.12.249.

- González, Z., Flox, C., Blanco, C., Granda, M., Morante, J. R., Menéndez, R. & Santamaria, R. (2017). Outstanding electrochemical performance of a graphene-modified graphite felt for vanadium redox flow battery application. *Journal of Power Sources*, 338, 155–162. doi: 10.1016/j.jpowsour.2016.10.069.
- González, Z., Sánchez, A., Blanco, C., Granda, M., Menéndez, R. & Santamaria, R. (2011). Enhanced performance of a Bi-modified graphite felt as the positive electrode of a vanadium redox flow battery. *Electrochemistry Communications*, 13(12), 1379–1382. doi: 10.1016/j.elecom.2011.08.017.
- Guin, P. S., Das, S. & Mandal, P. (2011). Electrochemical reduction of quinones in different media: a review. *International Journal of Electrochemistry*, 2011. doi: 10.4061/2011/816202.
- Gür, T. M. (2018). Review of electrical energy storage technologies, materials and systems: challenges and prospects for large-scale grid storage. *Energy & Environmental Science*, 11(10), 2696–2767. doi: 10.1039/C8EE01419A.
- Hawthorne, K. L. (2014). *Iron-Ligand Electrokinetics towards an all-Iron Hybrid Redox Flow Battery*. (Doctorate dissertation, Case Western Reserve University, United States of America) Retrieved from <https://etd.ohiolink.edu>.
- Heinzel, A. (1989). U.S. Patent No. 4882241. *Redox battery*. Washington, DC: U.S. Patent and Trademark Office.
- Hofmann, J. D., Pfanschilling, F. L., Krawczyk, N., Geigle, P., Hong, L., Schmalisch, S., ... Schröder, D. (2018). Quest for Organic Active Materials for Redox Flow Batteries: 2, 3-Diaza-anthraquinones and Their Electrochemical Properties. *Chemistry of Materials*, 30(3), 762–774. doi: 10.1021/acs.chemmater.7b04220.
- Hosseini, M. G., Mousavihashemi, S., Murcia-López, S., Flox, C., Andreu, T. & Morante, J. R. (2018). High-power positive electrode based on synergistic effect of N-and WO<sub>3</sub>-decorated carbon felt for vanadium redox flow batteries. *Carbon*, 136, 444–453. doi: 10.1016/j.carbon.2018.04.038.
- Hosseiny, S., Saakes, M. & Wessling, M. (2011). A polyelectrolyte membrane-based vanadium/air redox flow battery. *Electrochemistry Communications*, 13(8), 751–754. doi: 10.1016/j.elecom.2010.11.025.
- Hruska, L. & Savinell, R. (1981). Investigation of Factors Affecting Performance of the Iron-Redox Battery. *Journal of the Electrochemical Society*, 128(1), 18–25. doi: 10.1149/1.2127366.
- Huang, Q. & Wang, Q. (2015). Next-Generation, High-Energy-Density Redox Flow Batteries. *ChemPlusChem*, 80(2), 312–322. doi: 10.1002/cplu.201402099.
- Huang, Y., Deng, Q., Wu, X. & Wang, S. (2017). N, O Co-doped carbon felt for high-performance all-vanadium redox flow battery. *International Journal of Hydrogen Energy*, 42(10), 7177–7185. doi: 10.1016/j.ijhydene.2016.04.004.

- Hunt, J. D., Zakeri, B., Lopes, R., Barbosa, P. S. F., Nascimento, A., de Castro, N. J., ... Wada, Y. (2020). Existing and new arrangements of pumped-hydro storage plants. *Renewable and Sustainable Energy Reviews*, 129, 109914. doi: 10.1016/j.rser.2020.109914.
- Huskinson, B., Marshak, M., Aziz, M. J., Gordon, R. G., Betley, T. A., Aspuru-Guzik, A., ... Suh, C. (2015). U.S. Patent No. 20150243991A1. *Small organic molecule based flow battery*. Washington, DC: U.S. Patent and Trademark Office.
- Huskinson, B., Marshak, M. P., Suh, C., Er, S., Gerhardt, M. R., Galvin, C. J., ... Aziz, M. J. (2014). A metal-free organic-inorganic aqueous flow battery. *Nature*, 505(7482), 195–198. doi: 10.1038/nature12909.
- Ito, Y., Nyce, M., Plivelich, R., Klein, M., Steingart, D. & Banerjee, S. (2011). Zinc morphology in zinc-nickel flow assisted batteries and impact on performance. *Journal of Power Sources*, 196(4), 2340–2345. doi: 10.1016/j.jpowsour.2010.09.065.
- Jalan, V., Reid, M. A. & Charleston, J. A. (1984). U.S. Patent No. 4454649. *Chromium electrodes for REDOX cells*. Washington, DC: U.S. Patent and Trademark Office.
- Jiang, H., Shyy, W., Ren, Y., Zhang, R. & Zhao, T. (2019). A room-temperature activated graphite felt as the cost-effective, highly active and stable electrode for vanadium redox flow batteries. *Applied Energy*, 233, 544–553. doi: 10.1016/j.apenergy.2018.10.059.
- Jorné, J., Kim, J. & Kralik, D. (1979). The zinc-chlorine battery: half-cell overpotential measurements. *Journal of Applied Electrochemistry*, 9(5), 573–579. doi: 10.1007/BF00610944.
- Kabir, H., Gyan, I. O. & Cheng, I. F. (2017). Electrochemical modification of a pyrolytic graphite sheet for improved negative electrode performance in the vanadium redox flow battery. *Journal of Power Sources*, 342, 31–37. doi: 10.1016/j.jpowsour.2016.12.045.
- Kabtamu, D. M., Chen, J.-Y., Chang, Y.-C. & Wang, C.-H. (2017). Water-activated graphite felt as a high-performance electrode for vanadium redox flow batteries. *Journal of Power Sources*, 341, 270–279. doi: 10.1016/j.jpowsour.2016.12.004.
- Khan, K., Karodi, R., Siddiqui, A., Thube, S. & Rub, R. (2012). Development of anti-acne gel formulation of anthraquinones rich fraction from *Rubia cordifolia* (Rubiaceae). *International Journal of Applied Research in Natural Products*, 4(4), 28–36.
- Khan, N., Dilshad, S., Khalid, R., Kalair, A. R. & Abas, N. (2019). Review of energy storage and transportation of energy. *Energy Storage*, 1(3), 1–49. doi: 10.1002/est2.49.



- Khor, A., Leung, P., Mohamed, M., Flox, C., Xu, Q., An, L., ... Shah, A. (2018). Review of zinc-based hybrid flow batteries: From fundamentals to applications. *Materials Today Energy*, 8, 80–108. doi: 10.1016/j.mtener.2017.12.012.
- Killer, M., Farrokhseresht, M. & Paterakis, N. G. (2020). Implementation of large-scale Li-ion battery energy storage systems within the EMEA region. *Applied Energy*, 260, 114166. doi: 10.1016/j.apenergy.2019.114166.
- Kim, J. G., Son, B., Mukherjee, S., Schuppert, N., Bates, A., Kwon, O., ... Park, S. (2015). A review of lithium and non-lithium based solid state batteries. *Journal of Power Sources*, 282, 299–322. doi: 10.1016/j.jpowsour.2015.02.054.
- Kim, K. J., Kim, Y.-J., Kim, J.-H. & Park, M.-S. (2011). The effects of surface modification on carbon felt electrodes for use in vanadium redox flow batteries. *Materials Chemistry and Physics*, 131(1), 547–553. doi: 10.1016/j.matchemphys.2011.10.022.
- Kocak, B., Fernandez, A. I. & Paksoy, H. (2020). Review on sensible thermal energy storage for industrial solar applications and sustainability aspects. *Solar Energy*, 209, 135–169. doi: 10.1016/j.solener.2020.08.081.
- Krishan, O. & Suhag, S. (2019). An updated review of energy storage systems: Classification and applications in distributed generation power systems incorporating renewable energy resources. *International Journal of Energy Research*, 43(12), 6171–6210. doi: 10.1002/er.4285
- Kumaresan, T., Velumani, T., Chandran, M., Palaniswamy, K., Thirkell, A., Fly, A., ... Sundaram, S. (2020). Effect of Nafion loading and the novel flow field designs on Innovative anode electrocatalyst for improved DMFCs performance. *Materials Letters*, 128222. doi: 10.1016/j.matlet.2020.128222.
- Kwabi, D. G., Lin, K., Ji, Y., Kerr, E. F., Goulet, M.-A., De Porcellinis, D., ... others. (2018). Alkaline quinone flow battery with long lifetime at pH 12. *Joule*, 2(9), 1894–1906. doi: 10.1016/j.joule.2018.07.005.
- Lai, Q., Zhang, H., Li, X., Zhang, L. & Cheng, Y. (2013). A novel single flow zinc-bromine battery with improved energy density. *Journal of Power Sources*, 235, 1–4. doi: 10.1016/j.jpowsour.2013.01.193.
- Lalanne, P. & Byrne, P. (2019). Large-Scale Pumped Thermal Electricity Storages—Converting Energy Using Shallow Lined Rock Caverns, Carbon Dioxide and Underground Pumped-Hydro. *Applied Sciences*, 9(19), 4150. doi: 10.3390/app9194150.
- Lantz, A. W., Shavaliar, S. A., Schroeder, W. & Rasmussen, P. G. (2019). Evaluation of an Aqueous Biphenol-and Anthraquinone-Based Electrolyte Redox Flow Battery. *ACS Applied Energy Materials*, 2(11), 7893–7902. doi: 10.1021/acsaem.9b01381.

- Le, T. X. H., Bechelany, M. & Cretin, M. (2017). Carbon felt based-electrodes for energy and environmental applications: a review. *Carbon*, 122, 564–591. doi: 10.1016/j.carbon.2017.06.078.
- Lee, H., Jung, S., Cho, Y., Yoon, D. & Jang, G. (2013). Peak power reduction and energy efficiency improvement with the superconducting flywheel energy storage in electric railway system. *Physica C: Superconductivity*, 494, 246–249. doi:10.1016/j.physc.2013.04.033.
- Lee, W., Park, G., Kim, Y., Chang, D. & Kwon, Y. (2020). Nine Watt-Level Aqueous Organic Redox Flow Battery Stack Using Anthraquinone and Vanadium as Redox Couple. *Chemical Engineering Journal*, 125610. doi: 10.1016/j.cej.2020.125610.
- Leung, P. K. (2011). *Development of a zinc-cerium redox flow battery*. (Doctoral Dissertations, University of Southampton, United Kingdom). Retrieved from <https://eprints.soton.ac.uk/333334/>.
- Leung, P. K., Martin, T., Shah, A. A., Mohamed, M. R., Anderson, M. A. & Palma, J. (2017). Membrane-less hybrid flow battery based on low cost elements. *Journal of Power Sources*, 341, 36–45. doi: 10.1016/j.jpowsour.2016.11.062.
- Leung, P. K., Ponce de leon, C., Low, C. T. J. & Walsh, F. C. (2011). Characterization of a zinc-cerium flow battery. *Journal of Power Sources*, 196, 5174–5185. doi: 10.1016/j.jpowsour.2011.01.095.
- Leung, P. K., Ponce de Leon, C. & Walsh, F. C. (2012). The influence of operational parameters on the performance of an undivided zinc-cerium flow battery. *Electrochimica Acta*, 80, 7–14. doi: 10.1016/j.electacta.2012.06.074.
- Leung, P. K., Xu, Q. & Zhao, T. S. (2012). High-potential zinc-lead dioxide rechargeable cells. *Electrochimica Acta*, 79, 117–125. doi: 10.1016/j.electacta.2012.06.089.
- Leung, P., Martin, T., Shah, A., Anderson, M. & Palma, J. (2016). Membrane-less organic-inorganic aqueous flow batteries with improved cell potential. *Chemical Communications*, 52(99), 14270–14273. doi: 10.1039/C6CC07692K.
- Leung, P., Shah, A., Sanz, L., Flox, C., Morante, J., Xu, Q., ... Walsh, F. (2017). Recent developments in organic redox flow batteries: A critical review. *Journal of Power Sources*, 360, 243–283. doi: 10.1016/j.jpowsour.2017.05.057.
- Li, B., Li, L., Wang, W., Nie, Z., Chen, B., Wei, X., ... Sprenkle, V. (2013). Fe/V redox flow battery electrolyte investigation and optimization. *Journal of Power Sources*, 229, 1–5. doi: 10.1016/j.jpowsour.2012.11.119.
- Li, B. & Liu, J. (2017). Progress and directions in low-cost redox-flow batteries for large-scale energy storage. *National Science Review*, 4(1), 91–105. doi: 10.1093/nsr/nww098.

- Li, B., Nie, Z., Vijayakumar, M., Li, G., Liu, J., Sprenkle, V. & Wang, W. (2015). Ambipolar zinc-polyiodide electrolyte for a high-energy density aqueous redox flow battery. *Nature Communications*, 6, 6303. doi: 10.1038/ncomms7303.
- Li, W., Liu, J. & Yan, C. (2012). The electrochemical catalytic activity of single-walled carbon nanotubes towards VO<sub>2</sub><sup>+</sup>/VO<sub>2</sub><sup>+</sup> and V<sup>3+</sup>/V<sup>2+</sup> redox pairs for an all vanadium redox flow battery. *Electrochimica Acta*, 79, 102–108. doi: 10.1016/j.electacta.2012.06.109.
- Li, W., Liu, J. & Yan, C. (2013). Modified multiwalled carbon nanotubes as an electrode reaction catalyst for an all vanadium redox flow battery. *Journal of Solid State Electrochemistry*, 17(5), 1369–1376. doi: 10.1007/s10008-013-2006-6.
- Likit-Anurak, K., Uthaichana, K., Punyawudho, K. & Khunatorn, Y. (2017). The performance and efficiency of organic electrolyte redox flow battery prototype. *Energy Procedia*, 118, 54–62. doi: 10.1016/j.egypro.2017.07.012.
- Lim, H., Lackner, A. & Knechtli, R. (1977). Zinc-bromine secondary battery. *Journal of the Electrochemical Society*, 124(8), 1154–1157. doi: 10.1149/1.2133517.
- Lin, K., Gómez-Bombarelli, R., Beh, E. S., Tong, L., Chen, Q., Valle, A., ... Gordon, R. G. (2016). A redox-flow battery with an alloxazine-based organic electrolyte. *Nature Energy*, 1, 16102. doi: 10.1038/nenergy.2016.102.
- Liu, Q., Sleightholme, A. E., Shinkle, A. A., Li, Y. & Thompson, L. T. (2009). Non-aqueous vanadium acetylacetonate electrolyte for redox flow batteries. *Electrochemistry Communications*, 11(12), 2312–2315. doi: 10.1016/j.elecom.2009.10.006.
- Luo, X., Wang, J., Dooner, M. & Clarke, J. (2015). Overview of current development in electrical energy storage technologies and the application potential in power system operation. *Applied Energy*, 137, 511–536. doi: 10.1016/j.apenergy.2014.09.081.
- Ma, C., Li, X., Lin, L., Chen, L., Wang, M. & Zhou, J. (2018). A two-dimensional porous electrode model for designing pore structure in a quinone-based flow cell. *Journal of Energy Storage*, 18, 16–25. doi: 10.1016/j.est.2018.04.007.
- May, G. J., Davidson, A. & Monahov, B. (2018). Lead batteries for utility energy storage: A review. *Journal of Energy Storage*, 15, 145–157. doi: 10.1016/j.est.2017.11.008.
- Mehari, A., Xu, Z. & Wang, R. (2020). Thermal energy storage using absorption cycle and system: A comprehensive review. *Energy Conversion and Management*, 206, 112482. doi: 10.1016/j.enconman.2020.112482.
- Melke, J., Jakes, P., Langner, J., Riekehr, L., Kunz, U., Zhao-Karger, Z., ... others. (2014). Carbon materials for the positive electrode in all-vanadium redox flow batteries. *Carbon*, 78, 220–230.

- Menéndez, J., Fernández-Oro, J. M., Galdo, M. & Loredó, J. (2019). Pumped-storage hydropower plants with underground reservoir: Influence of air pressure on the efficiency of the Francis turbine and energy production. *Renewable Energy*, 143, 1427–1438. doi: 10.1016/j.carbon.2014.06.075.
- Menéndez, J. & Loredó, J. (n.d.). *Compressed Air Energy Storage plants in abandoned underground mines: Preliminary analysis and potential*.
- Milner, E. M., Scott, K., Head, I. M., Curtis, T. & Yu, E. H. (2017). Evaluation of porous carbon felt as an aerobic biocathode support in terms of hydrogen peroxide. *Journal of Power Sources*, 356, 459–466. doi: 10.1016/j.jpowsour.2017.03.079.
- Milshtein, J. D., Su, L., Liou, C., Badel, A. F. & Brushett, F. R. (2015). Voltammetry study of quinoxaline in aqueous electrolytes. *Electrochimica Acta*, 180, 695–704. doi:10.1016/j.electacta.2015.07.063.
- Miyake, S. & Tokuda, N. (2001). Vanadium Redox-Flow Battery for a Variety of Applications. *2001 Power Engineering Society Summer Meeting.*, 1, 450–451. doi: 10.1109/PESS.2001.970067.
- Mohamed, M., Leung, P. & Sulaiman, M. (2015). Performance characterization of a vanadium redox flow battery at different operating parameters under a standardized test-bed system. *Applied Energy*, 137, 402–412. doi: 10.1016/j.apenergy.2014.10.042.
- Mohamed, M. R., Sharkh, S. M. & Walsh, F. C. (2009). Redox flow batteries for hybrid electric vehicles: progress and challenges. *2009 IEEE Vehicle Power and Propulsion Conference*, 551–557. doi: 10.1109/VPPC.2009.5289801.
- Monteiro, R., Leirós, J., Boaventura, M. & Mendes, A. (2018). Insights into all-vanadium redox flow battery: A case study on components and operational conditions. *Electrochimica Acta*, 267, 80–93. doi: 10.1016/j.electacta.2018.02.054.
- Mukherjee, P. & Rao, V. (2019). Design and development of high temperature superconducting magnetic energy storage for power applications-A review. *Physica C: Superconductivity and Its Applications*, 563, 67–73. doi: 10.1016/j.physc.2019.05.001.
- Najib, S. & Erdem, E. (2019). Current progress achieved in novel materials for supercapacitor electrodes: mini review. *Nanoscale Advances*, 1(8), 2817–2827. doi: 10.1039/C9NA00345B.
- Olabi, A., Wilberforce, T., Ramadan, M., Abdelkareem, M. A. & Alami, A. H. (2020). Compressed air energy storage systems: Components and operating parameters-A review. *Journal of Energy Storage*, 102000. doi: 10.1016/j.est.2020.102000.
- Orazem, M. E. & Tribollet, B. (2011). *Electrochemical Impedance Spectroscopy* (Vol. 48). John Wiley & Sons.

- Orita, A., Verde, M., Sakai, M. & Meng, Y. (2016). The impact of pH on side reactions for aqueous redox flow batteries based on nitroxyl radical compounds. *Journal of Power Sources*, 321, 126–134. doi: 10.1016/j.jpowsour.2016.04.136.
- Ouyang, B., Zhang, Y., Wang, Y., Zhang, Z., Fan, H. J. & Rawat, R. S. (2016). Plasma surface functionalization induces nanostructuring and nitrogen-doping in carbon cloth with enhanced energy storage performance. *Journal of Materials Chemistry A*, 4(45), 17801–17808. doi: 10.1039/C6TA08155J.
- Pan, J., Ji, L., Sun, Y., Wan, P., Cheng, J., Yang, Y. & Fan, M. (2009). Preliminary study of alkaline single flowing Zn-O<sub>2</sub> battery. *Electrochemistry Communications*, 11(11), 2191–2194. doi: 10.1016/j.elecom.2009.09.028.
- Park, J. J., Park, J. H., Park, O. O. & Yang, J. H. (2016). Highly porous graphenated graphite felt electrodes with catalytic defects for high-performance vanadium redox flow batteries produced via NiO/Ni redox reactions. *Carbon*, 110, 17–26. doi: 10.1016/j.carbon.2016.08.094.
- Park, M., Jung, Y., Kim, J., Lee, H. I. & Cho, J. (2013). Synergistic effect of carbon nanofiber/nanotube composite catalyst on carbon felt electrode for high-performance all-vanadium redox flow battery. *Nano Letters*, 13(10), 4833–4839. doi: 10.1021/nl402566s.
- Park, M., Ryu, J., Kim, Y. & Cho, J. (2014). Corn protein-derived nitrogen-doped carbon materials with oxygen-rich functional groups: a highly efficient electrocatalyst for all-vanadium redox flow batteries. *Energy & Environmental Science*, 7(11), 3727–3735. doi: 10.1039/C4EE02123A.
- Park, M., Ryu, J., Wang, W. & Cho, J. (2017). Material design and engineering of next-generation flow-battery technologies. *Nature Reviews Materials*, 2(1), 16080. doi: 10.1038/natrevmats.2016.80.
- Pasala, V., Ramavath, J. N., He, C., Ramani, V. K. & Ramanujam, K. (2018). N- and P-co-doped Graphite Felt Electrode for Improving Positive Electrode Chemistry of the Vanadium Redox Flow Battery. *ChemistrySelect*, 3(30), 8678–8687. doi: 10.1002/slct.201801446.
- Pellow, M. A., Ambrose, H., Mulvaney, D., Betita, R. & Shaw, S. (2020). Research gaps in environmental life cycle assessments of lithium ion batteries for grid-scale stationary energy storage systems: End-of-life options and other issues. *Sustainable Materials and Technologies*, 23, 1–20. doi: 10.1016/j.susmat.2019.e00120.
- Permatasari, A., Lee, W. & Kwon, Y. (2020). Performance improvement by novel activation process effect of aqueous organic redox flow battery using Tiron and anthraquinone-2, 7-disulfonic acid redox couple. *Chemical Engineering Journal*, 383, 123085.

- Perry, M. L. & Weber, A. Z. (2016). Advanced Redox-Flow Batteries: A Perspective. *Journal of The Electrochemical Society*, 163(1), A5064–A5067. doi: 10.1149/2.0101601jes.
- Petek, T. J. (2015). *Enhancing the Capacity of All-Iron Flow Batteries: Understanding Crossover and Slurry Electrodes*. (Doctorate dissertation, Case Western Reserve University, United states of America) Retrieved from <https://etd.ohiolink.edu>.
- Pineda Flores, S. D., Martin-Noble, G. C., Phillips, R. L. & Schrier, J. (2015). Bio-inspired electroactive organic molecules for aqueous redox flow batteries. 1. thiophenoquinones. *The Journal of Physical Chemistry C*, 119(38), 21800–21809. doi: 10.1021/acs.jpcc.5b05346.
- Pivac, I. & Barbir, F. (2016). Inductive phenomena at low frequencies in impedance spectra of proton exchange membrane fuel cells-A review. *Journal of Power Sources*, 326, 112–119. doi: 10.1016/j.jpowsour.2016.06.119.
- Raza, R., Zhu, B., Rafique, A., Naqvi, M. R. & Lund, P. (2020). Functional ceria-based nanocomposites for advanced low-temperature (300-600° C) solid oxide fuel cell: A comprehensive review. *Materials Today Energy*, 15, 100373. doi: 10.1016/j.mtener.2019.100373.
- Raza, W., Ali, F., Raza, N., Luo, Y., Kim, K.-H., Yang, J., ... Kwon, E. E. (2018). Recent advancements in supercapacitor technology. *Nano Energy*, 52, 441–473. doi: 10.1016/j.nanoen.2018.08.013.
- Rehman, S., Al-Hadhrami, L. M. & Alam, M. M. (2015). Pumped hydro energy storage system: A technological review. *Renewable and Sustainable Energy Reviews*, 44, 586–598. doi: 10.1016/j.nanoen.2018.08.013.
- Roch, A., Greifzu, M., Talens, E. R., Stepien, L., Roch, T., Hege, J., ... others. (2015). Ambient effects on the electrical conductivity of carbon nanotubes. *Carbon*, 95, 347–353. doi: 10.1016/j.carbon.2015.08.045.
- Samineni, S., Johnson, B. K., Hess, H. L. & Law, J. D. (2006). Modeling and analysis of a flywheel energy storage system for voltage sag correction. *IEEE Transactions on Industry Applications*, 42(1), 42–52. doi: 10.1109/TIA.2005.861366.
- Savinell, R. F. & Wainright, J. S. (2012). U. S. Patent No. 20140227574A1. *Iron flow battery*. Washington, DC: U.S. Patent and Trademark Office.
- Scrosati, B. & Garche, J. (2010). Lithium batteries: Status, prospects and future. *Journal of Power Sources*, 195(9), 2419–2430. doi: 10.1016/j.jpowsour.2009.11.048.
- Selverston, S., Savinell, R. F. & Wainright, J. S. (2017). Zinc-Iron Flow Batteries with Common Electrolyte. *Journal of The Electrochemical Society*, 164(6), A1069–A1075. doi: 10.1149/2.0591706jes.
- Sheng, W., Zhou, X., Wu, L., Shen, Y., Huang, Y., Liu, L., ... Li, N. (2020). Quaternized poly (2, 6-dimethyl-1, 4-phenylene oxide) anion exchange membranes with

pendant sterically-protected imidazoliums for alkaline fuel cells. *Journal of Membrane Science*, 601, 117881. doi: 10.1016/j.memsci.2020.117881.

Shi, L., Liu, S., He, Z. & Shen, J. (2014). Nitrogen-Doped Graphene: Effects of nitrogen species on the properties of the vanadium redox flow battery. *Electrochimica Acta*, 138, 93–100. doi: 10.1016/j.electacta.2014.06.099.

Shigematsu, T. & others. (2011). Redox flow battery for energy storage. *SEI Technical Review*, 73, 5–13.

Singh, V., Kim, S., Kang, J. & Byon, H. R. (2019). Aqueous organic redox flow batteries. *Nano Research*, 12, 1988–2001. doi: 10.1007/s12274-019-2355-2.

Skyllas-Kazacos, M. (2004). U. S. Patent No. 20040241552A1. *Vanadium Redox Battery Electrolyte*. Washington, DC: U.S. Patent and Trademark Office.

Skyllas-Kazacos, M., Chakrabarti, M., Hajimolana, S., Mjalli, F. & Saleem, M. (2011). Progress in flow battery research and development. *Journal of The Electrochemical Society*, 158(8), R55–R79. doi: 10.1149/1.3599565.

Skyllas-Kazacos, M., Kazacos, G., Poon, G. & Verseema, H. (2010). Recent advances with UNSW vanadium-based redox flow batteries. *International Journal of Energy Research*, 34(2), 182–189. doi: 10.1002/er.1658.

Skyllas-Kazacos, M., Kazacos, M. & Mousa, A. (2003). U.S. Patent No. 20050244707A1. *Metal halide redox flow battery*. Washington, DC: U.S. Patent and Trademark Office.

Skyllas-Kazacos, M., Rychick, M. & Robins, R. U.S. Patent No. 4798567. *All-vanadium redox battery*, (1988). Washington, DC: U.S. Patent and Trademark Office.

Soloveichik, G. L. (2011). Battery technologies for large-scale stationary energy storage. *Annual Review of Chemical and Biomolecular Engineering*, 2, 503–527. doi:10.1146/annurev-chembioeng-061010-114116.

Soloveichik, G. L. (2015). Flow Batteries: Current Status and Trends. *Chemical Reviews*, 115(20), 11533–11558. doi: 10.1021/cr500720t.

Son, E. J., Kim, J. H., Kim, K. & Park, C. B. (2016). Quinone and its derivatives for energy harvesting and storage materials. *Journal of Materials Chemistry A*, 4(29), 11179–11202. doi: 10.1039/C6TA03123D.

Sun, B. & Skyllas-Kazacos, M. (1992a). Chemical modification of graphite electrode materials for vanadium redox flow battery application—part II. Acid treatments. *Electrochimica Acta*, 37(13), 2459–2465. doi: 10.1016/0013-4686(92)87084-D.

Sun, B. & Skyllas-Kazacos, M. (1992b). Modification of graphite electrode materials for vanadium redox flow battery application—I. Thermal treatment. *Electrochimica Acta*, 37(7), 1253–1260. doi: 10.1016/0013-4686(92)85064-R.

- Tabor, D. P., Gómez-Bombarelli, R., Tong, L., Gordon, R. G., Aziz, M. J. & Aspuru-Guzik, A. (2019). Mapping the frontiers of quinone stability in aqueous media: implications for organic aqueous redox flow batteries. *Journal of Materials Chemistry A*, 7(20), 12833–12841. doi: 10.1039/C9TA03219C.
- Tamtögl, A., Sacchi, M., Calvo-Almazán, I., Zbiri, M., Koza, M. M., Ernst, W. E. & Fouquet, P. (2018). Ultrafast molecular transport on carbon surfaces: The diffusion of ammonia on graphite. *Carbon*, 126, 23–30. doi: 10.1016/j.carbon.2017.09.104.
- Thaller, L. H. U. S. Patnt No. 3996064. *Energy storage system.*, (1976). Washington, DC: U.S. Patent and Trademark Office.
- Tseng, T.-M., Huang, R.-H., Huang, C.-Y., Liu, C.-C., Hsueh, K.-L. & Shieu, F.-S. (2014). Carbon felt coated with titanium dioxide/carbon black composite as negative electrode for vanadium redox flow battery. *Journal of The Electrochemical Society*, 161(6), A1132–A1138. doi: 10.1149/2.082308jes.
- Wang, R. & Li, Y. (2020). Carbon electrodes improving electrochemical activity and enhancing mass and charge transports in aqueous flow battery: Status and perspective. *Energy Storage Materials*, 31, 230–251. doi: 10.1016/j.ensm.2020.06.012.
- Wang, R., Li, Y. & He, Y.-L. (2019). Achieving gradient-pore-oriented graphite felt for vanadium redox flow batteries: meeting improved electrochemical activity and enhanced mass transport from nano-to micro-scale. *Journal of Materials Chemistry A*, 7(18), 10962–10970. doi: 10.1039/C9TA00807A.
- Wang, W. & Wang, X. (2007). Investigation of Ir-modified carbon felt as the positive electrode of an all-vanadium redox flow battery. *Electrochimica Acta*, 52(24), 6755–6762. doi: 10.1016/j.electacta.2007.04.121.
- Wedge, K., Drazevic, E., Konya, D. & Bientien, A. (2016). Organic Redox Species in Aqueous Flow Batteries: Redox Potentials, Chemical Stability and Solubility. *Scientific Reports (Nature Publisher Group)*, 6, 39101. doi: 10.1038/srep39101.
- Wei, G., Jia, C., Liu, J. & Yan, C. (2012). Carbon felt supported carbon nanotubes catalysts composite electrode for vanadium redox flow battery application. *Journal of Power Sources*, 220, 185–192. doi: 10.1016/j.jpowsour.2012.07.081.
- Wei, L., Zhao, T., Zeng, L., Zeng, Y. & Jiang, H. (2017). Highly catalytic and stabilized titanium nitride nanowire array-decorated graphite felt electrodes for all vanadium redox flow batteries. *Journal of Power Sources*, 341, 318–326. doi: 10.1016/j.jpowsour.2016.12.016.
- Wei, L., Zhao, T., Zeng, L., Zhou, X. & Zeng, Y. (2016). Copper nanoparticle-deposited graphite felt electrodes for all vanadium redox flow batteries. *Applied Energy*, 180, 386–391. doi: 10.1016/j.apenergy.2016.07.134.



- Wei, L., Zhao, T., Zhao, G., An, L. & Zeng, L. (2016). A high-performance carbon nanoparticle-decorated graphite felt electrode for vanadium redox flow batteries. *Applied Energy*, 176, 74–79. doi: 10.1016/j.apenergy.2016.05.048.
- Wei, Z., Zhao, J., Skyllas-Kazacos, M. & Xiong, B. (2014). Dynamic thermal-hydraulic modeling and stack flow pattern analysis for all-vanadium redox flow battery. *Journal of Power Sources*, 260, 89–99. doi: 10.1016/j.jpowsour.2014.02.108.
- Wei, Z., Zhao, J. & Xiong, B. (2014). Dynamic electro-thermal modeling of all-vanadium redox flow battery with forced cooling strategies. *Applied Energy*, 135, 1–10. doi: 10.1016/j.apenergy.2014.08.062.
- Wicki, S. & Hansen, E. G. (2017). Clean energy storage technology in the making: An innovation systems perspective on flywheel energy storage. *Journal of Cleaner Production*, 162, 1118–1134. doi: 10.1016/j.jclepro.2017.05.132.
- Winsberg, J., Hagemann, T., Janoschka, T., Hager, M. D. & Schubert, U. S. (2017). Redox-flow batteries: From metals to organic redox-active materials. *Angewandte Chemie International Edition*, 56(3), 686–711. doi: 10.1002/anie.201604925.
- Winsberg, J., Janoschka, T., Morgenstern, S., Hagemann, T., Muench, S., Hauffman, G., ... Schubert, U. S. (2016). Poly (TEMPO)/Zinc Hybrid-Flow Battery: A Novel, “Green,” High Voltage, and Safe Energy Storage System. *Advanced Materials*, 28(11), 2238–2243. doi: 10.1002/adma.201505000.
- Wu, X., Xu, H., Shen, Y., Xu, P., Lu, L., Fu, J. & Zhao, H. (2014). Treatment of graphite felt by modified Hummers method for the positive electrode of vanadium redox flow battery. *Electrochimica Acta*, 138, 264–269. doi: 10.1016/j.electacta.2014.06.124.
- Wu, X., Xu, H., Xu, P., Shen, Y., Lu, L., Shi, J., ... Zhao, H. (2014). Microwave-treated graphite felt as the positive electrode for all-vanadium redox flow battery. *Journal of Power Sources*, 263, 104–109. doi: 10.1016/j.jpowsour.2014.04.035.
- Wu, Z., Liu, Y., Deng, C., Zhao, H., Zhao, R. & Chen, H. (2020). The critical role of boric acid as electrolyte additive on the electrochemical performance of lead-acid battery. *Journal of Energy Storage*, 27, 101076. doi: 10.1016/j.est.2019.101076.
- Xiang, Y. & Daoud, W. A. (2018). Cr<sub>2</sub>O<sub>3</sub>-modified graphite felt as a novel positive electrode for vanadium redox flow battery. *Electrochimica Acta*, 290, 176–184. doi: 10.1016/j.electacta.2018.09.023.
- Xu, J., Ma, Q., Xing, L., Li, H., Leung, P., Yang, W., ... Xu, Q. (2020). Modeling the effect of temperature on performance of an iron-vanadium redox flow battery with deep eutectic solvent (DES) electrolyte. *Journal of Power Sources*, 449, 227491. doi: 10.1016/j.jpowsour.2019.227491.
- Yang, B., Hooper-Burkhardt, L., Krishnamoorthy, S., Murali, A., Prakash, G. S. & Narayanan, S. (2016). High-Performance Aqueous Organic Flow Battery with

Quinone-Based Redox Couples at Both Electrodes. *Journal of The Electrochemical Society*, 163(7), A1442–A1449. doi: 10.1149/2.1371607jes.

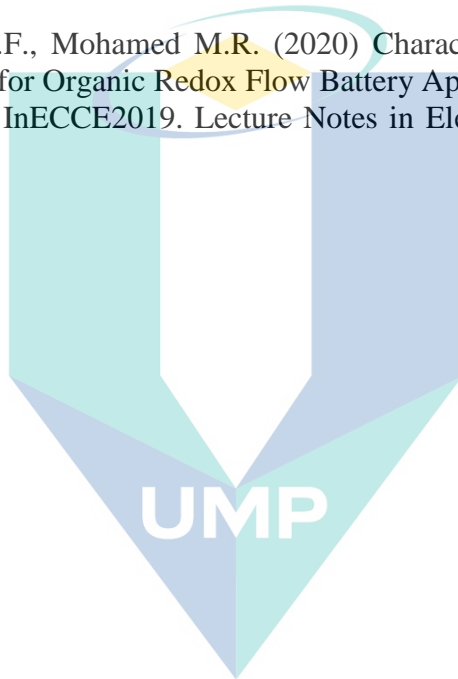
- Yang, B., Hooper-Burkhardt, L., Wang, F., Prakash, G. S. & Narayanan, S. (2014). An inexpensive aqueous flow battery for large-scale electrical energy storage based on water-soluble organic redox couples. *Journal of The Electrochemical Society*, 161(9), A1371–A1380. doi: 10.1149/2.1001409jes.
- Yang, C., Wang, H., Lu, S., Wu, C., Liu, Y., Tan, Q., ... Xiang, Y. (2015). Titanium nitride as an electrocatalyst for V (II)/V (III) redox couples in all-vanadium redox flow batteries. *Electrochimica Acta*, 182, 834–840. doi: 10.1016/j.electacta.2015.09.155.
- Yang, D.-S., Lee, J. Y., Jo, S.-W., Yoon, S. J., Kim, T.-H. & Hong, Y. T. (2018). Electrocatalytic activity of nitrogen-doped CNT graphite felt hybrid for all-vanadium redox flow batteries. *International Journal of Hydrogen Energy*, 43(3), 1516–1522. doi: 10.1016/j.ijhydene.2017.11.145.
- Yang, H. S., Park, J. H., Ra, H. W., Jin, C.-S. & Yang, J. H. (2016). Critical rate of electrolyte circulation for preventing zinc dendrite formation in a zinc-bromine redox flow battery. *Journal of Power Sources*, 325, 446–452. doi: 10.1016/j.jpowsour.2016.06.038.
- Yang, Z., Zhang, J., Kintner-Meyer, M. C., Lu, X., Choi, D., Lemmon, J. P. & Liu, J. (2011). Electrochemical energy storage for green grid. *Chemical Reviews*, 111(5), 3577–3613. doi: 10.1021/cr100290v
- Yun, N., Park, J. J., Park, O. O., Lee, K. B. & Yang, J. H. (2018). Electrocatalytic effect of NiO nanoparticles evenly distributed on a graphite felt electrode for vanadium redox flow batteries. *Electrochimica Acta*, 278, 226–235. doi: 10.1016/j.electacta.2018.05.039.
- Zach, K., Aeur, H. & Lettner, G. (2012). Facilitating energy storage to allow high penetration of intermittent renewable energy. *7th International Renewable Energy Storage Conference and Exhibition (IRES 2012)*.
- Zeng, Y., Zhao, T., An, L., Zhou, X. & Wei, L. (2015). A comparative study of all-vanadium and iron-chromium redox flow batteries for large-scale energy storage. *Journal of Power Sources*, 300, 438–443. doi: 10.1016/j.jpowsour.2015.09.100.
- Zeng, Y., Zhao, T., Zhou, X., Wei, L. & Jiang, H. (2016). A low-cost iron-cadmium redox flow battery for large-scale energy storage. *Journal of Power Sources*, 330, 55–60. doi: 10.1016/j.jpowsour.2016.08.107.
- Zeng, Y., Zhao, T., Zhou, X., Wei, L. & Ren, Y. (2017). A novel iron-lead redox flow battery for large-scale energy storage. *Journal of Power Sources*, 346, 97–102. doi: 10.1016/j.jpowsour.2017.02.018.

- Zeng, Y., Zhao, T., Zhou, X., Zeng, L. & Wei, L. (2016). The effects of design parameters on the charge-discharge performance of iron-chromium redox flow batteries. *Applied Energy*, 182, 204–209. doi: 10.1016/j.apenergy.2016.08.135.
- Zeng, Y., Zhou, X., An, L., Wei, L. & Zhao, T. (2016). A high-performance flow-field structured iron-chromium redox flow battery. *Journal of Power Sources*, 324, 738–744. doi: 10.1016/j.jpowsour.2016.05.138.
- Zhang, C., Wei, Y.-L., Cao, P.-F. & Lin, M.-C. (2017). Energy storage system: Current studies on batteries and power condition system. *Renewable and Sustainable Energy Reviews*. doi: 10.1016/j.rser.2017.10.030.
- Zhang, H., Baeyens, J., Caceres, G., Degreve, J. & Lv, Y. (2016). Thermal energy storage: Recent developments and practical aspects. *Progress in Energy and Combustion Science*, 53, 1–40. doi: 10.1016/j.pecs.2015.10.003.
- Zhang, H., Chen, N., Sun, C. & Luo, X. (2020). Investigations on physicochemical properties and electrochemical performance of graphite felt and carbon felt for iron-chromium redox flow battery. *International Journal of Energy Research*, 44 (5), 3839-3853. doi: 10.1002/er.5179.
- Zhang, S., Li, X. & Chu, D. (2016). An Organic Electroactive Material for Flow Batteries. *Electrochimica Acta*, 190, 737–743. doi: 10.1016/j.electacta.2015.12.139.
- Zhang, Z., Xi, J., Zhou, H. & Qiu, X. (2016). KOH etched graphite felt with improved wettability and activity for vanadium flow batteries. *Electrochimica Acta*, 218, 15–23. doi: 10.1016/j.electacta.2016.09.099.
- Zhang, Z., Zhao, T., Bai, B., Zeng, L. & Wei, L. (2017). A highly active biomass-derived electrode for all vanadium redox flow batteries. *Electrochimica Acta*, 248, 197–205. doi: 10.1016/j.electacta.2017.07.129.
- Zhao, Q., Zhu, Z. & Chen, J. (2017). Molecular engineering with organic carbonyl electrode materials for advanced stationary and redox flow rechargeable batteries. *Advanced Materials*, 29(48), 1607007. doi: 10.1002/adma.201607007.
- Zhao, Y., Si, S. & Liao, C. (2013). A single flow zinc//polyaniline suspension rechargeable battery. *Journal of Power Sources*, 241, 449–453. doi: 10.1016/j.jpowsour.2013.04.095.
- Zhou, X., Zeng, Y., Zhu, X., Wei, L. & Zhao, T. (2016). A high-performance dual-scale porous electrode for vanadium redox flow batteries. *Journal of Power Sources*, 325, 329–336. doi: 10.1016/j.jpowsour.2016.06.048.
- Zhu, H., Zhang, Y., Yue, L., Li, W., Li, G., Shu, D. & Chen, H. (2008). Graphite-carbon nanotube composite electrodes for all vanadium redox flow battery. *Journal of Power Sources*, 184(2), 637–640. doi: 10.1016/j.jpowsour.2008.04.016.
- Zoski, C. G. (2006). *Handbook of electrochemistry*. Elsevier.

## LIST OF PUBLICATIONS

### Journal Papers/Book Chapter

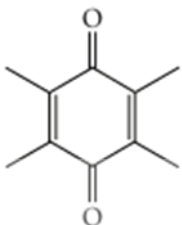
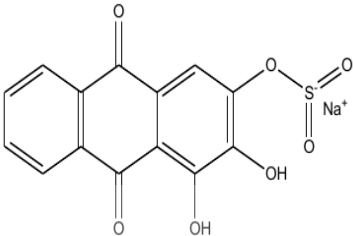
- A. Khor, P. Leung, M. Mohamed, C. Flox, Q. Xu, L. An, R. Wills, J. Morante, and A. Shah, "Review of zinc-based hybrid flow batteries: From fundamentals to applications," *Materials Today Energy*, vol. 8, pp. 80–108, 2018.
- A. C. Khor, M. Mohamed, K. F. Chong, and P. Leung, "Electrochemical Studies on Alizarin Red S as Negolyte for Redox Flow Battery: A Preliminary Study," *International Journal of Engineering & Technology*, vol. 7, pp. 375–377, 2018.
- Khor A.C., Chong K.F., Mohamed M.R. (2020) Characterization of Positive Porous Electrode Felt for Organic Redox Flow Battery Application. In: Kasruddin Nasir A. et al. (eds) InECCE2019. Lecture Notes in Electrical Engineering, vol 632. Springer



اونيورسيتي ملايسيا قهغ

UNIVERSITI MALAYSIA PAHANG

## APPENDIX A

Structure		
Name	1,4-benzoquinone	Alizarin red S
Abbreviation	1,4 – HQ	ARS
Solubility in water	5.9 g/100 mL (15 °C)	3.12 mol L <sup>-1</sup> (pH 6) (S. Zhang et al., 2016)
Solubility in 1 M H <sub>2</sub> SO <sub>4</sub>	0.7 M (Wedege et al., 2016)	<0.64 M (S. Zhang et al., 2016)

UMP

اونیورسیتی ملیسیا قهق

UNIVERSITI MALAYSIA PAHANG